

Functional Magnetic Resonance Imaging in Alert Behaving Monkeys

Blood-oxygen-level-dependent brain responses related to the
processing of visual stimuli and voluntary eye movements

Dissertation

zur Erlangung des Grades eines Doktors
der Naturwissenschaften

der Fakultät für Biologie

und

der Medizinischen Fakultät

der Eberhard-Karls-Universität Tübingen

vorgelegt

von

Hendrik Dietrich

aus Kiel, Schleswig-Holstein

2006

Tag der mündlichen Prüfung:

23. Juni 2006

Dekan der Fakultät für Biologie:

Prof. Dr. Friedrich Schöffl

Dekan der Medizinischen Fakultät:

Prof. Dr. Claus D. Claussen

1. Berichterstatter:

Prof. Dr. Peter Thier

2. Berichterstatter:

Prof. Dr. Werner J. Schmidt

Prüfungskommission:

Prof. Dr. Peter Thier

Prof. Dr. Werner J. Schmidt

Prof. Dr. Werner Lutzenberger

Prof. Dr. Uwe Ilg

Prof. Dr. Horst Herbert

Contents

1. INTRODUCTION.....	6
1.1: Functional Magnetic Resonance Imaging (fMRI)	6
The magnetic resonance imaging (MRI) signal.....	6
The blood oxygen level dependent (BOLD) contrast.....	9
How is the BOLD signal related to neural activity?.....	10
1.2: fMRI in monkeys.....	15
Motivation for fMRI studies in monkeys.....	15
fMRI in anaesthetized monkeys.....	16
fMRI in alert behaving monkeys.....	17
Sources of image artefacts.....	17
fMRI in humans vs. monkeys.....	18
1.3: Investigating visual processing and voluntary eye movements with fMRI.....	21
Visual field mapping.....	21
Optic flow.....	22
Voluntary eye movements.....	24
2. MATERIAL & METHODS.....	28
2.1: Animals.....	28
Subjects.....	28
Anaesthesia, surgical procedures and implants.....	28
2.2: Experimental procedures	32
Experimental environment.....	32
Body movements.....	34
Training and behavioural control.....	36
2.3: Behavioural paradigms.....	40
Visual field mapping paradigm.....	40
Optic flow paradigm.....	40
Saccadic eye movement paradigm.....	41
Smooth pursuit eye movement paradigm.....	41
Implementation of the behavioural paradigms in the fMRI design.....	41
2.4: Image acquisition	43
Structural MR imaging.....	43
Functional MR imaging.....	43

2.5: Functional image analysis.....	45
Standard procedures using software package 'SPM2'.....	45
Correction for multiple comparisons.	46
Selection and pooling.	46
2.6: Superimposition, projection and evaluation of SPMs.....	47
Projection of SPMs onto structural images.....	47
Projection of SPMs onto cortical surface reconstruction models.	48
Evaluation of SPMs by co-registration with rhesus monkey atlas.	48
 FIGURES & TABLES	 50
 3. RESULTS	 98
3.1: Presentation of BOLD responses.....	98
3.2: Visual field mapping	99
Representation of meridians of the visual field.....	99
Representation of different degrees of eccentricity of the visual field.	99
3.3: Optic flow	100
3.4: Voluntary eye movements.....	101
Saccadic eye movements.....	101
Smooth pursuit eye movements.	101
Saccadic vs. smooth pursuit eye movements.	102
 4. DISCUSSION & CONCLUSIONS.....	 104
4.1: Technical constraints	104
Image artefacts.	104
EPI sequence parameters.	105
Coil configuration.	105
Eye-gaze-control.....	106
Presentation screen.....	107
Auditory noise.	107
Misalignment of functional and structural images.....	107
Misprojection of functional data onto cortical surface reconstructions.	108
Deviations of brain areas from atlas.	109
Definition of BOLD response peaks.....	109

4.2: Visual field mapping	110
Representation of meridians of the visual field.....	110
Representation of different degrees of eccentricity of the visual field.	111
4.3: Optic flow	112
Areas MT/MST.....	112
Motion sensitivity.....	112
Cerebellum.....	115
4.4: Voluntary eye movements.....	116
Comparison across studies.	116
Areas LIP, FEF and SEF.	116
Area 6.	117
Area 46.	117
Area DP and area 5.	117
Areas MT/MST.....	118
Superior colliculus.....	118
Saccadic eye movements vs. SPEMs.	119
4.5: Future improvements.....	120
5. SUMMARY / ZUSAMMENFASSUNG	122
Summary.	122
Zusammenfassung.....	123
6. ACKNOWLEDGEMENTS.....	124
7. REFERENCES.....	126

1. Introduction

1.1: Functional Magnetic Resonance Imaging (fMRI)

Blood oxygen level dependent (BOLD) functional magnetic resonance imaging (fMRI) has been commonly used by a large group of scientists since its introduction (Ogawa and Lee, 1990; Ogawa *et al.*, 1990a; Ogawa *et al.*, 1990b; Bandettini *et al.*, 1992; Kwong *et al.*, 1992; Ogawa *et al.*, 1992; Ogawa *et al.*, 1998), and, within a very short time period, has become a very popular method for investigating human brain function. Its success is based on the availability of magnetic resonance scanners, on the fact that fMRI is non-invasive and therefore allows repeated measurements in human subjects and also on its high spatiotemporal resolution relative to other methods that can be used in human research (Fig. 1).

However, the understanding of the causal relationship between neural activity and the *BOLD signal*, as measured with fMRI, is still limited and needs to be further investigated. Until now, it is still unclear, which aspects of the neural signal is measured by BOLD fMRI (see below) and how these measurements relate to those obtained with other methods (for review, see Logothetis, 2002; Logothetis, 2003a; Logothetis, 2003b; Logothetis and Wandell, 2004).

The magnetic resonance imaging (MRI) signal. (Sections on MR physics are modified from Nensaiver, 1996; Grodd, 1998; Logothetis and Wandell, 2004). Magnetic resonance is based on nuclear magnetic properties. Atomic nuclei with odd atomic number, such as hydrogen, possess an angular momentum or spin. The moving charge generates a small magnetic field, which gives the nucleus its polarity.

MRI, as commonly used for human subjects and animals, relies on hydrogen nuclei that are present in the body in high enough density (primarily in water and, to a lesser extent, in fat) to allow for measurements at high spatial resolution.

When placed in a strong, uniform magnetic field, B_0 , hydrogen nuclei within the

tissue line up with the B_0 field, creating a longitudinal magnetization M_0 that will add to B_0 . In particular, each magnetic moment will experience a torque tending to align it either parallel or antiparallel to the B_0 field direction and around that axis, spins will precess. The angular *frequency of precession* is proportional to B_0 ,

$$\omega = \gamma B_0$$

(*Larmor's theorem*), where γ is the nuclear gyromagnetic ratio, 42.56 MHz/Tesla for protons. The *precession frequency* or *Larmor frequency* is defined as

$$\nu = \omega/2\pi.$$

Since nuclei that are in alignment with the field achieve a lower energetic state than those that are aligned antiparallel to the field, the population of nuclei aligned with the field is slightly higher than that of antiparallel aligned nuclei. The longitudinal magnetization M_0 is proportional to the difference in the number of nuclei parallel or antiparallel to the field, as well as to the quantum energy required for a nucleus to make a transition from the parallel to antiparallel state or vice versa. At room temperature at 1 T, the excess of parallel oriented spin accounts to seven to a million. This ratio reflects the relatively low *signal to noise ratio, SNR*, of MRI experiments.

The magnetic resonance measurement is initiated by introducing an electromagnetic field to the tissue, in form of a radiofrequency (RF) pulse perpendicular to the static B_0 field at the *Larmor frequency*. Through this excitation, the longitudinal magnetization M_0 is tilted away from the B_0 field direction and the nuclei will tend to synchronize their precession with the RF and precess around the RF axis. Following RF pulse application, relaxation processes take place and the absorbed energy is retransmitted. In a longitudinal relaxation process with exponential time constant T_1 , spins begin to fall back into an orientation parallel or antiparallel to B_0 . In a transverse relaxation process with exponential time constants T_2 , excited protons that have initially been in phase are caused to dephase due to *spin spin interactions* (i.e. energy transitions of a nucleus that changes the local field at nearby

nuclei). The retransmitted RF signal represents the MR signal that is measured by receiver coils.

In order to create MR images, spatial information must be recorded along with the received tissue relaxation information. Spatial encoding is achieved in three consecutive steps: *slice selection*, *phase encoding* and *frequency encoding*. Slice selection is accomplished by a magnetic gradient switching during the RF excitation with a pulse of a defined transmitter bandwidth. Once a slice has been selected, its signal has to be converted pixelwise along both axes by two additional magnetic field gradients that are orthogonal to each other. The phase encoding gradient is applied immediately after the excitation and causes a linear phase shift along its axis, which will add to the individual phase of each nucleus. The application of the frequency encoding gradient causes a linear frequency shift of the nuclear precession frequency along its axis. Since the MR signal is collected at the level of the frequency encoding gradient in the *read out period*, it is also termed *read out gradient*. For image formation, the measurement of an excited slice with a defined slice selection gradient has to be repeated in the phase encoding direction with different gradient strength to scan the excited plane in the second dimension, while slice selection and read out gradient remain unchanged. This is a time consuming process that accounts for the acquisition time T_a . T_a is dependent on the number of phase encoding steps, which determines the imaging matrix size MA and the repetition time TR (time between two consecutive sets of RF pulses):

$$T_a = MA \cdot TR.$$

Each measurement with a different phase encoding gradient is stored in a raw matrix, termed *k-space*. After complete data collection, the k-space will be 2D-*Fourier*-transformed from the time domain into the spatial domain. Phase memory and frequency shift of the spins are used to determine the spatial position and signal intensity of each pixel, which, together, are usually displayed as magnitude images.

RF excitation pulses, as well as the magnetic field gradients superimposed on the B_0 field, are applied in various different timing and amplitude parameters, called *pulse sequences*, in order to obtain contrasts that differentiate between various properties of the brain, such as structure (anatomical imaging), flow (perfusion imaging) and neural activity (functional imaging). Of special significance for fMRI is the transverse relaxation, caused by spin-spin interactions that would follow an exponential signal decay (*free-induction decay, FID*) with a time constant of T_2 in an ideal homogeneous magnetic field. But in physiological tissue, the transverse relaxation takes place more rapidly because of local field inhomogeneities, including those which are caused by the tissue itself. In the presence of such inhomogeneities, the decay constant is termed T_2^* . Field inhomogeneities change the frequency of the proton's precession, disturb phase coherence and speed up the transverse relaxation. Their size depends upon the physiological state of brain tissue and, in particular, the composition of the local blood supply, which serves as an indirect measure of neuronal activity (see below). T_2^* can be measured at fairly high spatiotemporal resolution across the entire brain and thus provides a valuable tool to neuroscience research.

The blood oxygen level dependent (BOLD) contrast. *BOLD contrast mechanisms* are those that are assumed to connect neural activity to the measured T_2^* . In the current report, I use the term *BOLD responses* in order to describe neuronal activity in response to specific stimuli or, more generally, I use the term *fMRI responses* in order to account for functional measures, including those dependent on blood oxygen or contrast agents.

BOLD contrast mechanisms alter the BOLD signal, as measured by T_2^* , by neural activity-dependent changes in relative concentration of oxygenated and deoxygenated blood. Very slight magnetic susceptibility differences – $\Delta\chi$: 0.27 ppm (Spees *et al.*, 2001) – between *oxygenated haemoglobin (Hb)*, which is isomagnetic relative to brain tissue and *deoxyhemoglobin (dHb)*, which is paramagnetic relative

to brain tissue (Pauling and Coryell, 1936), have to be detected in BOLD fMRI. Magnetic susceptibility is the degree of magnetization of a material in response to a magnetic field which is defined by the relationship

$$M = \chi \cdot B,$$

where M is the magnetic dipole moment per unit mass and B is the applied field.

Due to local oxygen consumption, as expected at brain sites of increased neural activity, levels of oxygenated blood would be expected to decrease in favour of deoxygenated blood. An increase in *cerebral blood volume* (CBV) and *cerebral blood flow* (CBF), however, does not only compensate for the decrease of levels of oxygenated blood, but actually overcompensates it (Fox and Raichle, 1986; Fox *et al.*, 1988), a mechanism that is still not fully understood (for review, see Boxerman *et al.*, 1995; Buxton and Frank, 1997; Ogawa *et al.*, 1998; Logothetis and Wandell, 2004).

The time course of the BOLD signal to a brief stimulus is often termed the *haemodynamic response function* (HRF). The HRF is assumed to be heterogeneous across cortex of individuals, between individuals and species. The data analysis package SPM2 (<http://www.fil.ion.ucl.ac.uk/spm/software/spm2>) utilizes a canonical HRF, that was used in the present study. As depicted in Fig. 2, six seconds after a brief, intense period of neural stimulation, this HRF exhibits a peak, followed by an undershoot that lasts a few seconds.

How is the BOLD signal related to neural activity? In the last four decades, investigations of cortical processing have been dominated by the analysis of action potentials, mainly by recording *single unit-activity* in the monkey, the animal of choice for studying cognitive behaviour. An important question, controversially discussed in the current literature, is how results obtained with fMRI are related to neural processing and, especially *whether the BOLD signal reflects neuronal action potentials*.

In the following, I will discuss some examples of recent studies relevant for ques-

tions on the relationship between neural activity and vascular changes in the brain.

It has been assumed that the spike rate of neurons is quantitatively related to the BOLD signal (Heeger *et al.*, 2000; Rees *et al.*, 2000). Mukamel and coworkers (2005) combined electrophysiological recordings with BOLD fMRI in humans. In two neurosurgical patients suffering from epilepsy, which underwent electrophysiological recordings of single unit activity and *local field potentials* (LFPs) in auditory cortex, it was demonstrated that single unit activity can be used to predict BOLD responses in healthy human subjects. During the presentation of natural stimuli, a linear correlation was found between spikes, as recorded from auditory cortex neurons in the two patients and the BOLD signal within the corresponding area of auditory cortex in healthy human subjects that attended to the same stimuli. However, since both high-frequency LFPs and spikes predicted BOLD responses, the authors could not identify one or the other as the driving force underlying the BOLD response.

In order to understand the relative contribution of several types of neural signals to the haemodynamic response, Logothetis and coworkers (2001) compared BOLD signals to LFPs, to single-unit activity and to *multi-unit activity* (MUA), which were recorded simultaneously intracortically in the visual cortex of anaesthetized monkeys (LFPs: 10-130 Hz, MUA: 300-3,000 Hz of the broadband electrode recordings). The researchers found that the BOLD signal indeed directly reflected neural responses elicited during stimulation, possibly linearly for short stimulus presentations. The SNR of haemodynamic responses was thereby found to be relatively low with respect to the associated neuronal responses, suggesting that the extent of such responses could be underestimated in fMRI experiments. The largest magnitude changes were observed in LFPs which, at recording sites characterized by transient responses, were the only signal that significantly correlated with the haemodynamic response. Furthermore, the authors argue that LFPs

yielded a better estimate of BOLD responses than MUA. Logothetis and coworkers (2001) concluded that BOLD responses could represent input and processing of neural information, as reflected by LFPs, rather than the output signal transmitted to other regions of the brain, as reflected by spikes. Thus, fMRI experiments may reveal activations in areas in which no single-unit activity is found in single-unit recordings.

Other animal studies deemphasize the contribution of spikes to the BOLD signal. Spiking activity recorded from primary and higher visual cortex of alert cats only showed a low concordance with the BOLD signal in anaesthetized cats (Kayser *et al.*, 2004). In rat cerebellar cortex, a dissociation of CBF (see above), as measured by *Laser Doppler Flowmetry*, *LDF* and changes in spike rate of the principal output neurons, *Purkinje cells*, *PCs*, as measured by microelectrode recordings, was demonstrated by a series of experiments (Fig. 3) (Lauritzen, 2005). In the following, results from these experiments are shortly summarized based on a review by Lauritzen (2005). Although the overall change in spiking output of *PCs* did not change (due to a reduced number of simple spikes in favour of an enhanced number of complex spikes), CBF increased in response to stimulation of the *cerebellar climbing fibres* (*CF*) (Lauritzen, 2001) (Fig. 3a). When, additionally to *CF* stimulation, the parallel fibre pathway was stimulated, spiking output of Purkinje cells was eliminated, but LFPs as well as CBF increased (Mathiesen *et al.*, 1998) (Fig. 3b). Functional ablation of the cerebral cortex led to a reduction of spike rate in the contralateral cerebellar cortex, but there was only little decrease in CBF; the coupling between synaptic activity and CBF was not impaired (Gold and Lauritzen, 2002) (Fig. 3c). When cerebellar cortex was superfused with agonists of the *γ-aminobutyric acid type A* (*GABA_A*) receptor, inducing tonic synaptic inhibition, spiking output of *PCs* was eliminated within seconds, whereas CBF remained constant; moreover, not only was spiking activity dissociated from CBF, but synaptic activity as well, because the CBF response to *CF* stimulation gradu-

ally diminished with prolonged exposure to the GABA_A receptor agonist, despite an increase in LFP amplitude (Caesar *et al.*, 2003) (Fig. 3d). Disinhibition, in addition to CF stimulation, increased spiking output of PCs two to threefold, but did not lead to a change in CBF; the coupling between excitatory synaptic activity evoked by CF stimulation and CBF was not impaired (Thomsen *et al.*, 2004) (Fig. 3e). In conclusion, these experiments fail to provide clear evidence for either LFPs or spikes underlying changes of the CBF.

Regardless of whether spikes, LFPs or other characteristics of neural activity eventually lead to an increase of CBF and the BOLD response, the relationship between neural activity and the induced vascular changes has to be identified. Since an increased blood flow provides substrates for energy metabolism such as glucose and oxygen, energy consumption is often assumed to be the driving force behind the haemodynamic response. In rodent brain, energy demands for pre-synaptic and postsynaptic activity, the generation of action potentials, the maintenance of membrane potentials and interactions with glia cells have been estimated (Attwell and Laughlin, 2001). It has been suggested that, although areas that show increased neural activity are as well likely to show increased metabolism, CBF and energy utilization might represent different processes which operate in parallel (Attwell and Iadecola, 2002).

Furthermore, it has been suggested that intracellular calcium might be the key that links neural activity to changes in CBF and oxygen consumption (Lauritzen, 2005). Vasodilator substances that mediate increases in CBF, such as potassium, hydrogen, prostaglandins, epoxyeicosatrienoic acid and nitric oxide are dependent on increases in intracellular calcium. Moreover, intracellular calcium is strongly related to oxygen consumption in mitochondria (Gunter *et al.*, 2004). Furthermore, if the amplitude of the vascular signals is controlled by the activation of dendritic calcium channels that are highly sensitive to synaptic inhibition in cerebral pyramidal and cerebellar PCs, but not in interneurons (Goldberg *et al.*, 2003;

Tsay and Yuste, 2004), the haemodynamic response could be controlled by different mechanisms for principal neurons and interneurons (Lauritzen, 2005). Although *synaptic excitation* might have a deeper impact on CBF than *synaptic inhibition*, the latter is also capable of modulating CBF. Inhibitory interneurons can contain vasodilator substances or enzymes that produce them on excitation of those neurons or even vasoconstrictors, further illustrating the complexity and diversity of the action of interneurons upon CBF (Zhang *et al.*, 1991; Southam *et al.*, 1992; Porter *et al.*, 1998; Vaucher *et al.*, 2000; Cauli *et al.*, 2004; Hamel, 2004; Iadecola, 2004).

Although, as illustrated here, it remains still unclear *how BOLD signals* (as dependent on factors such as levels of oxygenated blood, CBF and CBV) and neural activity are related, the *existence* of such a relationship seems indisputable. Future comparisons of *fMRI* responses with data as obtained with other methods will have to clarify the underlying mechanisms.

1.2: fMRI in monkeys

Motivation for fMRI studies in monkeys. Invasive methods, based on electrophysiology, electrochemistry, microdialysis, tract tracing and histology have commonly been used to investigate the functional organization of the monkey brain. These methods are advantageous with respect to fMRI in various aspects.

As a non-invasive method, fMRI has become one of the preferred methods in human brain research. *Why is it worth performing fMRI in the monkey?* Most importantly, fMRI provides a method that can be applied to monkeys and humans and thereby allows for a direct comparison between species. Secondly, as mentioned earlier, a better understanding of the relationship between the classic approaches in the monkey on one hand and monkey fMRI on the other will help to understand the mechanisms underlying the BOLD signal. And finally, fMRI in humans and monkeys might serve as a ‘functional localizer’ for detecting candidate sites throughout the whole brain volume that show stimulus-specific functional responses. These candidate sites can be further investigated by invasive methods in the monkey: either directly at monkey brain sites showing BOLD responses in monkey fMRI experiments or at monkey brain sites that are known or assumed to be homologous to human brain sites showing BOLD responses in human fMRI experiments.

A number of fMRI studies have been performed in *anaesthetized* monkeys (Chen *et al.*, 1996; Chen *et al.*, 1999; Logothetis *et al.*, 1999; Hayashi *et al.*, 1999; Disbrow *et al.*, 2000; Logothetis *et al.*, 2001; Tolia *et al.*, 2001; Rainer *et al.*, 2001; Brewer *et al.*, 2002) or *alert* (or *awake*) monkeys (Dubowitz *et al.*, 1998; Stefanacci *et al.*, 1998; Logothetis *et al.*, 1999; Zhang *et al.*, 2000; Vanduffel *et al.*, 2001; Zhang *et al.*, 2001; Dubowitz *et al.*, 2001a; Dubowitz *et al.*, 2001b; Andersen *et al.*, 2002; Leite *et al.*, 2002; Vanduffel *et al.*, 2002; Nakahara *et al.*, 2002; Fize *et al.*, 2003; Tsao *et al.*, 2003; Denys *et al.*, 2004; Koyama *et al.*, 2004; Pinsk *et al.*, 2004; Pinsk *et al.*, 2005; Sawamura *et al.*, 2005; Nelissen *et al.*, 2005; Baker *et al.*, 2005a; Baker *et al.*, 2005b). These

studies mainly focussed on the *visual system* (Stefanacci *et al.*, 1998; Logothetis *et al.*, 1999; Logothetis *et al.*, 2001; Rainer *et al.*, 2001; Dubowitz *et al.*, 2001a; Dubowitz *et al.*, 2001b; Tsao *et al.*, 2003), especially on *visual field mapping* (Logothetis *et al.*, 1999; Brewer *et al.*, 2002; Fize *et al.*, 2003), on *visual motion processing* (Tolias *et al.*, 2001; Vanduffel *et al.*, 2001; Vanduffel *et al.*, 2002) and, to a lesser extent, they investigated specific functions, including *mapping of somatosensory cortices* (Hayashi *et al.*, 1999), *visually guided saccades* (Koyama *et al.*, 2004; Baker *et al.*, 2005a), *visually guided saccades and smooth pursuit eye movements* (Baker *et al.*, 2005b), *drug-induced activation of the basal ganglia* (Chen *et al.*, 1996; Chen *et al.*, 1999; Zhang *et al.*, 2000; Zhang *et al.*, 2001; Andersen *et al.*, 2002), *shape processing* (Denys *et al.*, 2004; Sawamura *et al.*, 2005), the *representation of face and body parts* (Pinsk *et al.*, 2004; Pinsk *et al.*, 2005) and *cognitive tasks* (Nakahara *et al.*, 2002; Nellissen *et al.*, 2005). In some studies, contrast agents were used to enhance the fMRI response (Vanduffel *et al.*, 2001; Dubowitz *et al.*, 2001a; Leite *et al.*, 2002; Vanduffel *et al.*, 2002; Fize *et al.*, 2003). Some of the listed authors compared monkey fMRI data to human fMRI data, as either part of the same or of independent studies.

fMRI in anaesthetized monkeys. Using anaesthetized animals circumvents a main problem in MR imaging, namely artefacts due to active body movements during scanning. Although a number of studies demonstrated successful application of fMRI in anaesthetized monkeys (see list above), there is a major drawback with using anaesthesia, i.e. anaesthesia can mute BOLD responses in non-human and human subjects (see Stefanacci *et al.*, 1998; Logothetis *et al.*, 1999; Zhang *et al.*, 2000; Andersen *et al.*, 2002; Nakahara *et al.*, 2002). Although BOLD responses under anaesthesia might differentiate from those found in the alert state, improvements in protocols may reduce muting of BOLD responses (Zhang *et al.*, 2000). Logothetis *et al.* (1999) stressed several parameters of critical importance in fMRI of anaesthetized monkeys, including the elimination of artefacts due to passive movements (e.g. caused by respiration and heart beat), regular respiration and

correct positioning of the visual stimulus. In addition, they suggested incorrect anaesthesia, perturbed neural activity or cerebral circulation and hypovolemia as possible reasons for why others might have failed to obtain any BOLD responses in anaesthetized monkeys.

fMRI in alert behaving monkeys. When conducting fMRI in monkeys, a couple of difficulties arise which are either specific to alert monkeys or concern both alert and anaesthetized monkeys. Key points include:

- protection of monkeys from and adaptation of alert monkeys to *auditory noise* (e.g. >120 dB for *MAGNETOM Trio, Siemens*),
- *spatial constraints* within the MR scanner and possibly the need of requiring alert monkeys to sit in a prone position (*'Sphinx' posture*) within the primate chair that is placed inside the bore of the MR scanner,
- the need to *reduce body movements* and, especially, to *restrain the head* of alert monkeys,
- the need to track eye-position for *eye-gaze-control* in alert behaving monkeys,
- the need to *apply rewards* during behavioural tasks in alert behaving monkeys,
- the need to use *non-ferromagnetic material* (e.g. for primate chair, rewarding system etc.) in order to reduce field inhomogeneity and
- *hygienic aspects*, especially when using clinical routine MR scanners that are also in use for humans.

In *section 2.2* I will discuss how these difficulties have been dealt with in the present study.

Sources of image artefacts. Image distortions and various types of artefacts (see also *section 4.1* for detailed discussion) may result from:

- field homogeneity changes caused by *objects of different magnetic susceptibility* brought inside the magnetic field of the MR scanner, e.g. implants, monkey chair, head holder, etc.,
- field homogeneity changes caused by *compounds of different magnetic susceptibil-*

ity present within head, as e.g. different kinds of tissues, bone, air-filled or liquor-filled spaces, etc. and

- body movements.

Body movements inside the scanner are especially problematic, since they not only contribute to field homogeneity distortions by shifting both body and parts of the used components, but also alter the positions of body parts within the MR images.

A *shimming procedure* is applied *before* the start of every MR experiment in order to compensate for the distortions of the magnetic field by all material brought inside the MR scanner. It is, however, extremely difficult to correct for non-linear field distortions that occur *during* MR scanning. In the present study no such correction was applied.

Image position alterations can be compensated after MR scanning by applying a motion correction algorithm that realigns all MR images obtained in a single session. If, however, head movements occur in between excitation pulses and read-out time, a misalignment may result between the retransmitted signal and the encoded spatial position (for details on the MR signal and spatial encoding, see *section 1.1*) that cannot be corrected for by motion correction algorithms.

Restraining the monkey cannot prevent residual movements, as such that are caused by respiration and heart beat, even in the anaesthetized monkeys. Furthermore, muscle tension might result from efforts of alert monkeys to move against the restraining apparatus.

Training alert monkeys to actively remain still during periods of scanning time is much more efficient in preventing body movements than any restraining approach alone (see *section 2.2*).

fMRI in humans vs. monkeys. One important difference for conducting fMRI experiments in humans and monkeys, is absolute brain volume (weight of human brain app. 1.3 kg; weight of monkey brain app. 90 g; Blinkov *et al.*, 1968). Thus,

distortions of the same magnitude affect larger portions of the whole brain volume in monkeys with respect to humans.

In most human fMRI experiments, subjects lie in a horizontal posture (spine, prone or on the side) which is most natural and comfortable to humans and thereby helps to reduce body movements. Such postures are rarely adapted by monkeys. Instead, a vertical sitting posture is preferred, as commonly accommodated for in behavioural experiments by the use of primate chairs. Due to the horizontal orientation of clinical routine scanner bores, such regular primate chairs cannot be used. Instead, in most monkey fMRI studies, the monkey chair is adapted to allow the monkey to sit in a *Sphinx posture*. These postures in between upright sitting and lying prone are also naturally taken by monkeys. – Most importantly, for experiments including the presentation of visual stimuli, the head has to stay in an upright position that allows the monkey to direct the view to visual stimuli that are presented on a screen positioned inside the MR scanner bore, oriented perpendicular to the bore walls.

Most receiver coils used in human fMRI experiments are optimized for head positions that cannot be achieved by a monkey in *Sphinx posture*. We therefore use custom-made coils in the present study that can be freely placed onto the head of the monkey.

Besides carefully padding the head, human subjects otherwise usually lie relatively unrestrained, while the monkey's head is usually restrained by a head holder and body movements are limited by the architecture of the primate chair.

While human subjects often are instructed about tasks that they are required to fulfil during fMRI scanning sessions *immediately before* the beginning of the actual experiment, monkeys have to be *extensively and persistently trained* for such tasks in order to yield reliable and precise performance. Training naïve monkeys can take up to several months.

Furthermore, while human subjects often receive compensation for participation

after experiments, monkeys have to be continuously rewarded *during* experiments, e.g. by the delivery of drops of juice.

While human subjects usually participate in experiments for a rather limited time before getting tired, monkeys can accurately perform tasks repetitive without long breaks for several hours.

1.3: Investigating visual processing and voluntary eye movements with fMRI

Visual field mapping. Visual cortical areas have classically been identified on the basis of differences in anatomical connections, cytoarchitecture, myeloarchitecture, functional properties and retinotopic organization. Using such technique, more than 30 different visual areas have been defined (Felleman and Van Essen, 1991). While borders of the early visual areas are well-established (Daniel and Whitteridge, 1961; Zeki, 1977; Van Essen *et al.*, 1984), defining borders in extrastriate cortex becomes more difficult (Van Essen, 2003).

Here, we focus on systematic stimulation of parts of the visual field as a tool to reveal retinotopic organization and boundaries of early visual areas. Many visual areas exhibit a retinotopic organization, i.e. a preservation of the spatial arrangement of inputs from the retina up to the visual cortex. Cortical retinotopic maps of the visual field are particularly suitable for defining borders of *visual areas V1* through *V4*, since the arrangement of those maps differ between areas.

Since non-invasive functional imaging techniques became available, the retinotopic organization of human visual cortex has been extensively and systematically mapped (Engel *et al.*, 1994; Sereno *et al.*, 1995; DeYoe *et al.*, 1996; Goebel *et al.*, 1998; Kastner *et al.*, 1998; Hadjikhani and Roland, 1998; Wandell, 1999; Grill-Spector *et al.*, 2000; Tootell and Hadjikhani, 2001; Huk *et al.*, 2002; for review on 'primate' visual cortex, see Tootell *et al.*, 2003).

In order to bridge the methodological gap between human fMRI studies and non-human primate data, fMRI studies have to be conducted in the monkey. Initial results on visual mapping in anaesthetized (Logothetis *et al.*, 1999; Brewer *et al.*, 2002) and alert monkeys (Fize *et al.*, 2003) are now available. Fize and coworkers (2003) revealed representations of meridians, as well as the central, peripheral, upper and lower visual field that were suited to serve as reference for the present study. In the present study, it was aimed to reproduce the representations of me-

ridians, as well as a central (albeit sparing the most central part of the fovea) and a peripheral portion of the visual field in order to validate the methods while material, procedures and MR scan parameters etc. were improved.

Optic flow. The visual effect that results from an individual's own movement through the environment is referred to as 'optic flow' (Wurtz and Kandel, 2000). In contrast to the local motion of relatively small-sized objects, in optic flow, the entire visual field moves. As first demonstrated by Gibson (Gibson, 1966) and further extensively investigated by others (Verri *et al.*, 1989; Lappe and Rauschecker, 1993; Wurtz and Kandel, 2000), optic flow is critical for indicating the direction of the observer's movement. Optic flow expands outward (centrifugally) from a point straight ahead in the visual field whenever the observer moves forward with his/her eyes and head directed straight ahead. Conversely, optic flow expands inward (centripetally) when the observer is moving backwards. In addition to provide perceptual cues about heading, optic flow as seen during self-motion provides cues about the structure of the environment (Werkhoven and Koenderink, 1990a; Werkhoven and Koenderink, 1990b; Beusmans, 1993).

Although objects are generally perceived in a holistic way, some of their visual attributes seem to be processed separately (although not exclusively) within different instances within distinct cortical pathways. Motion and depth information are mediated by neural mechanisms in the 'dorsal pathway' (or 'where-pathway'), while form and colour information is mediated by neurons in the 'ventral pathway' (or 'what-pathway') (for review, see Wurtz and Kandel, 2000). Of particular interest in relation to the perception of optic flow fields, which shall be discussed here, is the dorsal pathway. It extends from *V1*, through the *middle temporal visual area (area MT)* and the *medial superior temporal visual area (area MST)*, to the posterior parietal cortex. Area *MST* can be subdivided into two main parts, namely a dorsal part, *MSTd* and a lateral part, *MSTl*. Whereas in the latter neurons can be found that respond to smooth pursuit eye movements, neurons which predomi-

nantly respond to optic flow (Duffy and Wurtz, 1991a), as discussed below, are largely present within *MSTd*.

In the dorsal as well as in the ventral pathway, hierarchies for visual processing lead to a greater abstraction at successive levels: whereas *V1* neurons respond only to local motion of elements of a patterned stimulus, neurons in *area MT* compute global motion of single objects and *area MST* contains neurons that fulfil the requirements necessary for the perception of large-field motion in the visual field (for review, see Wurtz and Kandel, 2000). *MST* neurons (a) respond to optic flow fields that give information about the heading of self-movement relative to the direction of gaze (Saito *et al.*, 1986; Tanaka *et al.*, 1986a; Duffy and Wurtz, 1991b; Orban *et al.*, 1992; Graziano *et al.*, 1994), (b) are sensitive to speed gradients in optic flow that give information about the structure of the environment (Duffy and Wurtz, 1997) and (c) can be altered by vestibular input such that a differentiation becomes possible between optic flow created by self-movement versus movement of large objects (Duffy, 1998; Bremmer *et al.*, 1999). *Area MST* thereby contributes to self-movement perception and visuospatial orientation. Because *areas MT* and *MST* together form the core substrates essential for motion processing, they are often referred to as '*motion complex MT/MST*'.

Motion processing has been investigated in anaesthetized (Tolias *et al.*, 2001) as well as in alert behaving monkeys (Vanduffel *et al.*, 2001; Vanduffel *et al.*, 2002; Orban *et al.*, 2003) using displays of coherently moving visual patterns. The present study aimed at revealing brain areas involved in the processing of optic flow. We were especially interested in whether we would be able to demonstrate BOLD responses within the *cerebellum*. This idea originated from the findings of a clinical study by Thier and co-workers (Thier *et al.*, 1999) on patients suffering from cerebellar lesions that had demonstrated deficits in performing tasks involving motion perception in those patients. Since the critical locus for such lesions remained largely unknown, an animal model was needed in order to study the nature of the

deficit and to help identify a region of the *cerebellum* that may be involved. Within the context of the above-mentioned clinical study, two regions of the cerebellar cortex were likely candidates for representing the origin of the observed visual deficits, because they receive visual input (Waespe *et al.*, 1981; Stein, 1986; Noda and Mikami, 1986; Thielert and Thier, 1993) and hence may contribute to visual disturbances such as deficits in processing of visual motion: one region is the *oculomotor vermis*, including *lobules VI* and *VII*, the other region is the *dorsal paraflocculus*. We had designed a study in which two rhesus monkeys were trained to detect coherent motion in a subset of dots moving within a random dot field (Dietrich *et al.*, 2003). After surgically removing parts of the *cerebellar posterior vermis* in two rhesus monkeys, preliminary results indeed demonstrated deficits in the performance of motion discrimination tasks (Dietrich *et al.*, 2003), suggesting a role of the *cerebellum* in motion processing.

Voluntary eye movements. Foveal vision is most important in most aspects of visual processing and visually guided behaviour (Dow *et al.*, 1981; Van Essen *et al.*, 1984; as cited by Munoz, 2002). The fovea is a small pit located in the macula of the retina. In primates, the layers of the retina within the fovea are spread aside to let light fall directly on the cone photoreceptors. The latter are present within the fovea in high density, thereby providing the highest visual acuity. Primates use two kinds of voluntary eye movements to place and maintain objects of interest on the fovea thereby providing the visual system with time to perform comprehensive image analysis, namely saccadic eye movements (saccades) and smooth pursuit eye movements (SPEMs) (Munoz, 2002; Krauzlis, 2005). These two types have been traditionally assumed to be distinct from one other and driven automatically in response to visual inputs. This traditional view has recently been challenged on the basis of an improved understanding of the underlying neuronal substrates, suggesting that such a separation might be not as strict as previously assumed (Krauzlis, 2005). Furthermore, Krauzlis (2005) reports that saccades and

SPEMs do not simply respond automatically to retinal inputs, but are instead largely regulated by processes of target selection and guided by complex factors such as perception, attention, memory and expectation. In the following, I will review the neural circuitry underlying saccades and SPEMs, which is also summarized in Fig. 4 (for review, see Munoz, 2002; Krauzlis, 2005).

Cortical areas involved in saccadic eye movements include the *lateral intraparietal area*, *LIP*, the *frontal eye field*, *FEF* and the *supplementary eye field*, *SEF*. Cortical areas involved in SPEMs include the *middle temporal area*, *MT* and *medial superior temporal area*, *MST*, as well as subregions of *areas LIP*, *FEF* and *SEF*. Although many cortical areas are involved in both saccades and SPEMs each area contains separate subregions for the two types of eye movements, which are interconnected as a closely matched pair of cortical networks (Tian and Lynch, 1996a; Tian and Lynch, 1996b; as cited in Krauzlis, 2005). The idea of parallel but distinct cortical pathways for saccades and SPEMs is supported by functional imaging studies in humans (Petit and Haxby, 1999; Rosano *et al.*, 2002; as cited in Krauzlis, 2005).

By means of several descending pathways, these cortical areas influence motor-control-related structures in the brain stem, such as the *superior colliculus*, *SC* and premotor nuclei in the *reticular formation*, *PMN*, both directly and indirectly.

Indirect pathways include the *precerebellar pontine nuclei*, *PON*, the eye movement related *oculomotor vermis* (*lobules VI and VII*) and *ventral paraflocculus* of the *cerebellum*, which in turn access the output oculomotor nuclei by projections to the *vestibular nucleus* and brain stem *premotor nuclei*, *PMN*. This cortico-ponto-cerebellar route has long been considered the primary control pathway for SPEMs, but only as a regulatory side loop for saccades.

The oculomotor regions of the *cerebellum* play an important role in supporting the accuracy of voluntary eye movements, by compensating for mechanical constraints and by adapting movements to changing circumstances (Optican and Robinson, 1980; Zee, 1984; Barash *et al.*, 1999; Thier *et al.*, 2002; Optican and Quaia,

2002; Catz *et al.*, 2005). These mechanisms are still not completely understood and are the subject of recent investigations.

Basal ganglia nuclei, such as the *caudate nucleus*, CN and the *substantia nigra pars reticulata*, SNr, act upon eye movement control via the SC. The latter indirect projections are well established for saccades, but have recently also been demonstrated for SPEMs (Cui *et al.*, 2003). Saccades and SPEMs seem to share parts of a brain stem circuitry previously assigned entirely to saccades (Krauzlis, 2005), which, for saccades alone, is still not completely understood (Scudder *et al.*, 2002).

While the monkey oculomotor system has been investigated extensively for decades, investigations of the human oculomotor system benefited greatly from the introduction of non-invasive functional imaging methods. In order to bridge the methodological gap between data obtained for monkeys and humans, we aimed to study visually-guided saccades and SPEMs with fMRI in alert behaving monkeys. Recently two other groups have published monkey fMRI data on saccades (Koyama *et al.*, 2004; Baker *et al.*, 2005a) and both saccades and SPEMs (Baker *et al.*, 2005b).

1. Introduction

2. Material & Methods

2.1: Animals

Subjects. Experiments were conducted with three male rhesus monkeys (*Macaca mulatta*), monkey S, monkey Z and monkey H, app. 12, 5 and 5 years of age, weighing app. 11, 7 and 7 kg, respectively.

They were maintained on standard laboratory diet given *ad libitum* and received their daily fluid requirements as rewards during training and experiments. Additionally to that, monkeys received fruits and water *ad libitum* after each fMRI experiment and on weekends.

Monkey S had been utilised for electrophysiological and psychophysical experiments years before fMRI experiments. During app. 1 $\frac{3}{4}$ years monkey S was trained and utilised for data collection in fMRI experiments on a regular basis. FMRI experiments took place maximally once per week, on altogether 37 days.

Monkey Z had to be excluded from the study early during the initial training phase, because the re-implantation of a head post became finally impossible, following repetitive breakage of head-posts (Fig. 5E) (for further details, see section 2.2).

Monkey H is currently still in training phase, being adapted to routine procedures.

Anaesthesia, surgical procedures and implants. All experimental procedures fully complied with the *NIH Guide for Care and Use of Laboratory Animals* and with the guidelines of the local ethic committee. I will first give an overview about all implantations and de-implantations that the monkeys received, before going into details of anaesthesia and surgical procedures in general. Finally, I will describe the procedures used to implant different types of head-posts in particular.

App. 6 years before the beginning of fMRI experiments, monkey S was implanted with a standard head-post, allowing the painless restraint of the head (such as shown in Fig. 5D) and a recording chamber for electrophysiological ex-

periments and scleral eye coils (for eye position tracking: Robinson, 1963). Subsequently, implants were reconfigured and another eye coil was implanted. App. 2 years after the first surgical intervention, all implants were removed due to an infection resulting in osteomyelitis below the area of the head-post implant. During the following 4 years, bone re-grew in the previously affected area, as determined by structural MRI. Shortly before the beginning of the fMRI experiments, monkey S was newly implanted with a standard head-post. During training sessions, the head-post broke (similar to breakage #2 in monkey Z in Fig. 5E) and had to be repaired. App. 2 years after implantation for fMRI experiments, the area below the head post got infected, making it necessary to remove the head-post one more time (for further description see *section 2.2*). Monkey S is currently recovering and not involved in experiments. – Shortly after monkey S had to be withdrawn from fMRI experiments, monkey Z was implanted with a standard head-post. This head-post broke during initial training sessions – while the head post was used for head restraining – due to strong movements of the monkey against the head restraining apparatus. After being repaired the head-post broke again in subsequent trainings sessions. The head post was again repaired but broke one more time during training sessions. The last breakage removed the entire implant with parts of the skull (Fig. 5E) (for detailed description, see *section 2.2*). After receiving medical care, monkey Z was retired from experiments. – App. at the time, monkey Z was implanted with the standard head-post, monkey H underwent surgical procedures for implanting basement implants for a newly developed *three-point head restraining system (TPHRS)* (Fig. 5F) (for detailed description, see *section 2.2*). Although monkey H was trained for upcoming fMRI experiments the implants were not yet used for head restraining. Approximately three months later, the TPHRS was completed. One of the implanted basement implants had to be replaced due to a local infection below the implant. When the head was restrained in training sessions, various elements of the TPHRS broke and needed to be re-

paired (Fig. 5F).

Surgeries were carried out using adapted standard protocols (Thier and Erickson, 1992). In short, animals were pre-anaesthetized using ketamine hydrochloride, app. 10 mg/kg body mass (*Ketamin-Ratiopharm*[®], *Ratiopharm*, Germany) and xylazinehydrochloride, app. 6-10 mg/kg body mass (*Rompun*[®], *Bayer*, Germany). The latter also acted as sedative, analgesic, anaesthetic and muscle relaxant during the pre-anaesthesia-period. In order to reduce salivation and to prevent vagal reflexes, atropine sulfate, app. 0.03-0.05 mg/kg body mass (*Atropinsulfat B. Braun*[®], *B. Braun*, Germany), was administered app. 20 minutes before the initiation of pre-anaesthesia. Implantation manoeuvres were conducted under intubation anaesthesia, using app. 0.3-1% isoflurane, app. 70% nitrous oxide and app. 30% oxygen (monkey S) or app. 0.2-0.3% isoflurane, app. 0.5-1.5 µg/kg-min remifentanyl hydrochloride (*Ultiva*[®], *Abbott Laboratories*), normal air and <30% oxygen (monkey Z and monkey H). Heart rate, artificial respiration, body temperature, blood pressure, blood oxygen and carbon dioxide saturation and reflexes were continuously monitored throughout the duration of the surgical procedures. Post-operative analgesics and antibiotics were administered as needed and animals were allowed to recover fully before their training was resumed. – During structural MR imaging, the monkeys were anaesthetized using ketamine hydrochloride and xylazinehydrochloride only.

Standard head-posts, made of polyetheretherketone (PEEK), were placed in the middle of the sagittal suture, behind the frontal suture. Implants in monkey S and monkey Z were embedded and encased in a smoothed layer of dental acrylic cement, based on methacrylate copolymers (*Paladur*[®], *Heraeus Kulzer*, Germany), anchored by up to 12 screws made from circonoxid (ceramic screws, model 'SA06', *Thomas Recording*, Germany). The dental acrylic basement covered app. 25 cm² of bone surface and were surrounded with skin. For the intended fMRI experiments, it was important to choose dental acrylic cement that would not contain any me-

tallic dyes that would distort the magnetic field homogeneity of the MR scanner. In monkey H, three PEEK-made basement implants of the *TPHRS*, anatomically adapted based on structural MR scans, were placed on the skull in a triangular fashion (one more rostral in the middle, two more caudal and temporal, right and left) and each fixed with three ceramic screws that were covered slightly by dental acrylic cement to smooth implant surfaces. Screws, made of PEEK, were screwed into the basement implants. The scalp was then closed completely over the skull and all implants, allowing healing and partly regrowing of bone around the implants. Unlike the method used for the implantation of standard head-posts this method does not leave an open wound around the implants that facilitates contamination and entry of germs. After app. three months, small cuts were made at positions of the two posterior screws under ketamine hydrochloride and xylazine hydrochloride anaesthesia. The latter were then replaced by screws with a spherical head that remained outside the scalp and constituted the three 'miniature head posts' as part of the *TPHRS* (Fig. 5F) (for detailed description, see *section 2.2*). The anterior implant had to be replaced due to an infection. The replaced miniature head post was encased in a smoothed layer of dental acrylic cement anchored by six ceramic screws.

2.2: Experimental procedures

Before the beginning of the training, each monkey was trained to voluntarily enter an especially custom-made primate chair (Fig. 5A) from the home cage. Afterwards, the monkey had to place the head through the front opening of the primate chair. Inside the primate chair, the monkey was transported either to the place where the training took place or – with the primate chair inside a wooden container – to the MR scanner, where fMRI experiments took place. Shortly before the beginning of training or experiments, the monkey's head was restrained. It was made sure that the monkey was relaxed and cooperative, in home, transport, training site and MR scanner environment.

Experimental environment. Training and maintenance of learned behaviour was achieved with help of a specially constructed *dummy scanner* made of plastic and wooden elements that mimicked the MR scanner magnet bore. Inside the dummy scanner bore, within the primate chair, the monkey was adapted

- to stay calm in a *prone position*, within the *spatial limitations* of the primate chair,
- to head restrain,
- to receive *rewards* (e.g. drops of water) through a tube guided to the monkey's snout,
- to simulated MR scanning *noise* at app. similar sound pressure levels present during MR scanning, presented via ear phones (alternatively to wear surface coils, see below),
- to wear *ear-plugs* for protection from noise present during MR scanning (standard wax ear-plugs (*Ohropax*[®], *Ohropax GmbH*, Germany) or special addition vulcanizing ear impression silicone (*Otoform A/k*, *Dreve Otoplastik GmbH*, Germany) that could be formed in order to fit anatomically into the ear canals),
- to wear a pair of ear-phone-like elements containing two *receiver-surface-coils* (instead of speakers) that could be reproducibly placed onto the head. These coils were used for image acquisition during MR scanning (Fig. 5B) (see *section*

2.4).

- Fig. 5E schematically shows the experimental setup with the monkey inside the primate chair within the MR scanner.
- *Head position.* The monkey was situated within the primate chair inside the dummy bore or magnet bore of the MR scanner with the head app. in the centre (due to the Sphinx posture of the monkey, the head was slightly shifted upwards from the centre position).
- *Head orientation.* During training, as well as during MR scanning, the head was oriented, so that the monkey would look in direction parallel to the bore onto a back-projection-screen. The screen was placed inside the bore at a distance of 30 cm to the monkey's eyes.
- *Stimulus projection.* The projection area covered 36×48 cm or 11.25×30° of visual angle, with 600×800 pixels, each pixel representing 0.038×0.019 °/pixel, vertically and horizontally, respectively. The projector (for training: NEC VT560; for fMRI scanning: NEC GT950, NEC, Japan) back-projected directly onto the screen of the dummy bore and via a mirror onto the screen of the MR scanner bore. The bore of the MR scanner in some sessions was lined with black paper in order to reduce reflections of projected light onto the walls.
- *Eye-position-tracking.* The left eye of the monkey was monitored by a miniature infrared (IR) CMOS-camera (*S/W-Kamera Modul 1, Conrad-Electronic GmbH, Germany*), resolution, 352×288 pixels, dimension, 21×21×15 mm (Fig. 5C) that, together with an illuminating IR-diode, was mounted app. 4 cm in front of the left eye of the monkey. The pupil of the eye was detected and used for eye-gaze-tracking by a custom-made eye-position-tracking-software based on the video image of the monkey's eye; spatial resolution, app. 0.5° visual angle, temporal resolution, 50 Hz.
- *Connections.* Cables from the surface coils had to be connected to a pre-amplifier interface, which was lying on top or at the side of the primate chair.

The preamplifier interface, in turn, led to the MR scanner connections on the ‘patient table’. Cables from the eye-position-tracking-device as well as the reward application tube had to be guided along and out of the scanner bore. If the cable of the eye-position-tracking device was not guided straight and at a distance parallel to the walls of the bore, image artefacts were likely to occur. To prevent those artefacts it was necessary to use pair-wise finished wires and to avoid loops in the cable. Visual signals were delivered to projectors via analogue VGA-cables. In fMRI experiments, the projector was placed inside the magnet room.

- *Control.* Control computers running custom-made software for the interactive coordination of stimulus presentation, behavioural control, reward application, eye-position-information and MR-scanner-pulse-trigger-signals (simulated in training sessions) were situated beside the dummy scanner or – in MR experiments – in the control room, beside the MR scanner control console, outside the MR scanning room. Software used is altogether termed ‘*control software*’ in the following.

Primate chair and all experimental equipment used (except the IR-camera, camera cables and LED) were made out of non-ferromagnetic material.

The MR scanner environment, including bore, control elements and all parts which had possibly been in contact with the monkey, as well as the floors were cleaned and disinfected after each experiment.

Body movements. As already mentioned in the introduction (see *section 1.2*), body movements are very problematic in MR experiments because they represent a major source of image artefacts (see *section 4.1*). Body movements can be limited by restraining the head and reducing the space within the primate chair, but it is not possible to prevent them completely. This represents a common problem in fMRI studies on alert behaving monkeys. Even in human fMRI experiments when subjects try not to move, involuntary movements occur. With the help of operant

conditioning (see below), monkeys can be trained to actively remain motionless. Still, head movements occur e.g. when the monkey licks during the applications of juice or water rewards.

The use of standard head-posts reduced head motion in the present study, but the force applied to the head-posts by the monkeys lead them to break several times. Fig. 5E shows the standard head-post implant with lines of three breakages in monkey Z. In monkey S, the head-post broke as well, similar to breakage #2 in monkey Z in Fig. 5E. Possible reasons for those breakages will be discussed in the following. The prone position might have enabled the monkeys to direct more force against the head restraining apparatus than they usually can when sitting upright with the head fixed, as in conventional primate chairs. Additionally to the involvement of neck musculature, monkeys also use their hands and feet to push against the primate chair walls. 'Nodding' movements could possibly have been prevented by using a chin rest, in which case it has to be assured that the monkeys can comfortably swallow and receive water rewards. Aggressive, forceful movements against the head restraining apparatus or primate chair represent an exception in the behavioural repertoire of the monkeys after they have been effectively adapted to head restraining, primate chair, environment and experimental procedures. In this sense, monkey Z was probably not adapted well enough. A longer adaptation phase could have possibly prevented the monkey from breaking the implant.

The third breakage in monkey Z removed the entire implant as well as most of the screws, together with parts of the skull. This probably happened due to the fact that the implant was limited to a relatively confined area of the skull which was not only 'perforated' by the holes of the screws but, furthermore, might not have reached its final thickness and strength in the relatively young animal and was consequently destabilized. The reason for keeping the implant as small as possible was to reduce image artefacts that could have resulted from implanted material

during MR scanning.

As described before (see *section 2.1*), monkey H, unlike monkey S and monkey Z, was not implanted with a standard head-post, but rather with three miniature head-posts – as part of a newly developed *TPHRS* (Fig. 5F). Other than with the standard head-posts, no force was applied to parts of the *TPHRS* implant after surgery and before complete healing and regrowth of bone during a period of app. three months. Until completion of the *TPHRS*, the monkey was trained by using a ‘helmet’ for head restraining. The helmet was fixed to the primate chair and enclosed parts of the head, leaving openings for eyes, nose and snout and mimicked the function of a head restraining apparatus. It was not as effective in preventing head movements as head-posts are, but it allowed initial training and eye-position-tracking. In initial training sessions, with the head restrained by the completed *TPHRS*, parts of the latter broke (Fig. 5F) and had to be repaired. It still has to be evaluated whether the *TPHRS* approach contributes to more stability for head restraining than the standard head-post approach.

Training and behavioural control. Training and maintenance of learned behaviour was achieved by operant conditioning with positive reinforcement, applying drops of water as reward for fulfilling requirements of tasks. All paradigms used required the monkey to direct eye gaze or to maintain eye gaze at visual targets that were projected onto the screen (see *section 2.3*). In all experiments, behavioural control was achieved by *eye-gaze-control*. As mentioned above, the pupil of the left monkey’s eye was detected and used to determine the direction of eye gaze via the video image of the IR-camera. The *control software* was used to define a circumscribed squared area around visual targets that covered 6-9° of visual angle. Such areas included a tolerance range of a few degrees around visual targets, termed *tolerance windows* in the following. Once eye gaze was detected to be inside the tolerance window, a particular experiment was started that either required the monkey to stay with eye gaze on the target or to direct eye gaze either

together with moving targets or between subsequently appearing targets (for details see *section 2.3*).

Whenever the oculomotor requirements of tasks were not met – i.e. whenever the monkey’s eye gaze left the tolerance window – the current trial was aborted and repeated only, when eye gaze returned into the tolerance window. Operant conditioning was achieved by applying rewards depending on the oculomotor performance of the monkey: rewards were given only in periods when the monkey fulfilled oculomotor requirements (for detailed description of reward applications, see *section 2.3*); if trials had to be aborted because those requirements were not met, reward application stopped immediately; when requirements were met again, trials were repeated and application of rewards for the performance of appropriate oculomotor behaviour was continued. In order to exclude interruptions of eye gaze detection by eye blinks, short time periods were provided, in which eye gaze was allowed to be absent from the tolerance window. In cases that required the monkey to make saccades, eye gaze control was shortly deactivated, allowing eye gaze being moved from the previously defined tolerance window towards the newly defined one. These inactivation times were also useful to account for instances at which pupil detection did not work properly, as e.g. at extreme eye positions relatively to the IR-camera. Even if positioning of the IR-camera allowed pupil detection at all present eye positions, eye gaze detection could be disrupted by sporadic occurring artefacts present inside the video image of the IR-camera, which were caused by the application of magnetic field gradients during MR scanning sessions (see *Fig. 7*). These interferences were present at varying degree between fMRI experiments, suggesting that positioning of components such as primate chair, IR-camera, cables etc. slightly varied. It was also possible that video image artefacts were absent in the beginning of a particular scanning session and occurred spontaneously during MR scanning. Thus, eye-gaze-control had to be inactivated manually at some instances during fMRI experiments (see

section 4.1).

Moreover, strong movements of the monkey could shift the IR-camera-position in front of the monkeys. Following such shifts and depending on its extent, the experimenter had to either stop experiments and reconfigure IR-camera-position or recalibrate the eye-position-tracking system.

Apart from using eye-gaze-control in order to assure fulfilment of task requirements, eye-gaze-control was also used to indirectly control head movements, in other words, to train the monkey to maintain the head motionless. Whenever the monkey made head-movements that shifted the monitored eye outside the tolerance window, the trial was aborted. The experimenter had to observe the video image of the monkey's eye in order to differentiate between eye gaze errors and head movements. The experimenter could detect differences between eye gaze errors and head movements by attending to the area around the monkey's eye that was still visible in the video image and that showed parts of the head.

In order to train monkeys to actively remain motionless it would be necessary to provide monkeys with feedback information about movements of various body parts, including the head. While the monkey licks water rewards, snout, tongue and yaw move. In recent training sessions, we tested a method that could not yet be applied successfully in fMRI experiments. This method aimed at using a *movement-sensor* as another tool for behavioural control by providing the monkey with feedback information about body movements. We began by detecting chin movements of the monkey that were likely to occur whenever the monkey moved the head, e.g. during receiving rewards. For that purpose, we used an air-filled cushion that delivered air pressure changes via flexible tube outside the bore of the dummy scanner. These air pressure changes were transformed into electrical signals, which, in turn, were evaluated by the *control software* and used for both providing the monkey with feedback information about movements and controlling behaviour. Similar to the method used for eye-gaze-control, trials were

aborted (and reward delivery was discontinued) whenever chin movements were detected. Monkey S was retired from experiments, before training of using the movement-sensor was successfully finished. However, the use of such movement sensors seems to be a promising tool in reducing body movements of the monkey. Their use would not only be feasible in training sessions, but also in fMRI experiments, since cushion and tube are made out of non-metallic material. All electronic parts can be placed outside the magnet room.

The total time the monkey performed in training or fMRI experiments depended on the motivation of the monkey to participate in experiments in order to receive water rewards and on the actual amount of water drunken. Typically, the monkey participated app. two hours in fMRI experiments and drank app. 300 ml of water. Rewards were periodically delivered throughout 30-second-time-blocks. Depending on correct performance throughout these blocks, an additional reward was given (see *section 2.3*). Each reward application delivered a few drops of water to the monkey by opening a valve of a water reservoir that delivered water via a flexible tube to the monkey (Fig. 5G). After scanning, fruits were given to the monkey for positive association with fMRI experiments.

2.3: Behavioural paradigms

Visual field mapping paradigm. During fixation of a white fixation spot (diameter 25 minutes of arc) in the middle of the screen, one of four visual field mapping stimuli was presented to the monkey. Each of those stimuli consisted of red and green polar-shaped checkerboard patterns flickering in counterphase at 8.6 Hz. Flickering stimuli have been reported to represent strong visual stimuli; the optimal temporal frequency for driving cortical neurons has been reported as app. 4 Hz (Fox *et al.*, 1987). Field sizes were scaled linearly at a distance from the center of the screen toward the periphery and only roughly accounted for the retinal magnification factor (LeVay *et al.*, 1975; Tootell *et al.*, 1982; Sereno *et al.*, 1995). Scaling was equal for horizontal and vertical orientation, although it is controversially discussed whether the retinal magnification factor is isotropic along horizontal and vertical meridians (Sakitt, 1982; Letelier and Varela, 1984). Areas were shaped as follows:

(A) Two horizontally oriented wedges (sectors), covering 10 deg of visual angle, checkerboard field size, 5° tangential and 0.2° radial in the inner row and additional, 0.1° per row from inside to outside. Wedges covered 30° horizontally (Fig. 6A).

(B) Two vertically oriented wedges with the same stimulus parameters as in (A), except the orientation and limits of the wedges that covered 11.25° vertically (Fig. 6B).

(C) Small ring, centred in the middle of the screen, inner diameter, 2°, outer diameter, 3.4°, checkerboard field size, 5° tangential and 0.7° radial (2 rows) (Fig. 6C).

(D) Large ring, centred in the middle of the screen, inner diameter, 18°, outer diameter, 21.9°, checkerboard field size, 5° tangential and 1.9° radial in inner row and 2° in the second row (2 rows) (Fig. 6D).

Optic flow paradigm. During fixation of a white fixation spot (diameter 50

minutes of arc) in the middle of the screen, the monkey viewed 175 white randomly placed dots, each measuring 10 minutes of arc, which moved centrifugally from the centre of the screen with a velocity of 5° per second. At a time, only one hemifield was shown (Fig. 6E and 6F). Each dot was introduced to (and started moving from) the display at a randomly selected position within a circular aperture of 60° and had a lifetime of 200 ms, after which it disappeared. After its lifetime, it reappeared at (and started moving from) a new, randomly selected position.

Saccadic eye movement paradigm. The monkey had to repeatedly perform 15° saccades between two white spots (diameter 25 minutes of arc) lying in the horizontal line, each at 7.5° distance from the centre of the screen (Fig. 6G). At a time, only one of the two targets was displayed. At a rate of 1.5 Hz, one target was removed from the display and simultaneously the other one was shown. The monkey was asked to immediately perform a saccade towards a target, once it was introduced and maintain fixation throughout the time it was shown.

Smooth pursuit eye movement paradigm. The monkey had to repeatedly pursue a white spot (diameter 25 minutes of arc) that moved continuously in a sinusoidal fashion, at a frequency of 0.3 Hz between two positions within the horizontal line, each at 7.5° distance from the centre of the screen (Fig. 6G).

Implementation of the behavioural paradigms in the fMRI design. Oculomotor stimuli were presented in an epoch-related ‘blocked’ design, i.e. stimuli were presented in blocks that were interleaved with blocks of a ‘baseline condition’. Baseline conditions required pure fixation of a white fixation spot (diameter 25 minutes of arc) in the middle of the screen (Fig. 6H). In the visual field mapping paradigm and in the optic flow paradigm, each block contained a condition that could both serve as stimulus of interest and as baseline condition. All stimulus contrasts are listed in Table 1. Duration was 30 seconds for all block types.

Starting time of blocks of visual stimulation was triggered by pulses delivered by

the MR scanner, indicating times of image acquisition.

Reward was given in constant intervals of 2-5 seconds during each block and only interrupted when the oculomotor requirements were not met (see *section 2.2*).

When performance was $\frac{2}{3}$ error-free within a block, a large reward was additionally given at the end of each block.

2.4: Image acquisition

For BOLD imaging, we used a 3 T MRI scanner (*MAGNETOM Trio, Siemens, Germany*) and custom-made *linear polarized receiver-surface-coils (Stark Contrast, Germany)* (Fig. 5B) for functional and structural imaging and a standard knee coil (*Siemens, Germany*) for high-resolution structural imaging.

Structural MR imaging. High-resolution T1-weighted spin-echo images were obtained, averaged over several repetitions in order to improve SAR. Averaging and a high resolution both require considerable scanning time – app. 30 minutes in the present study (for reference: Logothetis and coworkers (1999) scanned and averaged 2 hours and 40 minutes in isoflurane/fentanyl anaesthetized monkey). It was necessary to anaesthetize (see *section 2.1*) the monkey to reduce body movements throughout scanning time as much as possible. Image acquisition parameters used were:

In-plane resolution, 0.625×0.625 mm, slice thickness, 0.48 mm (gapless); base resolution 256×256; 201 slices; repetition time, TR, 1940 ms; echo time, TE, 2.6 ms; flip angle, FA, 8 degrees; effective bandwidth, 200 Hz/pixel, number of total averages, 5.

Functional MR imaging. For functional imaging, *T2**-weighted *gradient-echo, GE, echo planar imaging, EPI*, was carried out. Two different sets of image acquisition parameters were used, F1 (used for visual field mapping paradigm and optic flow paradigm) and F2 (used for saccade paradigm and SPEM paradigm). These parameters were:

(F1) *In-plane resolution, 2×2 mm and slice thickness, 2 mm (gapless); base resolution 64×64; 25 contiguous slices, acquired in descending order and tilted coronal>transversal by 30° or 34° or 38°; TR, 2000 ms; TE, 35 ms; FA, 90°; effective bandwidth, 1955 Hz/pixel.*

(F2) *In-plane resolution, 1.3×1.3 mm or 1.4×1.4 mm and slice thickness, 1.9 mm (gapless); base resolution 128×88; 21 contiguous slices, acquired in ascending order and*

tilted coronal>transversal by 5° or 15° or 20° ; *TR*, 2000 ms; *TE*, 28 ms or 30 ms; *FA*, 70° ; *effective bandwidth*, 1220 or 1345 Hz/pixel.

The number of obtained images in single sessions varied between app. 150 and 1400, depending on the performance of the monkey.

2.5: Functional image analysis

Standard procedures using software package ‘SPM2’. Software package *SPM2* (<http://www.fil.ion.ucl.ac.uk/spm/software/spm2>) and custom-made *MATLAB* (*Mathworks*) software was used for data analysis. *SPM2* standard procedures (Friston, 2003) are illustrated schematically in Fig. 8. If not declared otherwise, *SPM2* default values were used in processing steps.

- *Motion correction.* Images of one series were spatially aligned with each other in order to reduce unwanted variance components in the voxel time-series induced by movement among a series of scans. This was achieved by a motion correction algorithm, using a six-parameter- (three translational and three rotational parameters, x , y , z , pitch, yaw and roll, respectively) linear-rigid-body-transformation.
- *Slice time correction.* The slice-by-slice-acquisition of images covering the entire brain is a time consuming process (see *section 1.1*). For statistical analysis, the time of the middle slice of the entire slice series is assumed to be the time of the image acquisition of the entire slice series.
- *Co-registration.* Images were spatially co-registered with structural images in a manual procedure (see below).
- *Spatial smoothing.* Images were spatially smoothed with a Gaussian kernel (full width at half maximum $5 \times 5 \times 5$ mm (F1) or $3 \times 3 \times 5$ mm (F2)).
- *Voxel-wise statistical analysis.* The experimental design and the nature of hypothesis testing was defined in the design matrix (Fig. 8), in which, for each scanning session, image scans are represented in rows and stimulus function (information about onset and duration of stimuli) and regressors in columns. In the present study, the six realignment parameters were used as covariates of no interest. Parameters were estimated using the *general linear model*. Specific profiles within these parameters were tested using a linear compound or contrast with the T -statistic. The resulting statistical map constitutes a *statistic paramet-*

ric map, SPM.

Correction for multiple comparisons. Significance of the resulting statistical parametric maps, SPMs, was assessed at a criterion of a single-voxel threshold of $p > 0.05$, corrected for multiple comparisons across the brain volume, examined by using the *False Discovery Rate, FDR* (Genovese *et al.*, 2002). *FDR* is an innovative approach to the multiple comparisons problem. While the *Familywise Error, FWE* (Nichols and Hayasaka, 2003) – the standard measure of *Type I Errors* in multiple testing, the chance of any false positives – is used by traditional methods such as *Bonferroni* or *Random Field* methods, *FDR* methods have weak control of *Familywise Type I Error*. Instead of controlling the *chance* of any false positives, the *FDR* controls the *expected proportion* of false positives among suprathreshold voxels. Because a *FDR* threshold is determined from the observed p-value distribution, it is adaptive to the amount of signal in the data. *FDR* is more sensitive than traditional methods because it uses a more lenient metric for false positives.

Selection and pooling. On 38 experimental days, more than 55,000 functional images were obtained, including early scanning sessions in which various parameter settings were tested and many improvements had to still be made. For final statistical analysis, functional images of several scanning sessions were pooled (see Table 1). Criteria for pooling were equal image acquisition parameters (F1 vs. F2) and overall quality of functional images. Quality levels could be assessed by various aspects, including examining the degree of motion correction that had to be applied to the functional data set of each session. Series containing movements that severely affected data quality were rejected. Series that included images containing a high degree of artefacts were also excluded. Pooling of sessions for each paradigm improves statistical power by increasing the overall number of images (sample size). For pooling, mean images resulting from the motion correction for each session (see above) were aligned with each other using standard algorithms of the software package *SPM2*.

2.6: Superimposition, projection and evaluation of SPMs

Projection of SPMs onto structural images. Statistical parametric maps (SPMs) resulting from functional image analysis (see *section 2.5*) were superimposed onto structural (reference) images using the software package *SPM2*. For that purpose, landmark structures, such as the *corpus callosum*, were used to manually co-register the functional brain volume onto the structural brain volume. Standard co-registration algorithms implemented in the software package *SPM2* were not suitable here, because a proper alignment was prevented by distortions of the functional brain volume at various sites relative to the structural brain volume. Manual co-registration could not correct those distortions but it assured the proper alignment of the majority of sites which were undistorted or less affected. This manual approach introduces some degree of subjectivity, by requiring the experimenter to identify landmark structures within the brain volumes of both the functional and the structural data sets and by choosing six parameters (three translational and three rotational parameters, x , y , z , pitch, yaw and roll, respectively) for orienting the functional brain volume to meet the orientation of the structural brain volume.

The structural brain volume itself was transformed into *monkey bicomissural space* (Hayashi *et al.*, 1999; Nakahara *et al.*, 2002), in which the origin lies in the *anterior commissure* and both the *anterior commissure* and the *posterior commissure* lie in a transversal and the inter-hemispheric, sagittal plane. After manual co-registration of functional and structural images and superimposition of SPMs onto structural images, anatomical landmarks of the structural images (such as gyri and sulci of the cerebral cortex) could be used to identify sites of BOLD responses. Giving coordinates in *monkey bicomissural space* has the potential to become a standard used by various laboratories (Hayashi *et al.*, 1999; Nakahara *et al.*, 2002; Koyama *et al.*, 2004; Baker *et al.*, 2005a; Baker *et al.*, 2005b) thereby facilitating inter-subject and inter-study comparisons. Nevertheless, inter-subject variability in gross anatomy,

including brain size, cortex folding etc., as well as improper transformations might still lead to a considerable difference in coordinates given for identified brain structures across subjects and studies.

Projection of SPMs onto cortical surface reconstruction models. In contrast to volume-based identification and comparison of brain structures, a localization of cortical sites, based on cortical surface, is well suited to provide a common standard for inter-subject comparisons. For this purpose, the cortical surface was reconstructed from structural images for each hemisphere, using 3D borders between grey and white mater (Fig. 9A). Co-registered SPMs were then projected onto the cortical surface.

Surface reconstruction procedures, projections and morphs (see below) were done with the *Caret* (*Computerized Anatomical Reconstruction and Editing Toolkit*) software package, version 5.3 (John Harwell, Heather Drury, Donna Hanlon and David Van Essen; <http://brainmap.wustl.edu/caret.html>), using standard procedures (Van Essen *et al.*, 2001).

Beside the naturally folded 'fiducial' 3D cortical surface reconstruction, the model could be further transformed, including virtual inflation and flattening of each hemisphere separately (Fig. 9B). For this purpose, parts of the medial wall had to be removed virtually and virtual cuts had to be made. The cortical surface was projected onto a plane and corrected for distortions. Such a flattened cortical reconstruction then represents the surface of a complete hemisphere, except parts of the medial wall. We used flattened cortex-surface reconstructions in addition to structural brain slices, in order to visualize and evaluate SPMs (superimposed on slices and projected onto reconstructions).

Evaluation of SPMs by co-registration with rhesus monkey atlas.

It has been suggested that the hierarchy of cortical areas can be delineated using anatomical criteria, i.e. landmarks of the cortical surface such as *gyri* and *sulci* (Rockland and Pandya, 1979; Friedman, 1983; Maunsell and Van Essen, 1983; Van

Essen, 1985). Under this assumption, it becomes feasible to map data obtained by any method that reports functional sites in relation to anatomical brain structures onto a common cortical template. This way, Felleman and Van Essen (1991) mapped data from studies of anatomical connections, cytoarchitecture, myeloarchitecture, functional properties, retinotopic organization etc. onto a common cortical surface reconstruction, a standard rhesus monkey template (F99UA1, <http://brainmap.wustl.edu:8081/sums/index.jsp>), subsequently serving as an atlas.

We used a surface-based co-registration procedure to morph the standard rhesus monkey template (F99UA1) with superimposed atlas (Felleman & Van Essen, 1991) to the individual's (monkey S) cortical surface (Fig. 10). Borders of all identified cortical areas of the atlas were then superimposed onto the individual's morphed flattened cortical surface reconstruction (Fig. 11). SPMs that are projected onto these flattened cortical surface reconstructions can then be analysed with respect to the atlas area borders that are derived from a multitude of studies (Felleman and Van Essen, 1991).

The standard rhesus monkey template with superimposed atlas provides an ideal common standard for inter-subject comparison, whenever group data of several subjects have to be evaluated or when fMRI data of different studies have to be compared (cortical surface reconstructions of all subjects morphed to template with atlas). The evaluation of BOLD responses with the help of the surface atlas represents an advantageous alternative or amendment to the identification of brain areas, using conventional brain slice atlases.

Figures & Tables

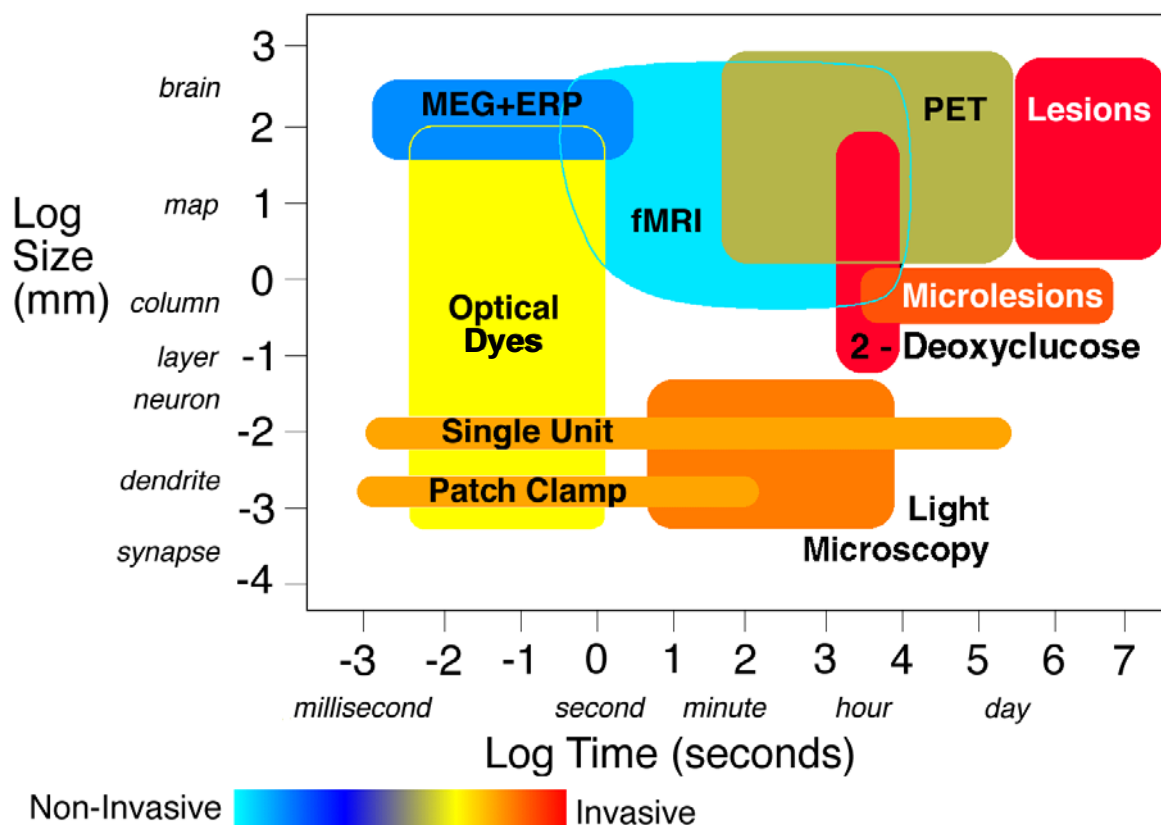


Fig. 1: Comparisons of spatiotemporal characteristics and invasiveness among methods commonly used in neuroscience research (adapted from Churchland & Sejnowski (1997) and Rosenbaum *et al.* (1991)).

Diagram showing spatial resolution (ordinate, log-scaled) over temporal resolution (abscissa, log-scaled) as well as invasiveness (colour-scale shown below diagram) of commonly used methods in neuroscience research. Advantages of fMRI are the fact that it represents a non-invasive method and that it has a relatively high spatiotemporal resolution with respect to various other methods.

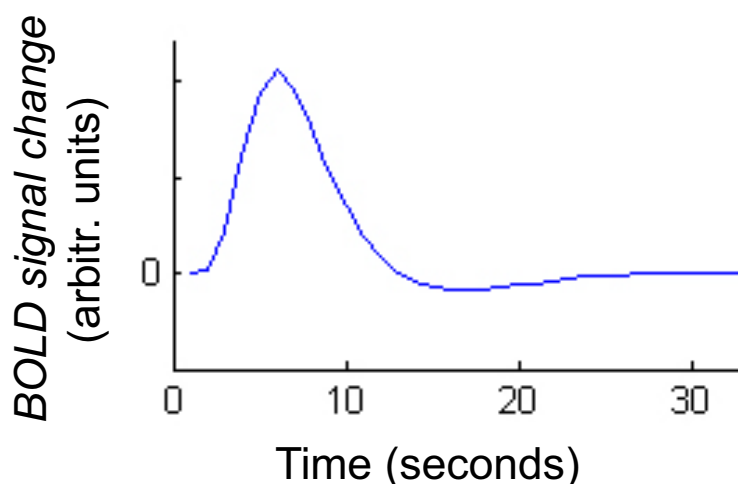


Fig. 2: Canonical haemodynamic response function (HRF), used by SPM2. Time course of the BOLD signal change to a brief stimulus.

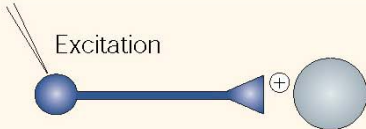
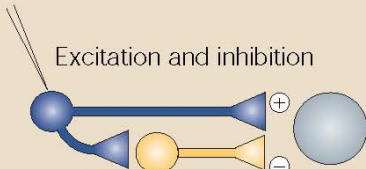
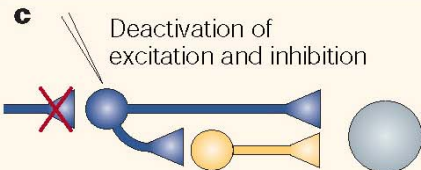
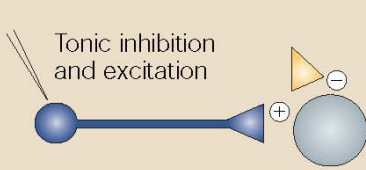
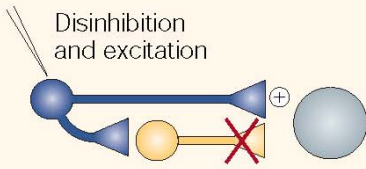
Neuronal network		Spiking output	Blood flow	Σ LFP–blood flow relationship
Intervention	Synaptic input			
a	Excitation 	Unchanged	Rise in CBF in response to stimulation	Linear and nonlinear
b	Excitation and inhibition 	Decreased	Rise in CBF in response to stimulation	Nonlinear
c	Deactivation of excitation and inhibition 	Decreased	Decrease or no change of baseline CBF	Unchanged linear
d	Tonic inhibition and excitation 	Decreased	Decrease of evoked rise in CBF in response to stimulation	Not available
e	Disinhibition and excitation 	Increased	Unchanged rise in CBF in response to stimulation	Unchanged linear or nonlinear

Fig. 3: Neurophysiological basis of activity-dependent increases in cerebral blood flow illustrated by examples obtained from rat cerebellar cortex (taken, with kind permission, from Lauritzen, 2005). See text for details.

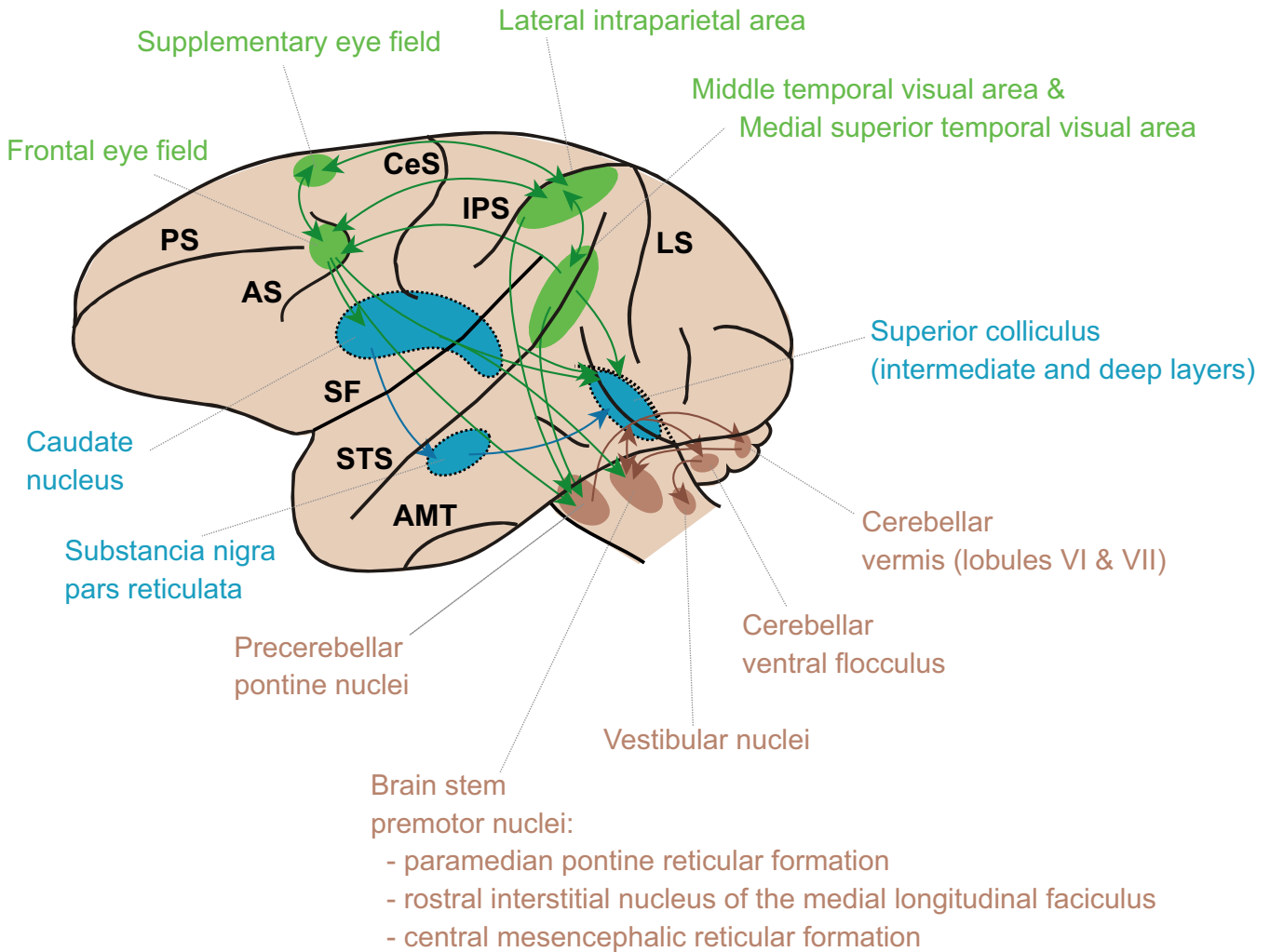


Fig. 4: Neuronal substrates and pathways involved in saccadic and smooth pursuit eye movements (adapted from Krauzlis, 2005).

Schematic diagram of neuronal substrates and descending pathways for saccadic and smooth pursuit eye movements on lateral view of monkey cortex. Cortical areas are shown in green. The brain structures that are normally covered by the cerebral cortex are shown in blue, surrounded by black dashed lines. Structures lying in the brain stem and cerebellum are shown in brown. Arrows indicate anatomical connections between brain structures. Not all relevant areas are depicted (e.g., ascending pathways are omitted) and arrows do not always correspond to direct anatomical connections.

AS, arcuate sulcus; CeS, central sulcus; IPS, intraparietal sulcus; LS, lunate sulcus, PS, principal sulcus; SF, sylvian fissure; STS, superior temporal sulcus.

Fig. 5: Material.

(A) Custom-made primate chair, entirely made of non-metallic material. (1) Head restraining apparatus, firmly attached to the primate chair. (2) IR-camera that can be adaptively placed in front of the monkeys eye. (3) Tubing for the delivery of rewards.

(B) Two linear polarized receiver surface coils, used for functional MR scanning.

(C) IR-CMOS camera and illuminating IR-LED used for monitoring the monkey's left eye during experiments.

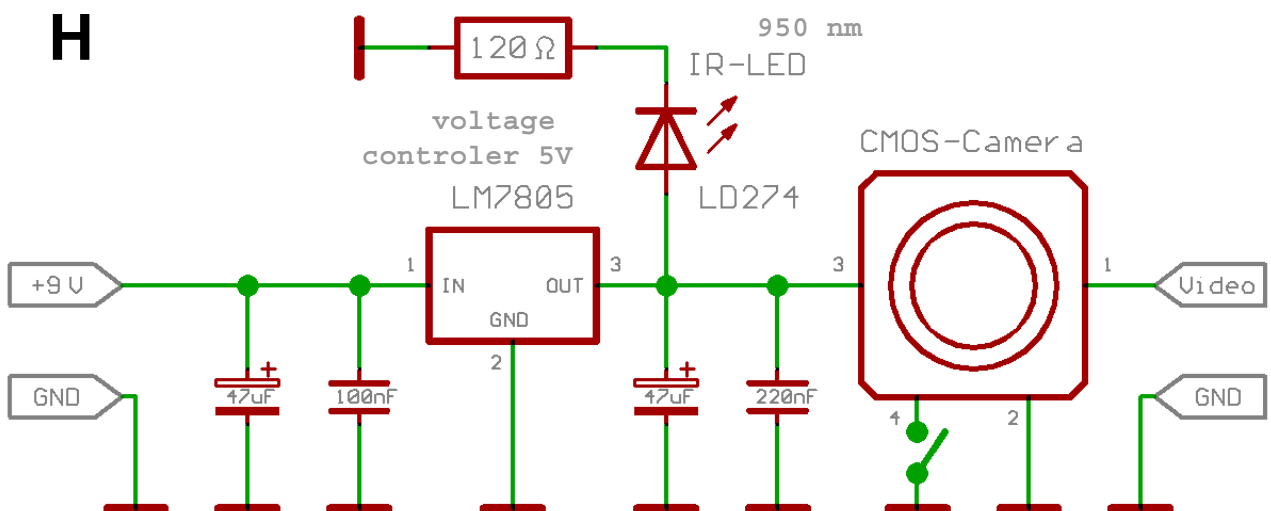
(D) Video image of left eye, with green ellipse superimposed onto it, demarcating the pupil that was used for *eye-position-tracking*.

(E) Schematic illustration of the standard head-post used in monkey S and monkey Z. The figures also show three lines that indicate the location of breakage of head posts.

(F) Schematic illustration of the *three-point head restraining system (TPHRS)*, used with monkey H.

(G) Experimental setup showing the monkey inside the primate chair within the MR scanner environment.

(H) Diagram of connections of IR-CMOS camera and IR-LED.



Figures & Tables

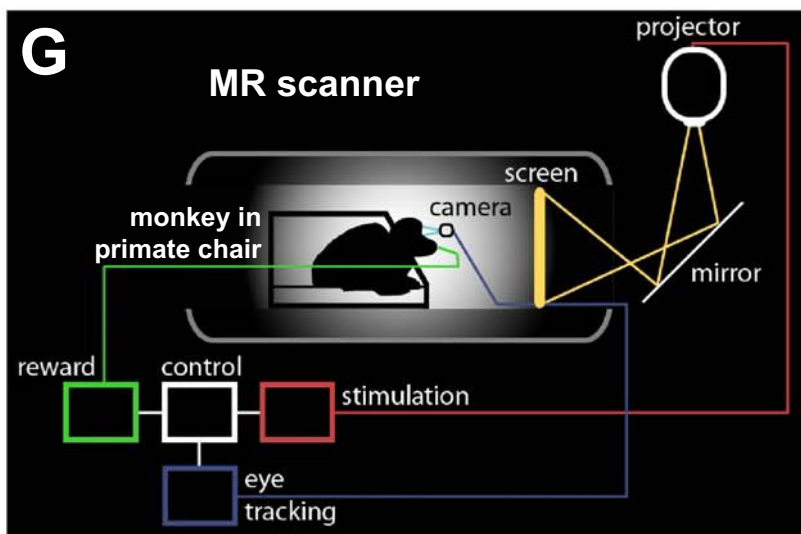
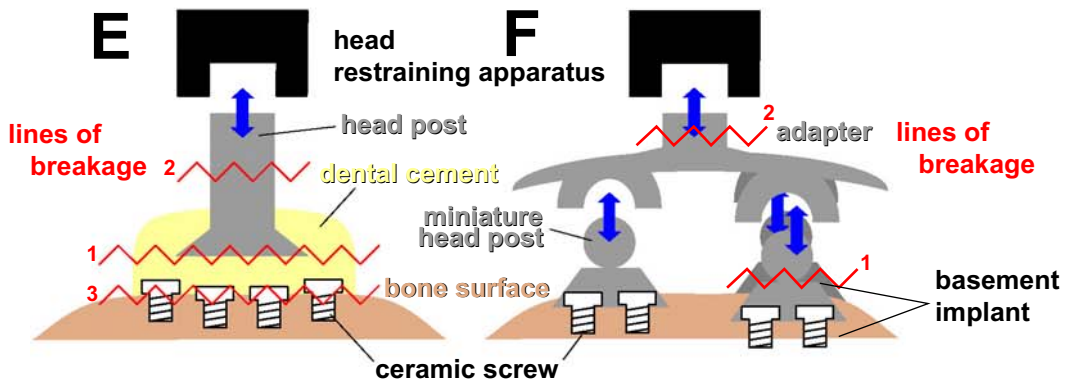
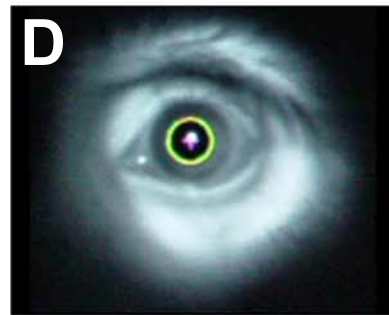
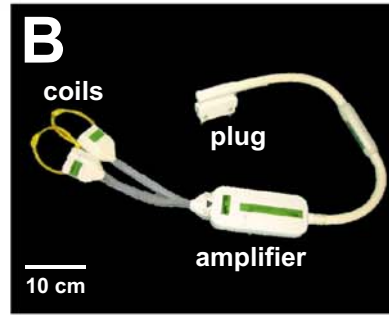
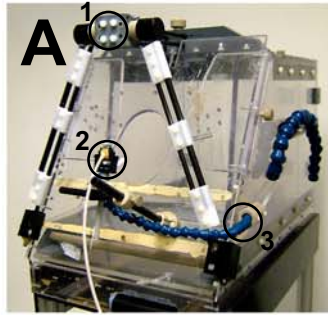


Fig. 6: Stimuli.

(A-D) Stimuli presented in the visual field mapping paradigm. Flickering checkerboard stimuli confined to (A) the horizontal meridian, (B) to the vertical meridian, (C) to 2-3.5° of eccentricity and (D) 18-22° of eccentricity of the visual field. White spot in the center is a fixation target.

(E-F) Stimuli presented in the optic flow paradigm. Random dot displays comprising centrifugal motion (optic flow) with an aperture diameter of 60°, covering left (E) or right (F) visual hemifield. Red spot in the center is a fixation target.

(G) In the saccadic eye movements paradigm, one of two targets were presented at a rate of 1.5 Hz, alternately at positions indicated by white double-arrow, 15° apart from each other. In the SPEM paradigm, the target moved continuously in a sinusoidal fashion, at a frequency of 0.3 Hz, between positions indicated by white double-arrow, 15° apart from each other. The target shown in figure (G) represents either the right saccade target or the SPEM target at right extreme position.

(H) Fixation target as present in baseline blocks in between blocks of oculomotor trials.

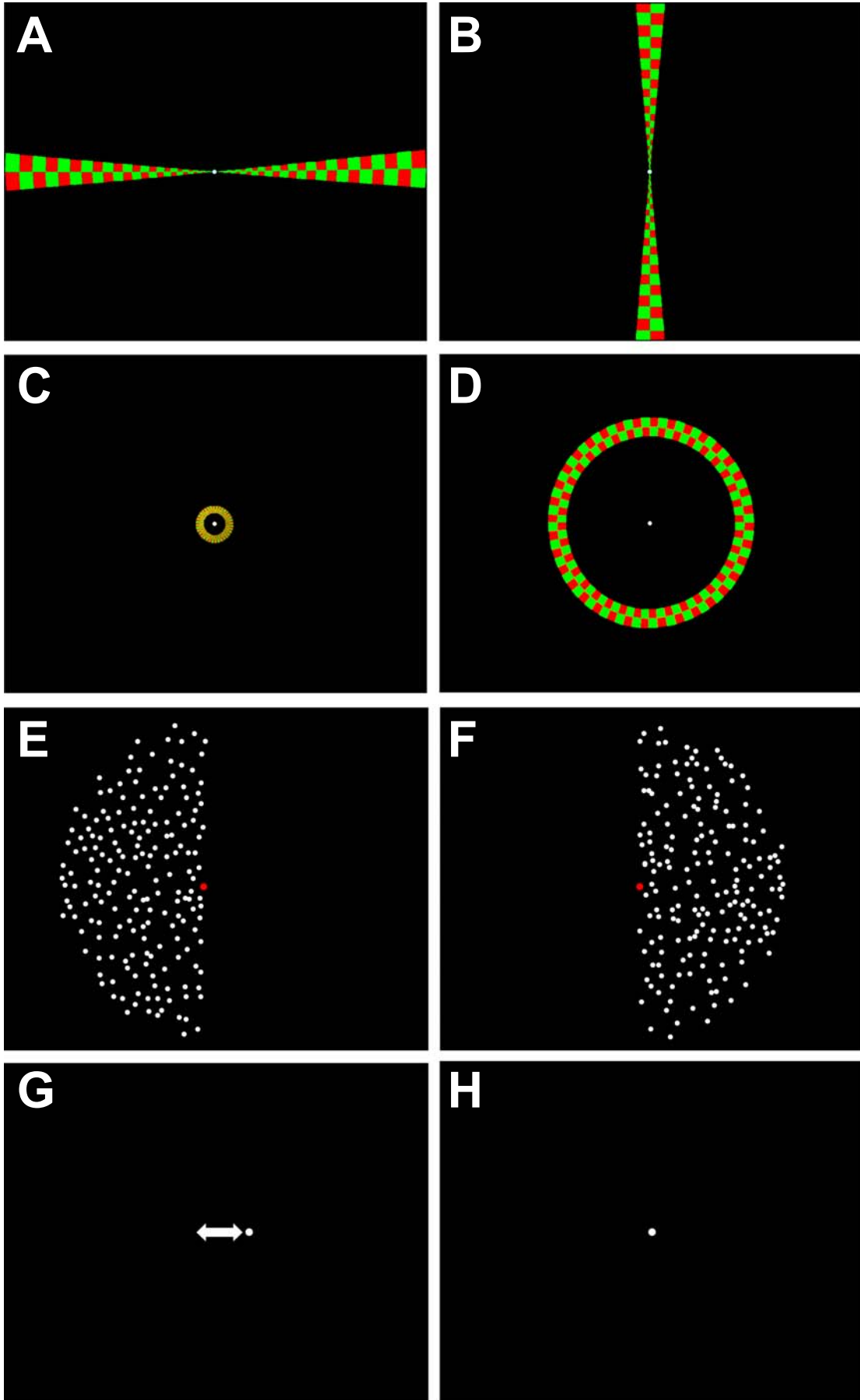


Fig. 7: Representative eye position traces.

Representative horizontal (left column) and vertical (right column) eye position traces during image acquisition in saccadic eye movements paradigm (A), SPEM paradigm (B) and during pure fixation (C).

In the saccadic eye movements paradigm, one of two targets were presented at a rate of 1.5 Hz, alternately at horizontal positions 15° apart from each other. In the SPEM paradigm, the target moved continuously in a sinusoidal fashion, at a frequency of 0.3 Hz, horizontally between positions 15° apart from each other.

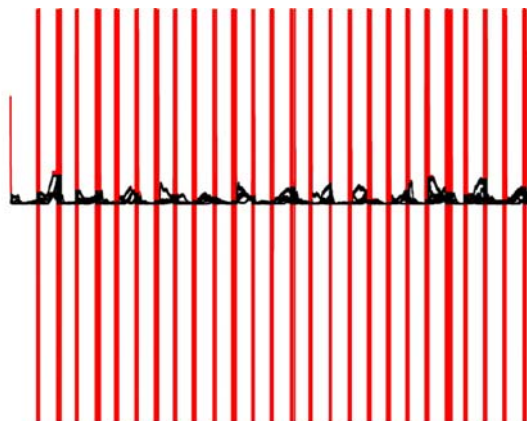
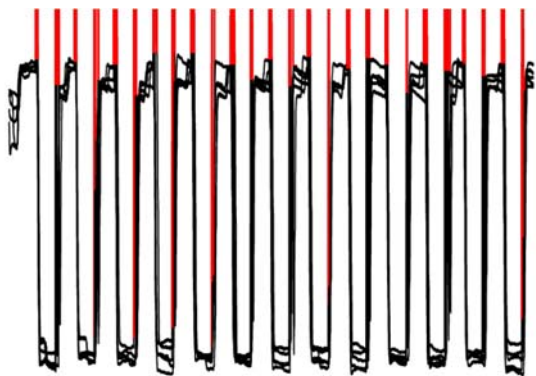
The vertical position traces of (B) show a slight modulation in phase with the modulations of the horizontal eye position. This could be explained by a slight horizontal tilt of the camera which led to wrong assignments of horizontal eye movement components to the measured vertical eye movements.

Artefacts in the video image of the IR-camera are marked in red colour. Blue arrows mark saccades made by the monkey during fixation blocks.

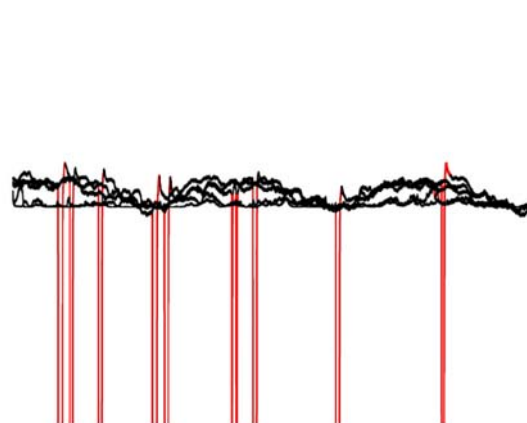
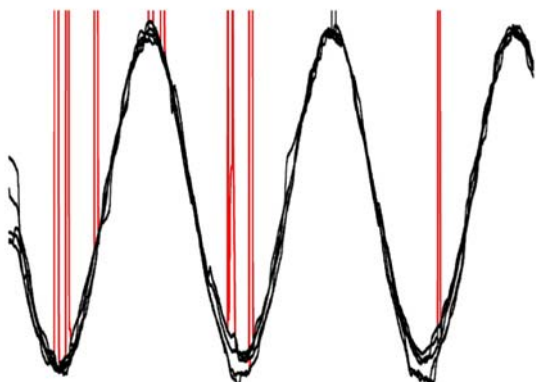
horizontal
eye position

vertical
eye position

A



B



C

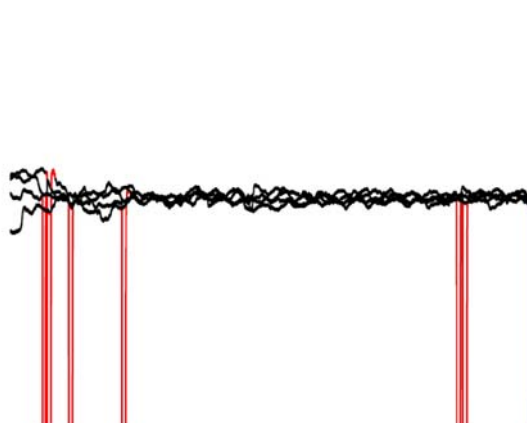
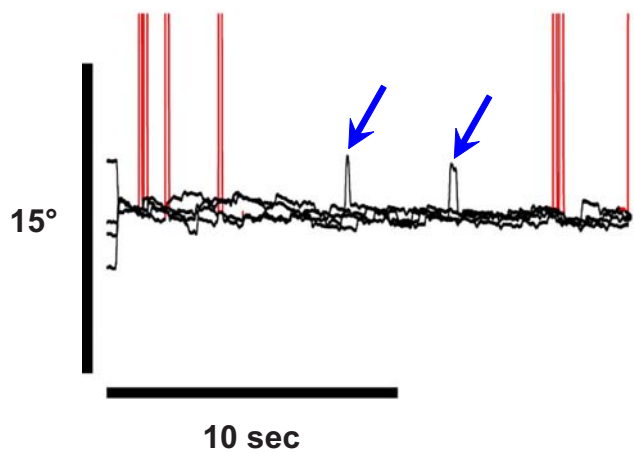


Fig. 8: Schematic illustration of standard procedure for fMRI data analysis in SPM2 (adapted from Friston, 2003).

Schematic illustration of the standard procedure that is applied to functional images in order to yield SPMs (See text for details). The design matrix shows stimulus function and regressors for three series that were pooled for analysis.

SPMs are superimposed onto the co-registered structural (reference) images in the SPM2 software (<http://www.fil.ion.ucl.ac.uk/spm/software/spm2/>), or projected onto cortical surface reconstructions (see Fig. 9).

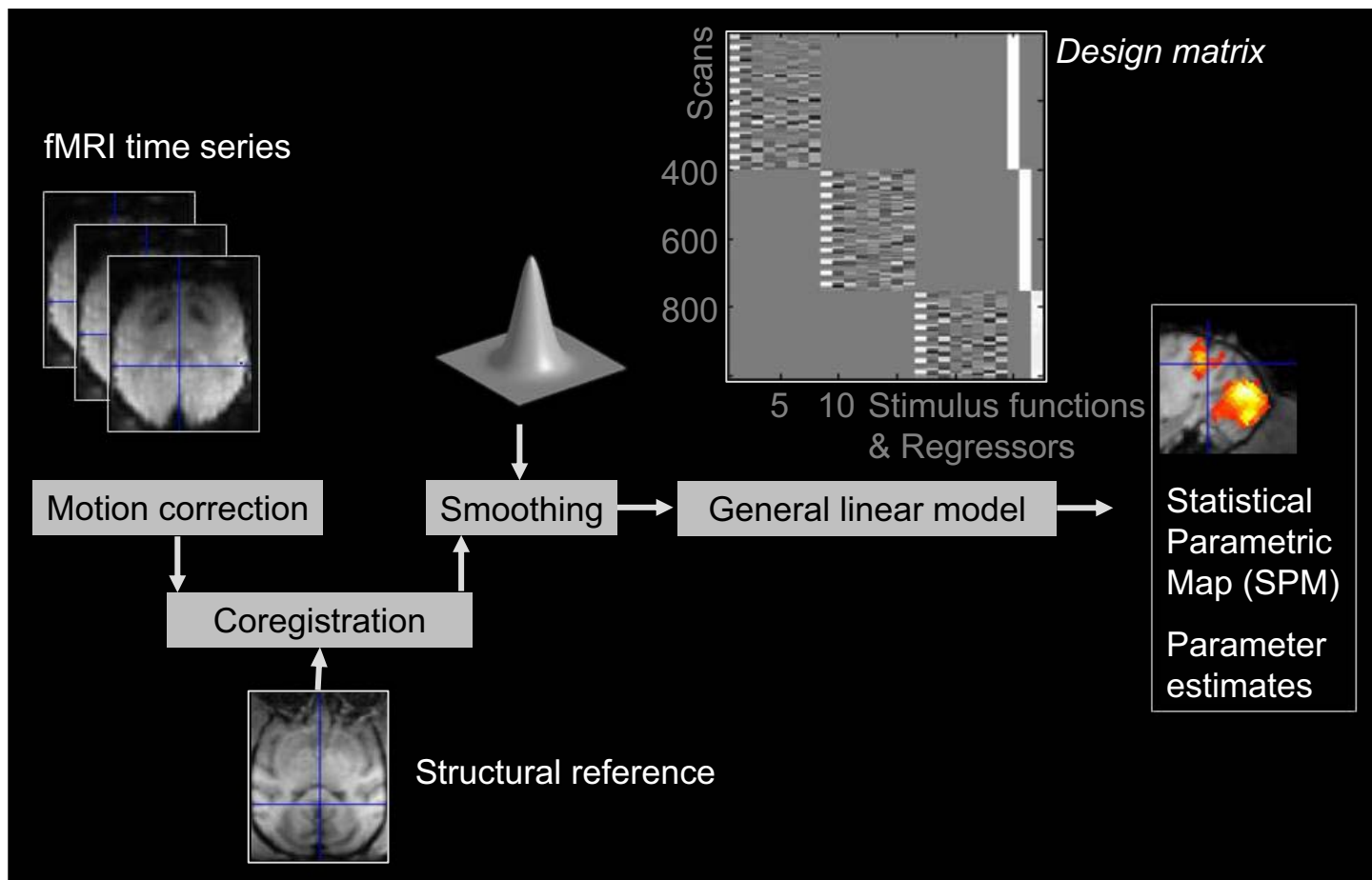


Fig. 9: White matter segmentation and cortex-surface reconstruction.

(A) Parasagittal (a), coronal (b) and transverse (c) cross-sections of the brain (monkey S) at positions indicated by coordinates (lower left in a, b, and c) in “monkey bicomissural space” (Hayashi *et al.*, 1999; Nakahara *et al.*, 2002) and in (d) by lines superimposed on lateral views of a 3D surface-reconstruction of the cortex. The segmentation of the white matter is indicated in red colour on cross-sections (only shown on right hemisphere). The border between grey and white matter was used to reconstruct the cortex-surface, as shown in (B) as fiducial (naturally folded) surface 3D model (a), as partly virtually inflated 3D model (b) and flattened representation (c) (only the right hemisphere shown). Parts of the medial wall are spared in the flattened reconstruction (c), which otherwise represents the surface of the complete right hemisphere. Scale and orientation bars in (B) apply to all subfigures of (B) (a, b, c).

All surface reconstruction procedures were performed with the *Caret* software package, version 5.3 (John Harwell, Heather Drury, Donna Hanlon, and David Van Essen; <http://brainmap.wustl.edu/caret.html>).

AC, anterior commissure (center, of “monkey bicomissural space” (Nakahara *et al.* 2002); *D-V* dorsal-ventral coordinate for transverse cross-sections; *M-L*, medial-lateral coordinate for parasagittal cross-sections; *C-R*, caudal-rostral coordinate for coronal cross-sections. *AMT*, anterior middle temporal sulcus; *AS*, arcuate sulcus; *CaS*, calcarine sulcus; *CeS*, central sulcus; *CiS*, cingulate sulcus; *IOS*, inferior occipital sulcus; *IPS*, intraparietal sulcus; *LS*, lunate sulcus; *OTS*, occipitotemporal sulcus; *POS*, parieto-occipital sulcus; *PS*, principal sulcus; *SF*, sylvian fissure; *STS*, superior temporal sulcus.

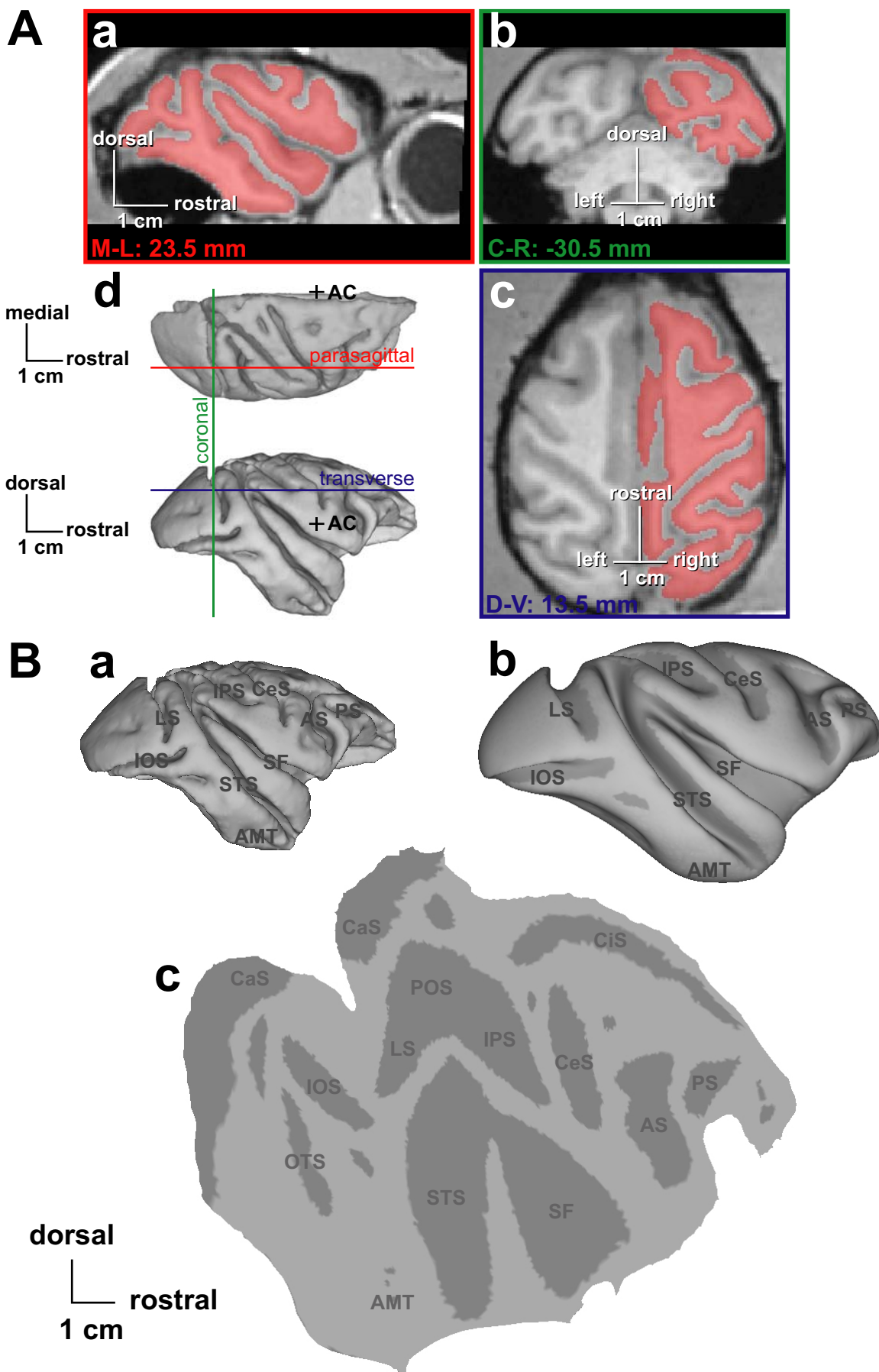


Fig. 10: Surface-based coregistration of a standard rhesus monkey template and atlas with the individual's cortical reconstruction.

A surface-based coregistration procedure was used to morph a standard rhesus monkey template (F99UA1, <http://brainmap.wustl.edu:8081/sums/index.jsp>) (A, right hemisphere; E, left hemisphere) with superimposed atlas (Felleman & Van Essen, 1991) (B, right hemisphere; F, left hemisphere) to the individual's (monkey S) cortical surface (C, right hemisphere; G, left hemisphere). For alignment, 29 (right hemisphere) and 38 (left hemisphere) landmarks were used that are shown in (A), (C), (E) and (G) as white lines on top of cortical surface reconstructions. Concave and convex folded structures of the original cortex model (sulci and gyri, respectively) are shown in darker and lighter gray, respectively. The individual's cortical surface reconstructions are shown in (D, right hemisphere) and (H, left hemisphere) with the morphed atlas superimposed. All atlas areas, as shown here in different colours, are based on Felleman & Van Essen, 1991. See Fig. 11 for the individual's cortical surface reconstructions with area borders and names superimposed.

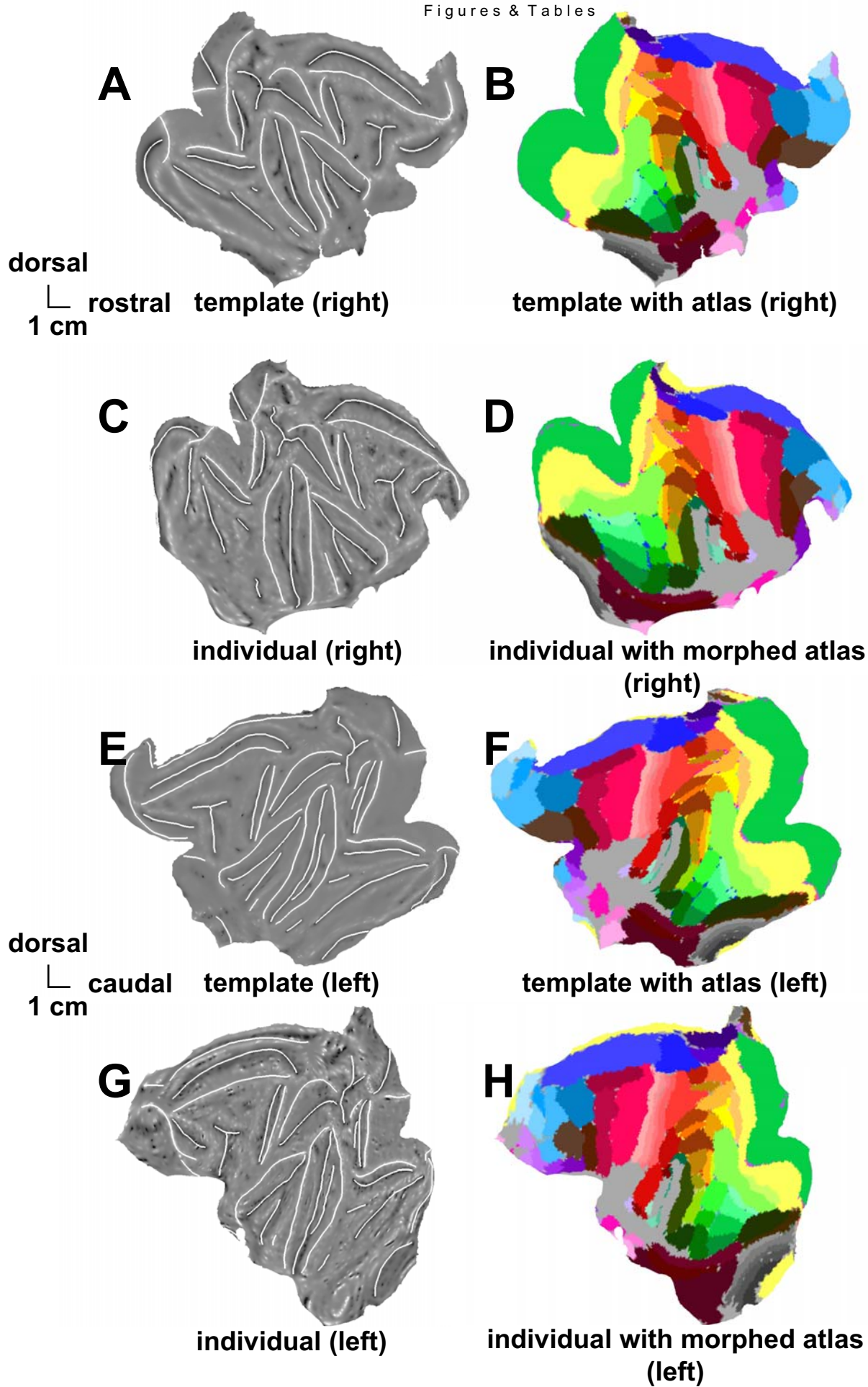


Fig. 11: Flattened cortical reconstructions with morphed rhesus monkey atlas (Felleman & Van Essen, 1991) superimposed.

Flattened cortical reconstructions of left (A) and right (B) hemisphere of monkey S with morphed rhesus monkey atlas (Felleman & Van Essen, 1991) superimposed.

Visual areas:

Visual areas in occipital lobe: *V1 (area 17), visual area 1; V2 (V-II), visual area 2; V3 (V3d), visual area 3; VP (V3v), ventral posterior; V3A, visual area V3A; V4, visual area 4; V4t, V4 transitional; VOT, ventral occipitotemporal; MT (V5), middle temporal.*

Visual areas in temporal lobe: *FST, floor of superior temporal; PITd (TEOd), posterior inferotemporal (dorsal); PITv (TEOv), posterior inferotemporal (ventral); CITd (TEd), central inferotemporal (dorsal); CITv (TEv), central inferotemporal (ventral); AITd, anterior inferotemporal (dorsal); AITv, anterior inferotemporal (ventral); STPp, superior temporal polysensory (posterior); STPa, superior temporal polysensory (anterior); TF, TF; TH, TH.*

Visual areas in parietal lobe: *MSTd (MSTc), medial superior temporal (dorsal); MSTl (MSTp), medial superior temporal (lateral); PO (V6), parieto-occipital; PIP, posterior intraparietal; LIP, lateral intraparietal; VIP, ventral intraparietal; MIP, medial intraparietal; MDP, medial dorsal parietal; DP (DPL), dorsal prelunate; 7a, 7a.*

Visual areas in frontal lobe: *FEF, frontal eye field; 46 (principal sulcus), 46.*

Non-visual areas:

Somatosensory areas: *1; 2; 3a; 3b; 5; 7b; SII; Ri, retroinsular; Pa, postauditory; Ig, insular granular; Id, insular dysgranular.*

Auditory areas: *A1, primary auditory; Aud, auditory; RL, rostromedial; CM, caudomedial; L, lateral.*

Areas of hippocampal complex, HC: *ER, entorhinal cortex; 35; 36; presubiculum; prosubiculum; subiculum; field CA1 and CA3.*

Olfactory areas: *PIR, piriform cortex; PAC, periamygdaloid cortex.*

Orbitofrontal areas: *11; 12; 13; Pro, proisocortex; Pall, periallocortex; lateral prefrontal area 45; dorsal prefrontal areas 9 and 10; medial prefrontal areas 14, 25 and 32.*

Motor areas: *4 (primary motor) and 6 (premotor and arcuate premotor or 6s and 6i); SMA (supplementary motor area); MEF (medial eye field, or SEF, supplementary eye field).*

Cingulate and other limbic areas: *23; 24; 29, retrosplenial; 30, PGm (7m); prostriate, PS.*

A few regions in the posterior orbitofrontal, lateral prefrontal and anterior sylvian cortices are left unspecified here. *UNK, unknown.*

Sulci:

AMT, anterior middle temporal sulcus; AS, arcuate sulcus; CaS, calcarine sulcus; CeS, central sulcus; CiS, cingulate sulcus; IOS, inferior occipital sulcus; IPS, intraparietal sulcus; LS, lunate sulcus; OTS, occipitotemporal sulcus; POS, parieto-occipital sulcus; PS, principal sulcus; SF, sylvian fissure; STS, superior temporal sulcus.

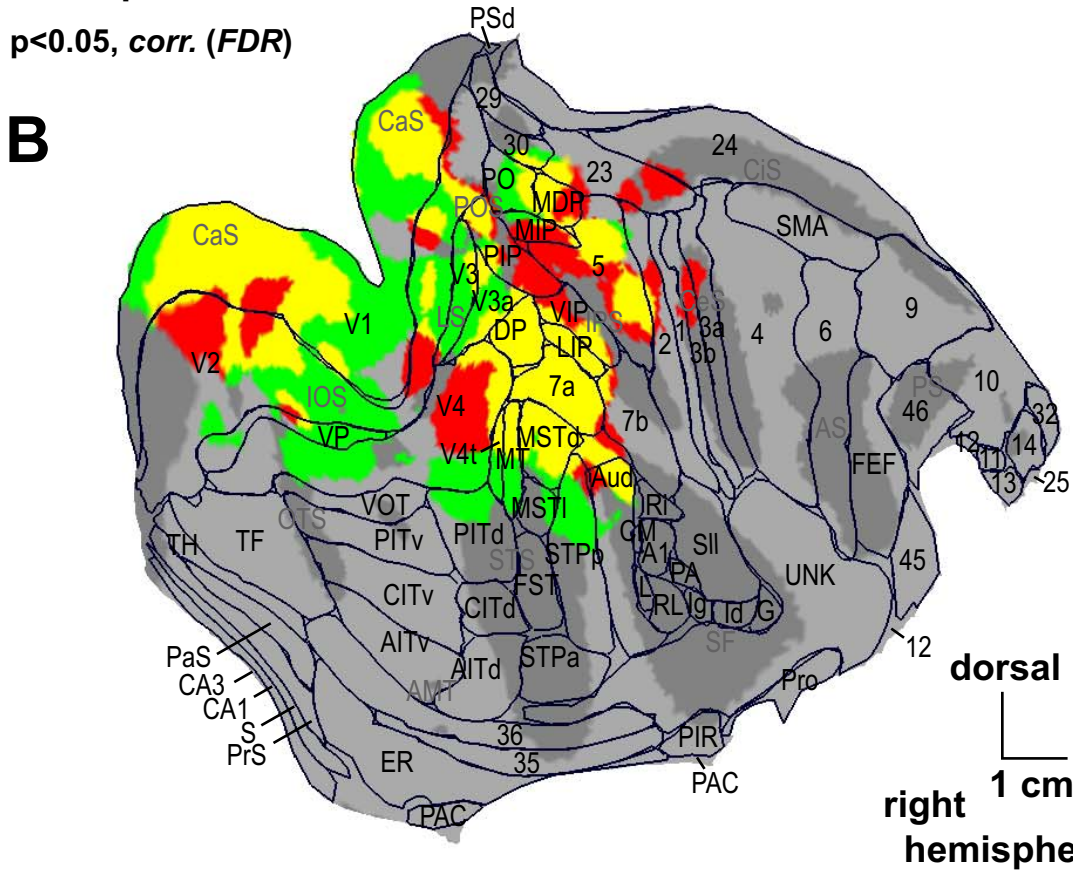
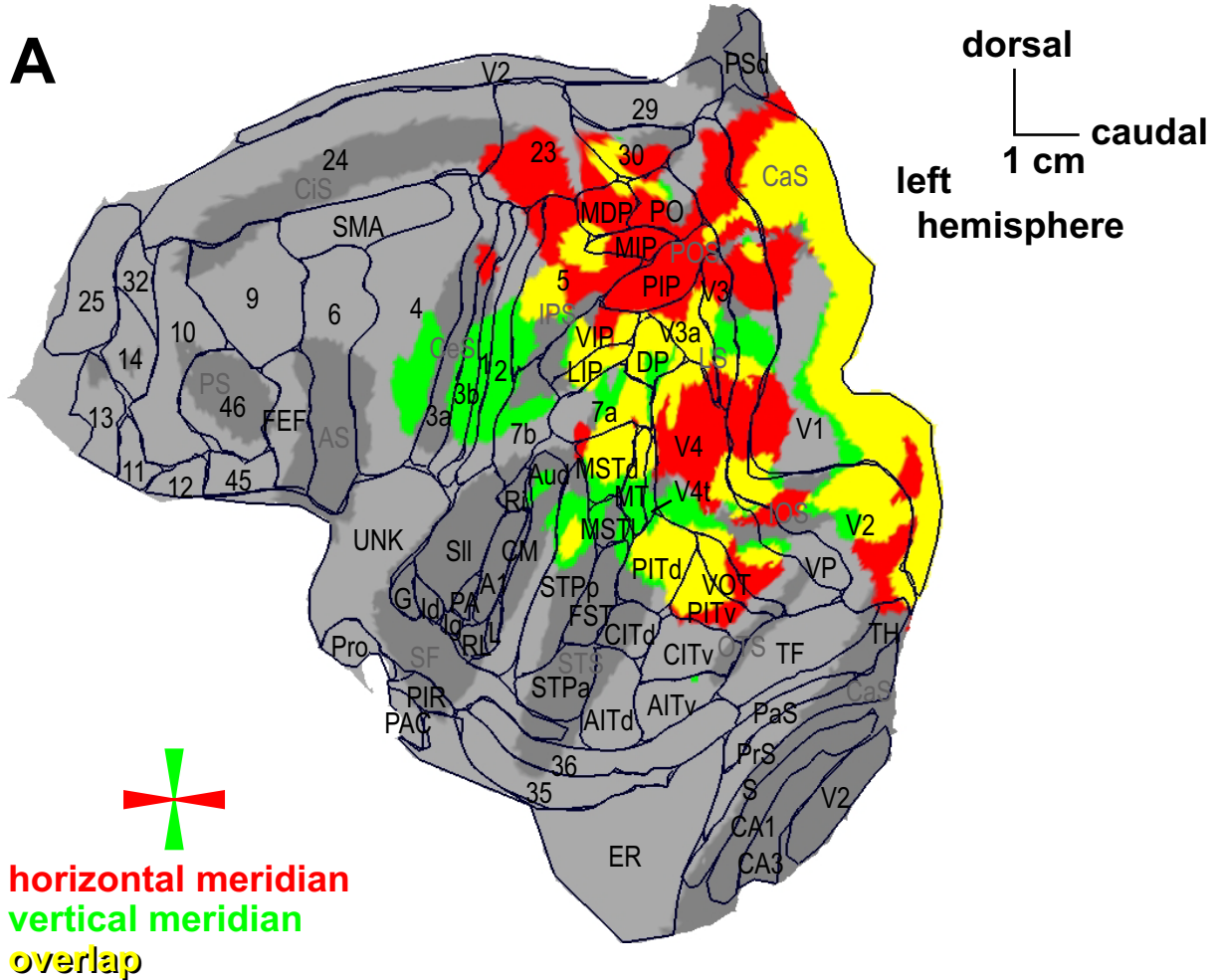
Table 1: Overview on stimulation paradigms, pools and stimulus contrasts.

Figs.	Paradigm	# Sessions in pool	# Functional images in pool	Stimulus contrast(s)
12	Visual field mapping	2	1373	<ul style="list-style-type: none"> Contrast 1: horizontal double-wedge vs. vertical double-wedge Contrast 2: vertical double-wedge vs. horizontal double-wedge Contrast 1: 2-3.5° annulus vs. 18-22° annulus Contrast 2: 18-22° annulus vs. 2-3.5° annulus
13&14	Optic flow	3	541	<ul style="list-style-type: none"> Contrast 1: right visual hemifield vs. left visual hemifield Contrast 2: left visual hemifield vs. right visual hemifield
15&16	Saccade eye movements	3	2639	Contrast: 15° horizontal saccades vs. fixation
17&18	Smooth pursuit eye movements	6	3003	Contrast: 15° horizontal smooth pursuit vs. fixation



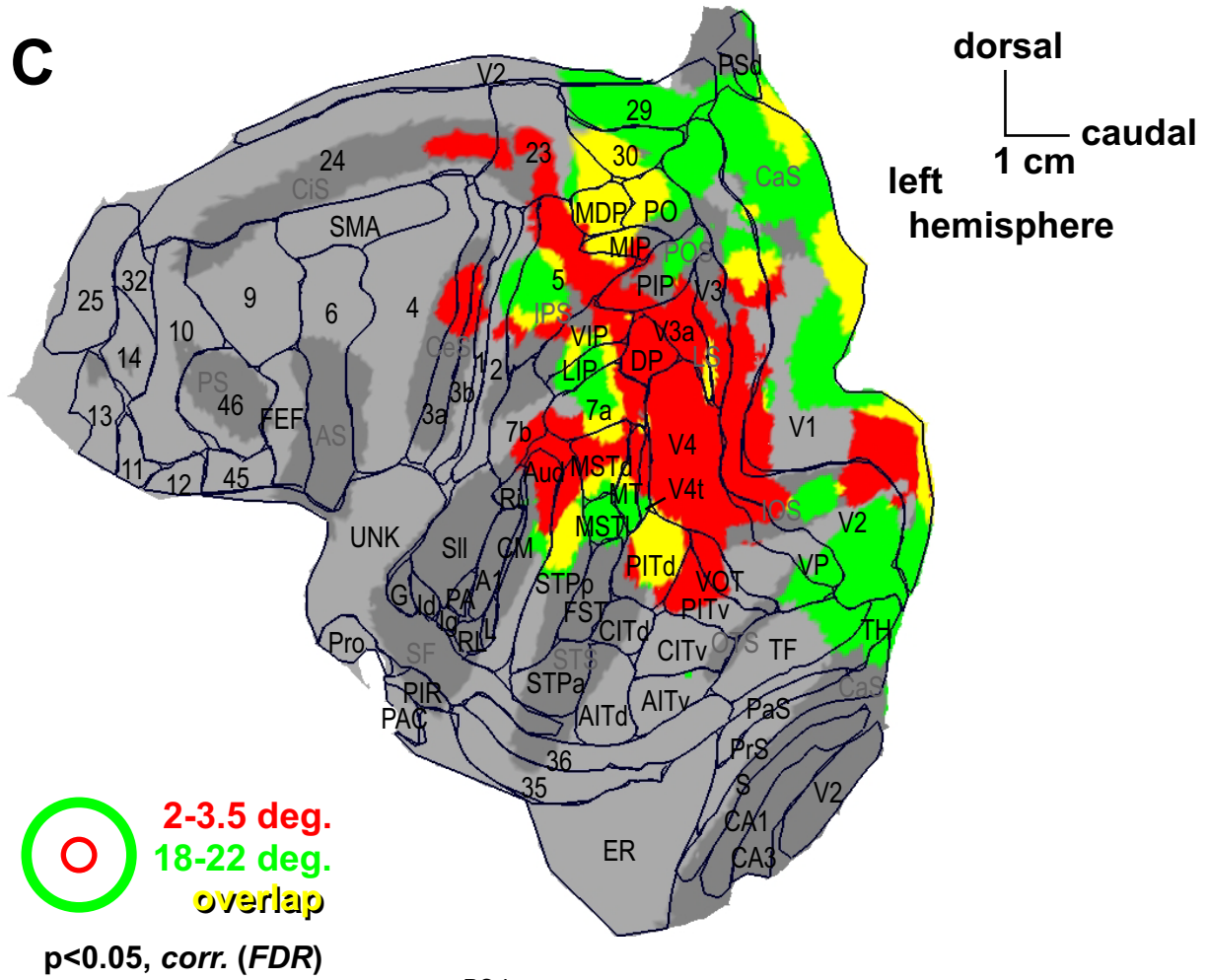
Fig. 12: Representation of meridians and different degrees of eccentricity of the visual field.

BOLD responses to flickering checkerboard stimuli confined to the meridians of the visual field (A-C, horizontal meridian, red; vertical meridian, green; overlapping areas, yellow) and to flickering checkerboard stimuli confined to certain degrees of eccentricity of the visual field (C-D, 2-3.5°, red; 18-22°, blue; overlapping areas, purple) are shown as *T*-score maps ($p < 0.05$, corrected for multiple comparisons using *FDR*) on the flattened cortical reconstructions of the left (A, C) and right (B, D) hemisphere of monkey S. Same conventions as in [Fig. 11](#).



$p < 0.05$, corr. (FDR)

C



D

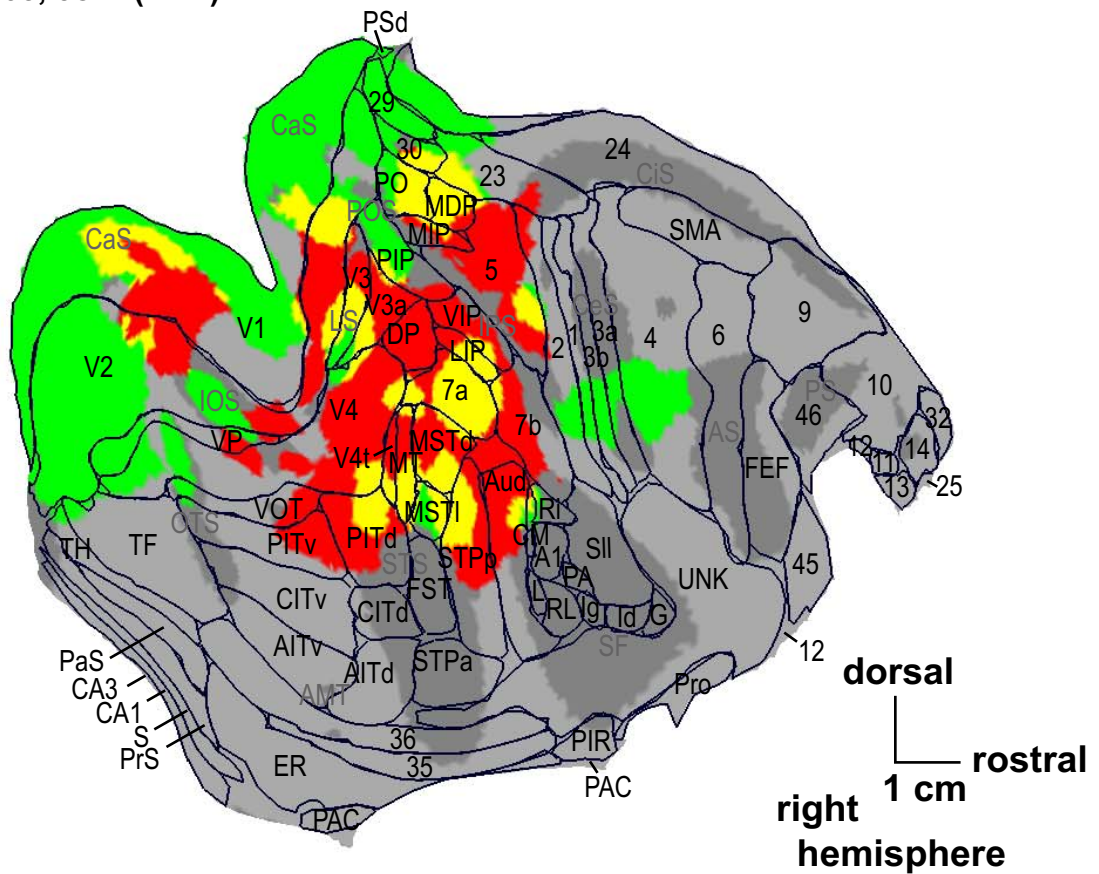


Table 2: Cortical brain regions involved in optic flow.

Area of peak response	Adjacent area(s) to peak response	AC-PC coordinates [mm]			Peak T value	Hemi-sphere
		ML	AP	DV		
5		-13.5	-14.5	16.0	6.7	L
5		14.5	-15.5	19.0	13.4	R
7a	MSTd	16.5	-18.5	15.5	13.9	R
Aud		-18.5	-15.0	10.5	6.4	L
Aud		19.0	-15.5	11.5	13.0	R
DP	LIP, VIP	-8.5	-25.5	19.0	8.4	L
LIP	VIP	15.0	-16.5	17.0	13.9	R
MDP	MIP, 5	-7.0	-27.0	19.5	8.4	L
MSTd	MT	-14.0	-19.5	11.5	7.9	L
MT	MSTd, 7a	16.5	-21.0	13.5	13.8	R
PIP		-9.5	-30.5	8.0	7.6	L
PIP		9.5	-34.5	8.5	12.6	R
V1		-12.0	-33.0	6.5	18.8	L
V1		-13.0	-36.0	5.0	20.1	L
V1		14.0	-36.0	5.5	17.4	R
V1		12.5	-34.0	6.5	17.3	R
V2		-4.5	-33.5	15.5	6.5	L
V2		-6.0	-33.0	6.0	8.4	L
V2		-12.5	-34.5	0.5	18.3	L
V2		13.5	-37.5	2.0	17.5	R
V3		-9.0	-31.0	15.0	6.7	L
V3	V3a	16.5	-31.0	9.5	10.8	R
V3a	V4	-17.5	-30.0	9.0	8.5	L
VIP	LIP	-13.5	-16.0	14.5	7.7	L

Area names taken from surface-based coregistration of the individual's cortical surface reconstruction to a rhesus monkey atlas (Felleman & Van Essen, 1991). Colour-code of area names corresponds to spherical symbols in the corresponding figure which represents the location of defined peak responses. Peak responses are manually defined, based on *T*-score maps as projected onto cortical surface reconstruction.

**Fig. 13: SPMs revealed by optic flow.**

BOLD responses to optic flow confined to the right (A) and left (B) visual hemifield are shown as *T*-score maps ($p < 0.05$, corrected for multiple comparisons using *FDR*) on the flattened cortical reconstructions of the left (A) and right (B) hemisphere of monkey S. Spherical symbols represent the location of defined peak BOLD responses (Table 2). Same conventions as in Fig. 11.

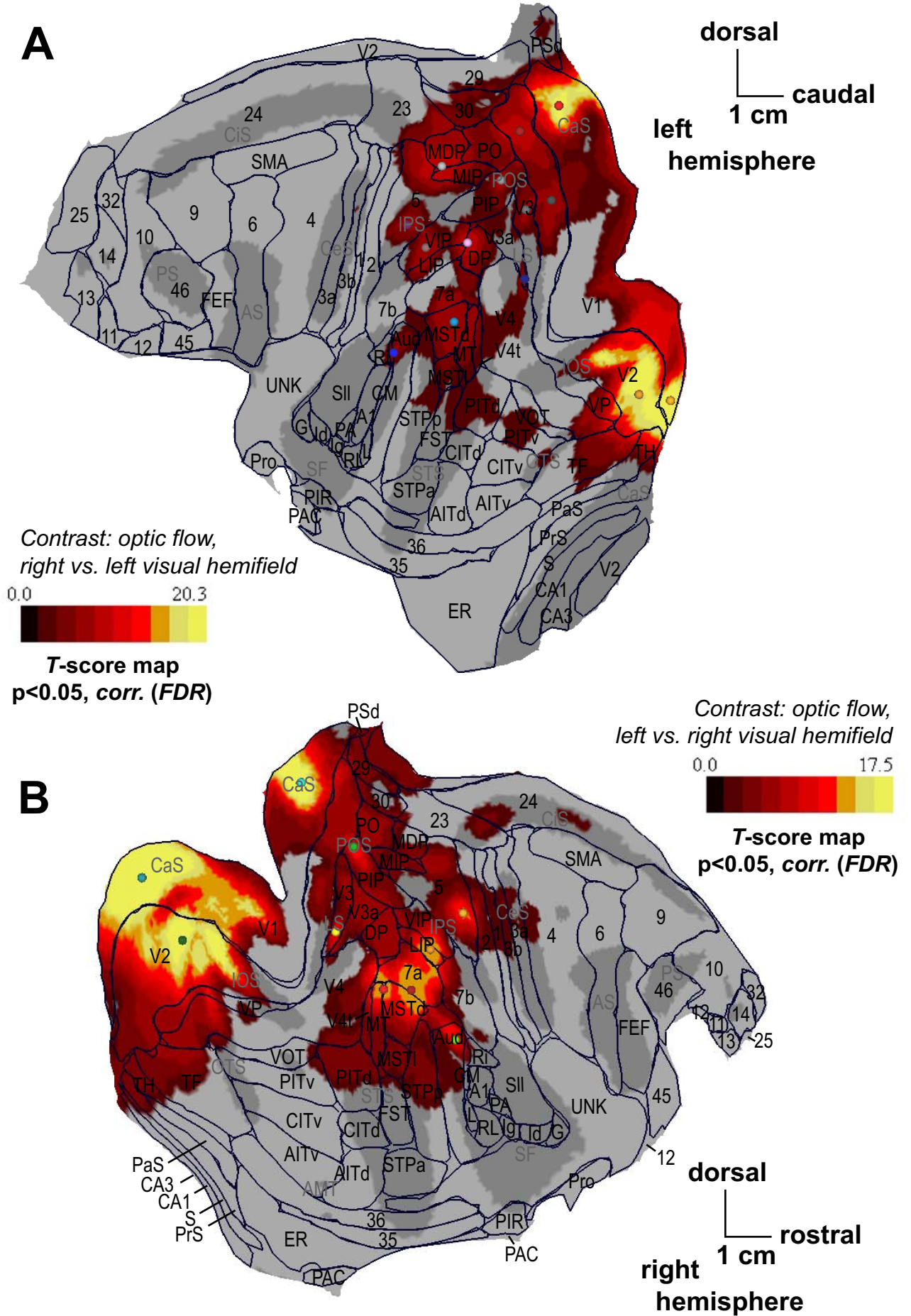
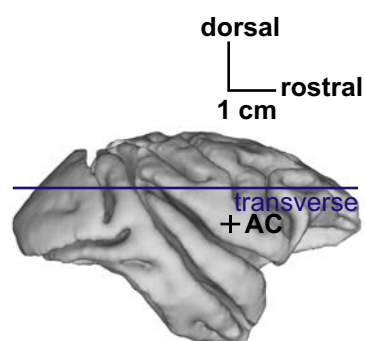
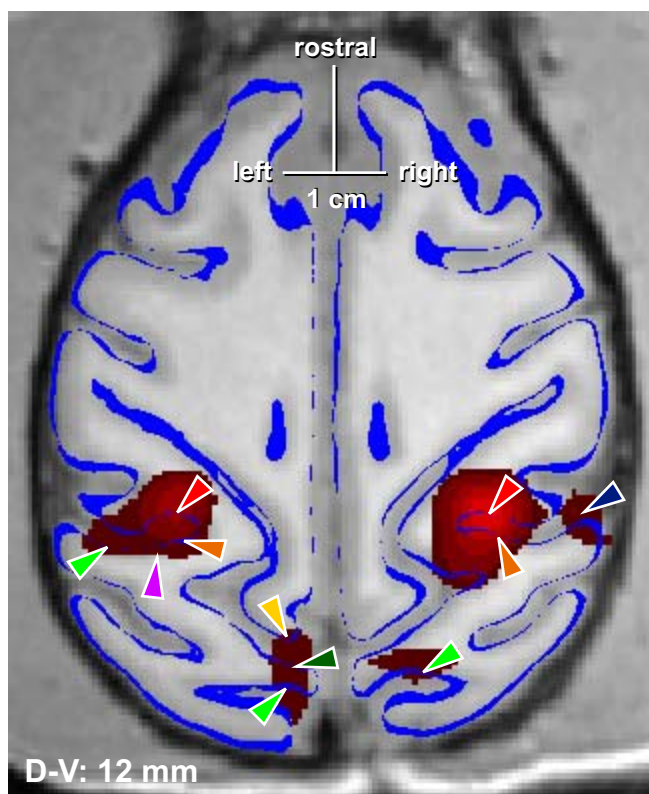


Fig. 14: SPMs revealed by optic flow within *motion complex MT/MST*.

BOLD responses to optic flow confined to the right and left visual hemifield are shown as *T*-score maps ($p < 0.05$, corrected for multiple comparisons using *FDR*) on transversal brain section (different contrasts for left and right hemisphere, merged into a single section). Dorsal-ventral position of section is indicated by line superimposed onto lateral view of a 3D surface reconstruction of the cortex (right). Blue outline superimposed on transversal brain section indicates borders between grey and white matter that was used in order to create cortical surface reconstructions. Coloured arrows indicate brain areas (rhesus monkey atlas, Felleman & Van Essen, 1991). Colour code and area names are given next to brain section.



- MSTd
- MT
- PO
- V1
- V2
- V4
- V4t

Left hemisphere
 Contrast: optic flow,
 right vs. left visual
 hemifield



T-score map
 $p < 0.05$, corr. (FDR)

Right hemisphere
 Contrast: optic flow,
 left vs. right visual
 hemifield



T-score map
 $p < 0.05$, corr. (FDR)

Fig. 15: SPMs revealed by saccadic eye movements.

BOLD responses to 15° horizontal saccadic eye movements are shown as *T*-score maps ($p < 0.05$, corrected for multiple comparisons using *FDR*) on the flattened cortical reconstructions of the left (A) and right (B) hemisphere of monkey S. Spherical symbols represent the location of defined peak BOLD responses ([Table 2](#)). Same conventions as in [Fig. 11](#).

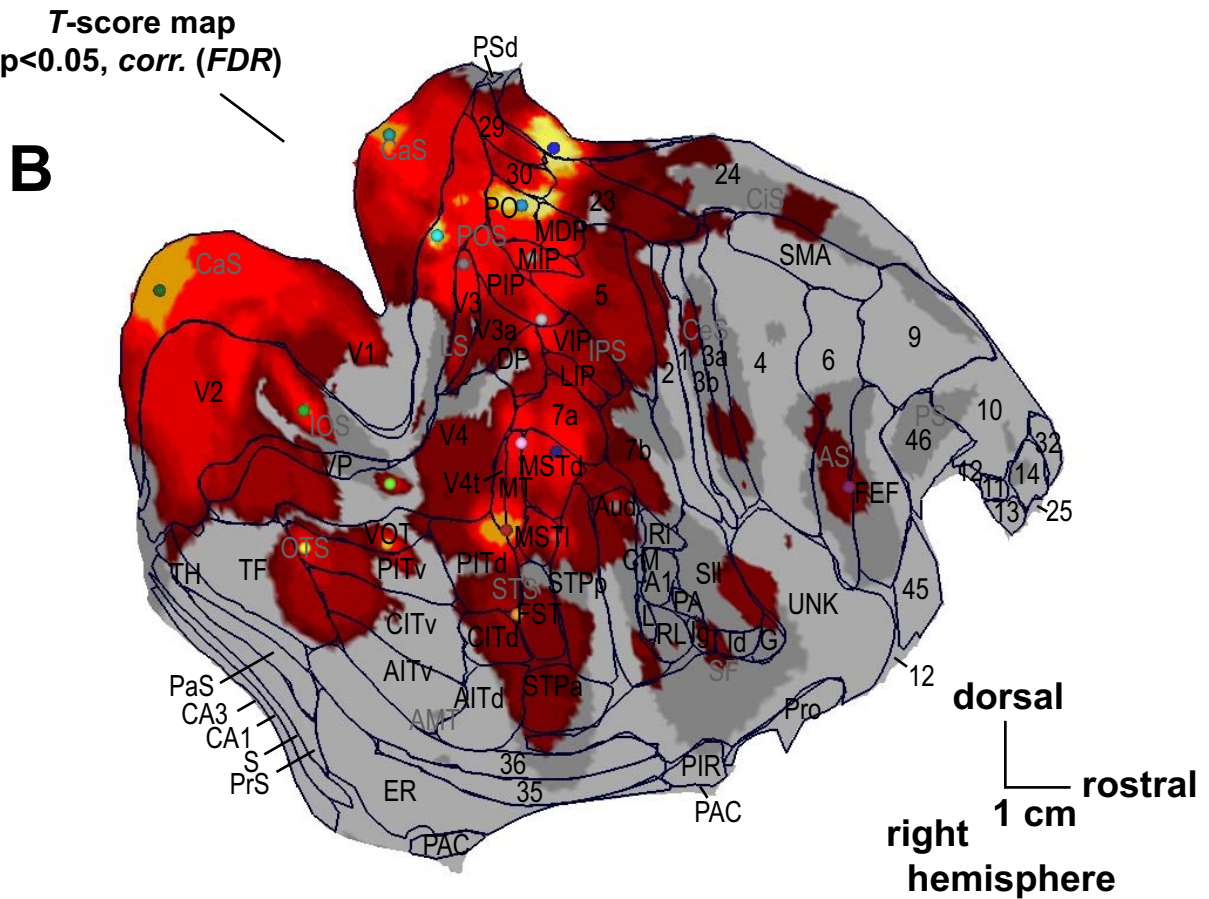
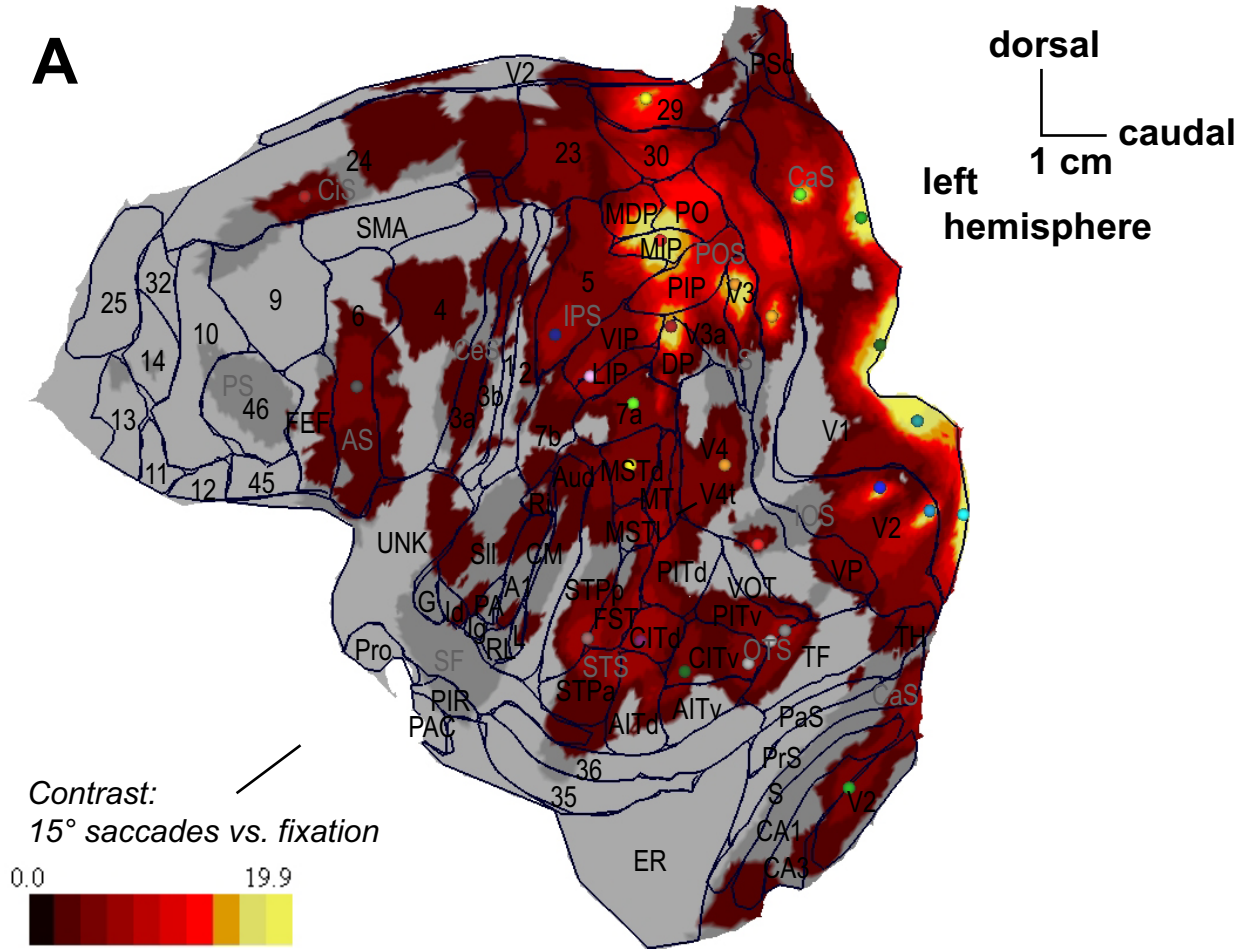


Fig. 16: SPMs revealed by saccadic eye movements within specific brain areas.

BOLD responses to 15° horizontal saccadic eye movements are shown as *T*-score maps ($p < 0.05$, corrected for multiple comparisons using *FDR*) on transversal (A), transversal cutout (B) and parasagittal (C) brain sections. Dorsal-ventral position or medial-lateral position of section is indicated by line superimposed onto lateral or dorsal views of a 3D surface reconstruction of the cortex, respectively (right in A-C). Blue outline superimposed on transversal brain section indicates borders between grey and white matter that was used in order to create cortical surface reconstructions. Coloured arrows or coloured outlines indicate brain areas (rhesus monkey atlas, Felleman & Van Essen, 1991). Colour code and area names are given next to each brain section. *T*-score scale valid for (A-C).

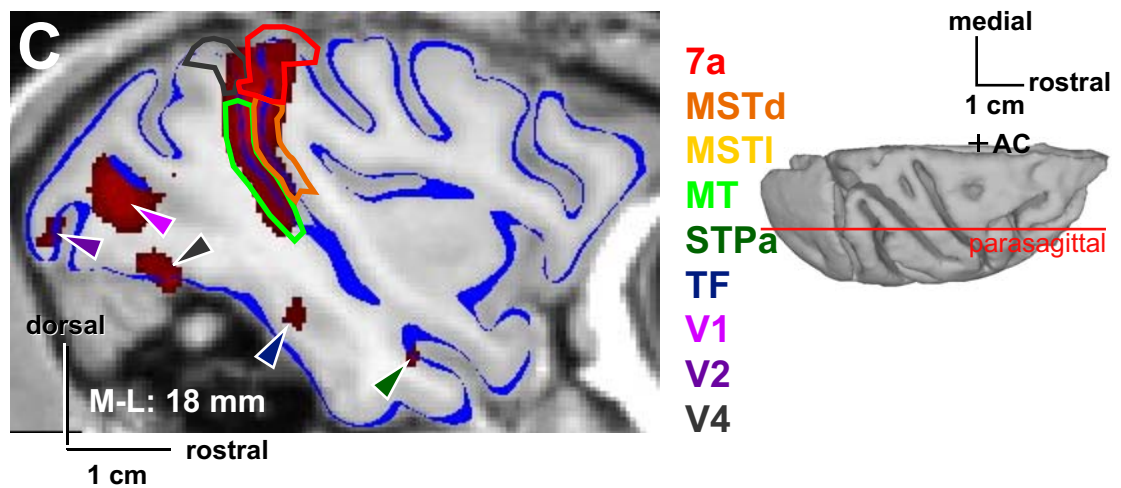
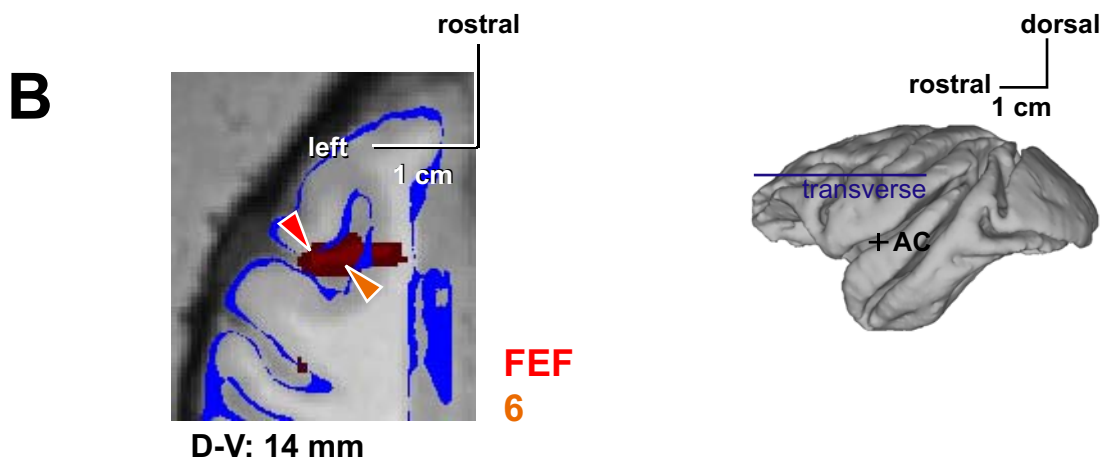
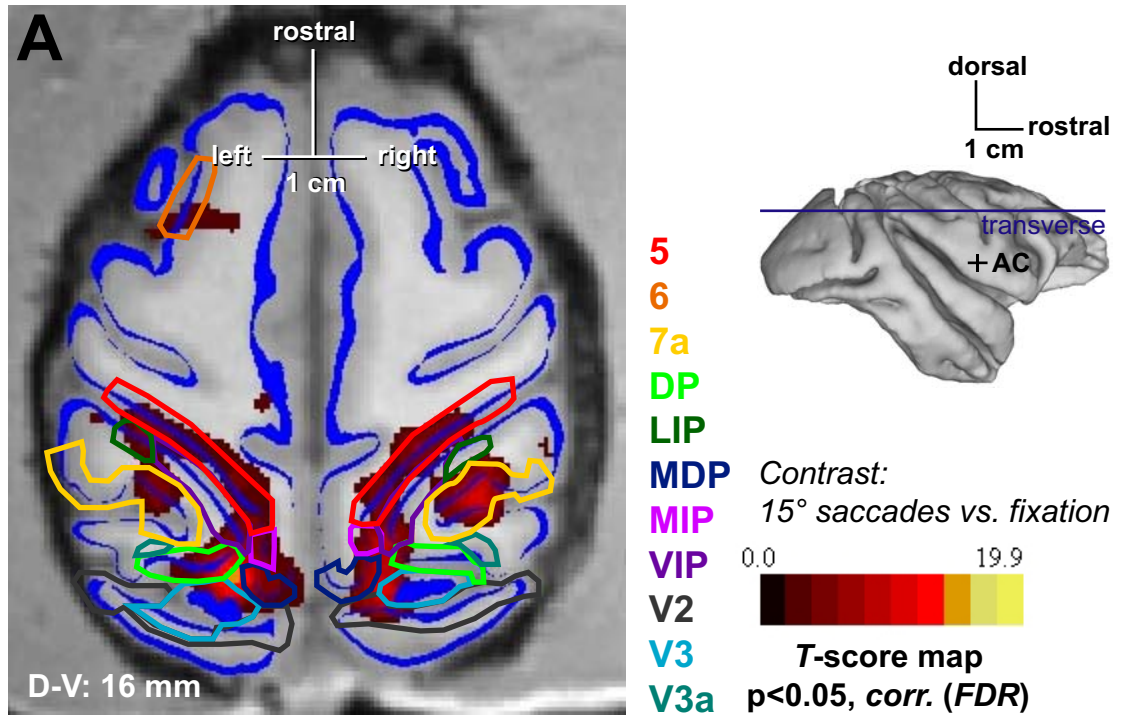


Table 3: Cortical brain regions involved in saccadic eye movements.

Area of peak response	Adjacent area(s) to peak response	AC-PC coordinates [mm]			Peak T value	Hemi-sphere
		ML	AP	DV		
5		-17.0	-13.0	17.0	6.2	L
6	4, FEF	-10.0	6.5	12.0	5.0	L
6	FEF	14.5	7.0	8.5	3.0	R
24		-6.0	7.5	13.5	4.2	L
29		-2.0	-23.0	5.0	14.2	L
7a		-16.0	-21.5	19.0	5.6	L
Aud		20.0	-17.0	12.0	5.8	R
CA3	V2	-17.5	-13.5	-7.0	4.9	L
CITd	AITd	-23.5	-9.5	-7.0	7.6	L
CITv		-21.0	-16.0	-7.0	6.0	L
CITv		-26.5	-11.5	-10.5	6.1	L
DP	PIP, VIP, V3a	-8.5	-26.5	15.5	16.6	L
FST	STPp, STPa	-22.5	-8.0	-5.5	7.6	L
FST	CITd, PITd	20.0	-11.0	-6.0	4.6	R
LIP	VIP	-17.0	-15.0	16.0	6.2	L
MIP	MDP, PO, 5, PIP	-6.0	-28.5	14.5	16.6	L
MIP	5, PIP	8.0	-28.0	12.5	10.1	R
MSTd		-17.0	-19.0	10.0	5.1	L
MSTd	7a	16.0	-19.0	13.5	9.5	R
MSTl	MT, PITd	-21.5	-18.5	2.5	6.8	L
MSTl	STPp	21.0	-16.0	3.5	9.7	R
MT	MSTd, 7a	16.5	-21.0	12.5	9.5	R
PIP	DP, VIP	8.5	-24.0	12.5	10.0	R
PITv	TF	-20.0	-21.5	-2.5	6.8	L
PITv	CITv	20.0	-21.0	-3.0	8.8	R
PO	23, 30, MDP	2.5	-31.5	10.0	12.7	R
V1		-10.5	-38.5	8.5	16.0	L
V1		-11.0	-41.0	8.5	19.9	L
V1		-12.0	-43.0	9.0	17.6	L
V1		-12.5	-45.5	4.5	19.8	L
V1		-10.5	-41.0	5.0	19.9	L
V1		16.0	-34.0	5.0	10.5	R
V1		15.5	-33.0	7.5	10.5	R
V2		-9.0	-31.0	18.0	15.8	L
V2		-10.5	-40.0	3.0	16.5	L
V2		-15.0	-42.0	2.5	16.5	L
V2		18.0	-36.5	3.5	10.5	R
V2		2.5	-34.5	11.0	12.0	R
V2	23	2.5	-24.0	5.0	14.5	R
V3	V3a, PIP	-9.0	-30.5	13.5	16.6	L
V3	V2, PIP	7.5	-31.0	12.5	9.9	R
V4		-25.0	-23.0	2.5	6.3	L
V4		-26.0	-25.0	11.0	4.8	L
V4		25.0	-22.5	2.5	8.8	R
V4t	MT, PITd	21.5	-18.5	1.5	11.0	R
VOT		25.0	-20.5	-2.5	10.5	R

Same conventions as for [Table 2](#).

Table 4: Cortical brain regions involved in SPEMs.

Area of peak response	Adjacent area(s) to peak response	AC-PC coordinates [mm]			Peak T value	Hemi-sphere
		ML	AP	DV		
5	MDP, MIP	6.0	-26.0	18.5	16.1	R
5	2.0	15.0	-15.5	20.0	8.1	R
7a	MSTd	17.0	-19.0	16.5	9.5	R
Aud		20.0	-16.5	13.0	9.5	R
DP	VIP, PIP	9.0	-26.5	17.5	16.1	R
FEF	6.0	-17.0	11.0	6.5	7.2	L
FEF	6	15.0	9.0	7.5	3.2	R
FST	PITd	-21.0	-15.5	0.0	13.1	L
LIP	VIP, 7a	16.0	-16.0	16.5	9.4	R
MDP	MIP, 5, 23, PO	-4.5	-29.0	19.5	13.8	L
MIP	MDP, 5	-5.0	-26.0	16.5	14.6	L
MSTI	STPp, MSTd	-22.0	-17.0	5.0	12.5	L
MSTI	STPp	21.5	-16.0	3.5	7.8	R
MT	MSTI, V4t, PITd	-20.5	-19.5	4.0	13.1	L
MT	MSTd, 7a, V4	16.5	-21.0	13.5	8.1	R
PITd	FST, MT	-24.0	-17.5	1.5	13.1	L
PITd	MT, V4t, V4	23.0	-18.0	1.0	8.2	R
PITv	PITd, VOT	28.5	-16.5	-2.5	6.7	R
PO		-3.0	-32.0	9.0	16.4	L
PO	MDP, 23, 30	2.5	-32.0	10.0	22.1	R
STPp	MSTI	-24.0	-15.0	4.0	11.3	L
STPp		28.0	-12.0	3.0	7.0	R
V1		-12.0	-40.0	9.0	20.1	L
V1		-10.5	-38.5	9.0	19.4	L
V1		-12.0	-43.0	9.0	20.1	L
V1		-13.5	-44.5	6.0	18.4	L
V1		-10.5	-39.5	6.0	20.1	L
V1		7.5	-44.0	5.0	19.2	R
V1		10.5	-37.5	8.5	15.5	R
V2		-10.5	-39.5	3.0	17.7	L
V2		-1.5	-37.0	11.0	21.4	L
V2	V1	10.5	-39.5	3.5	19.4	R
V2		16.0	-41.5	3.0	16.9	R
V2	V1	2.5	-35.5	11.0	22.1	R
V2		9.0	-30.5	18.5	15.6	R
V3		-9.0	-30.5	14.5	10.7	L
V3		9.5	-29.5	15.5	16.1	R
V4	VP	20.0	-31.0	-0.5	8.9	R
VIP	PIP, DP	-8.0	-25.0	17.0	14.6	L

Same conventions as for [Table 2](#).

Fig. 17: SPMs revealed by SPEMS.

BOLD responses to 15° horizontal smooth pursuit eye movements are shown as *T*-score maps ($p < 0.05$, corrected for multiple comparisons using *FDR*) on the flattened cortical reconstructions of the left (A) and right (B) hemisphere of monkey S. Spherical symbols represent the location of defined peak BOLD responses (Table 2). White star demarkates a cortical area at a location which could correspond to the *supplementary eye field*, *SEF*, (Schlag & Schlag-Rey, 1987; Felleman & Van Essen, 1991; Tehovnik, 1995; Tehovnik *et al.*, 2000). Same conventions as in Fig. 11.

Fig. 18: SPMs revealed by SPEMs within specific brain areas.

BOLD responses to 15° horizontal smooth pursuit eye movements are shown as *T*-score maps ($p < 0.05$, corrected for multiple comparisons using *FDR*) on transversal cutout (A) and parasagittal (B) brain sections. Dorsal-ventral position or medial-lateral position of section is indicated by line superimposed onto lateral or dorsal views of a 3D surface reconstruction of the cortex, respectively (right in A & B). Blue outline superimposed on transversal brain section indicates borders between grey and white matter that was used in order to create cortical surface reconstructions. Coloured arrows or coloured outlines indicate brain areas (rhesus monkey atlas, Felleman & Van Essen, 1991). Colour code and area names are given next to each brain section.

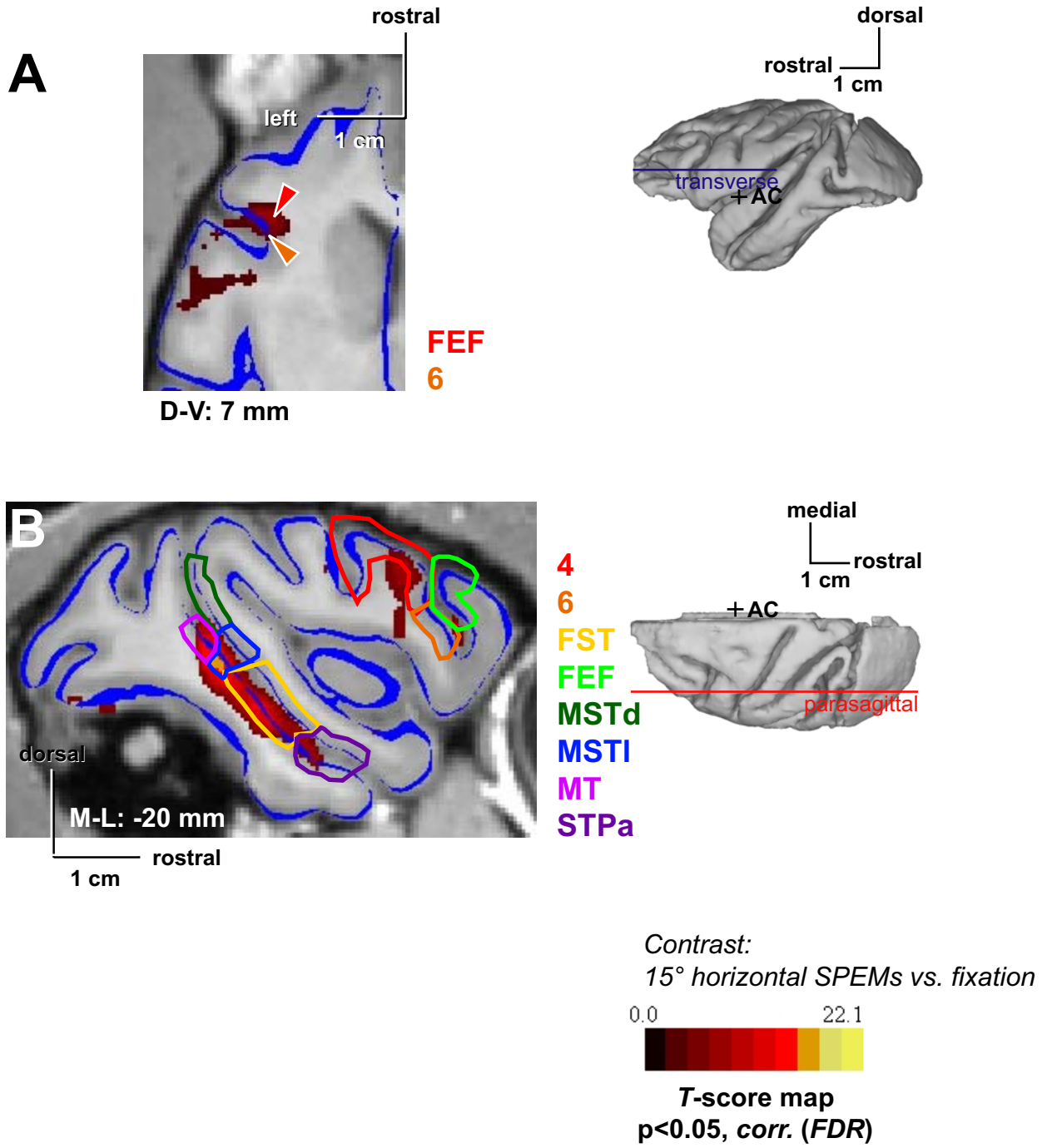
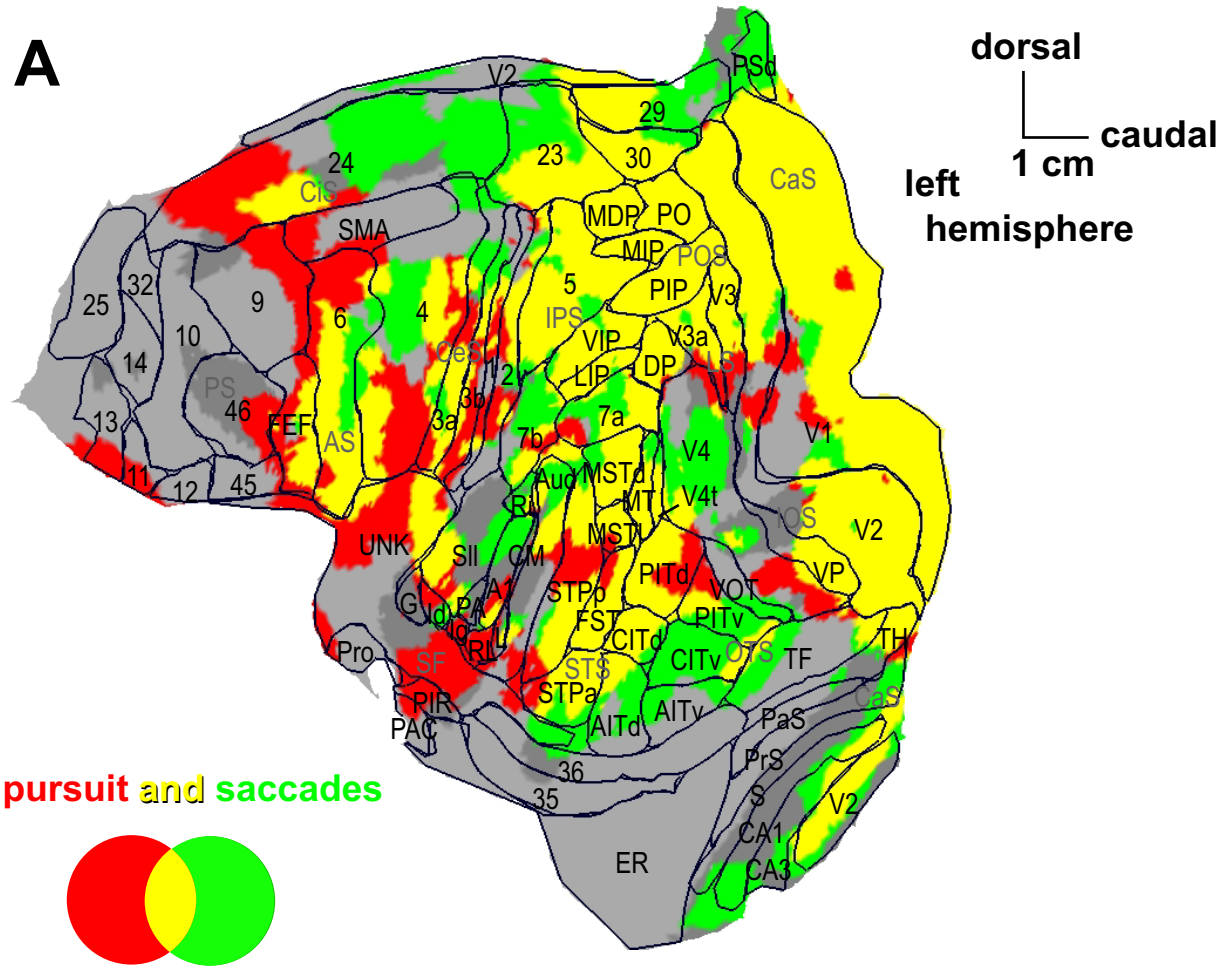


Fig. 19: SPMs revealed by saccadic eye movements and SPEMs.

BOLD responses to 15° horizontal saccadic eye movements (red colour, same *T*-score maps as shown in Fig. 15) and SPEMs (green colour, same *T*-score maps as shown in Fig. 17) are shown as *T*-score maps ($p < 0.05$, corrected for multiple comparisons using *FDR*) on the flattened cortical reconstructions of the left (A) and right (B) hemisphere of monkey S. Regions responding to both, saccadic and smooth pursuit eye movements are shown in yellow. Same conventions as in Fig. 11.

A



B

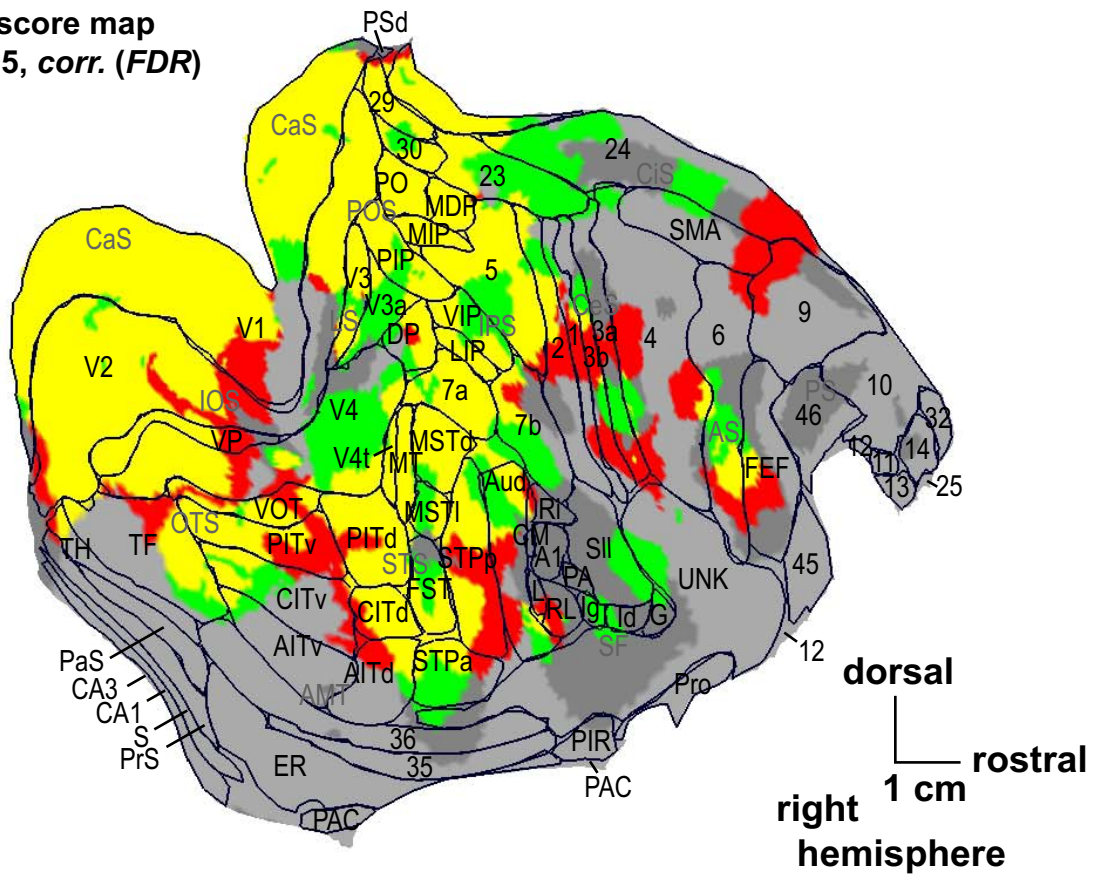
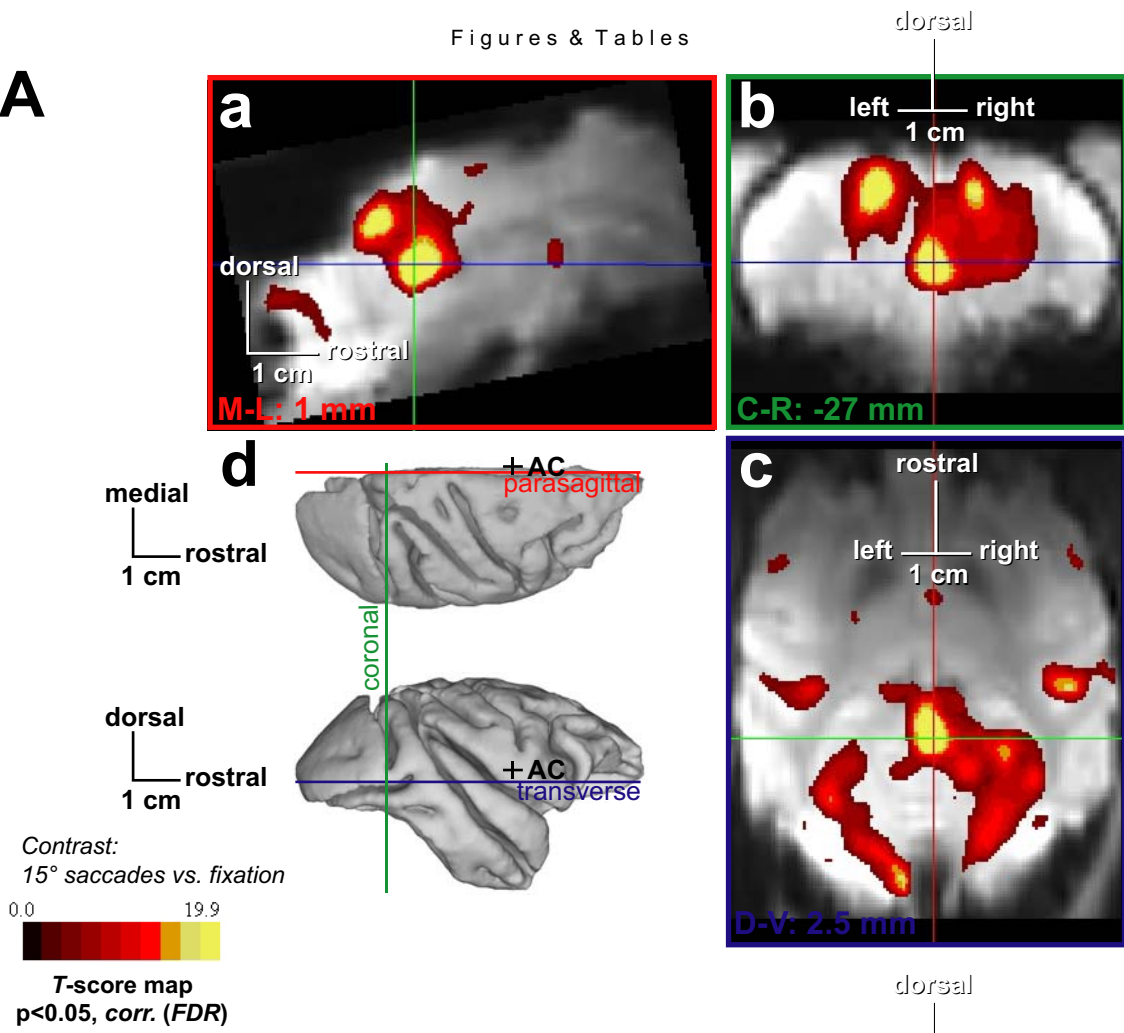


Fig. 20: SPMs revealed by saccade eye movements and SPEMs within the superior colliculus.

BOLD responses to 15° horizontal saccade eye movements (A) and 15° horizontal smooth pursuit eye movements (B) are shown as *T*-score maps ($p < 0.05$, corrected for multiple comparisons using *FDR*) on parasagittal (a), coronal (b) and transverse (c) brain sections, centered at the location of one peak response, at the putative position of the *superior colliculus*. Same conventions as in [Fig. 9A](#).

A



B

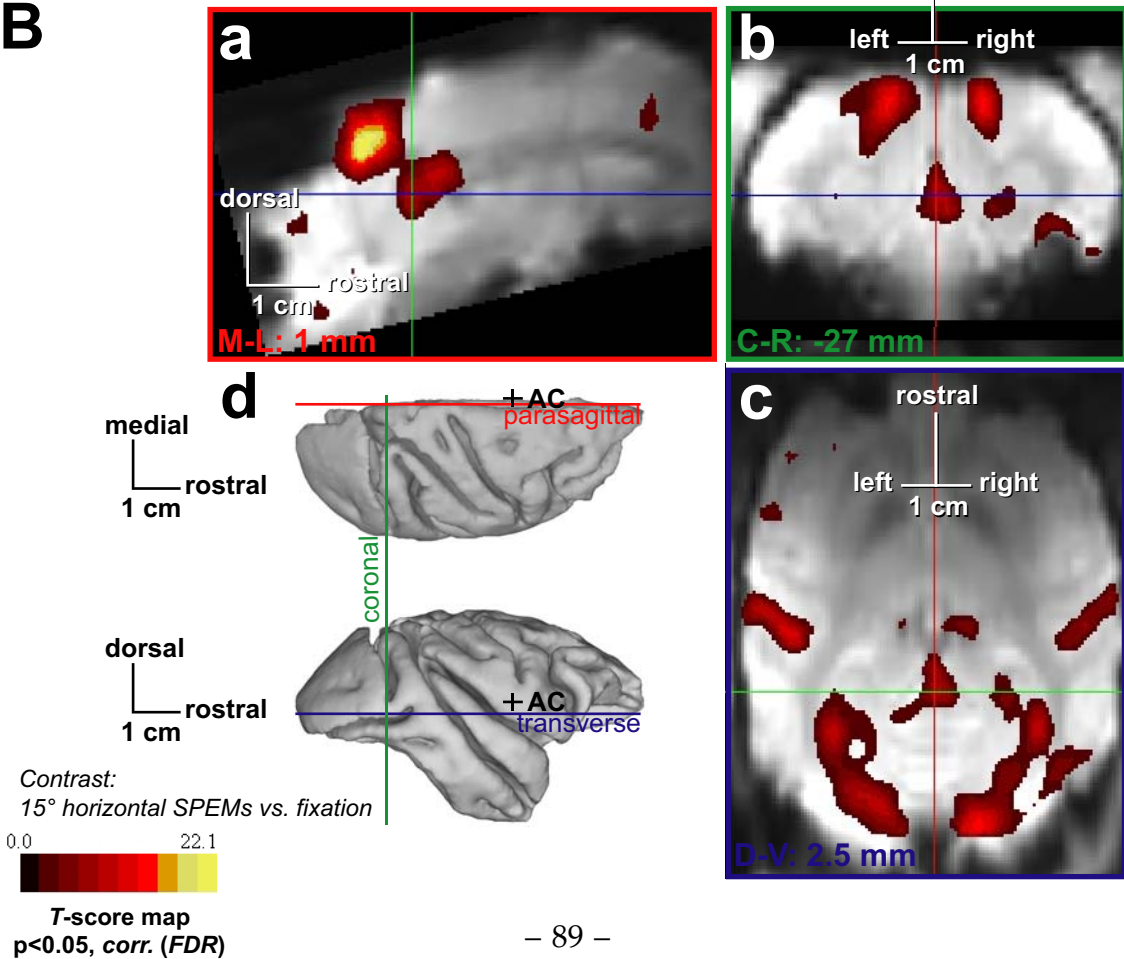


Fig. 21: Examples of image artefacts.

20 transversal slices of EPI images shown from left to right, line by line, from dorsal to ventral. Examples of various image artefacts are outlined with dashed, coloured lines: deletions, yellow; “ghosting” artefacts, blue; “zero-fill” artefacts, green. Red arrows show app. direction of image distortions. All images are shown in radiological convention (left on right).

EPI images, transversal slices, dorsal to ventral

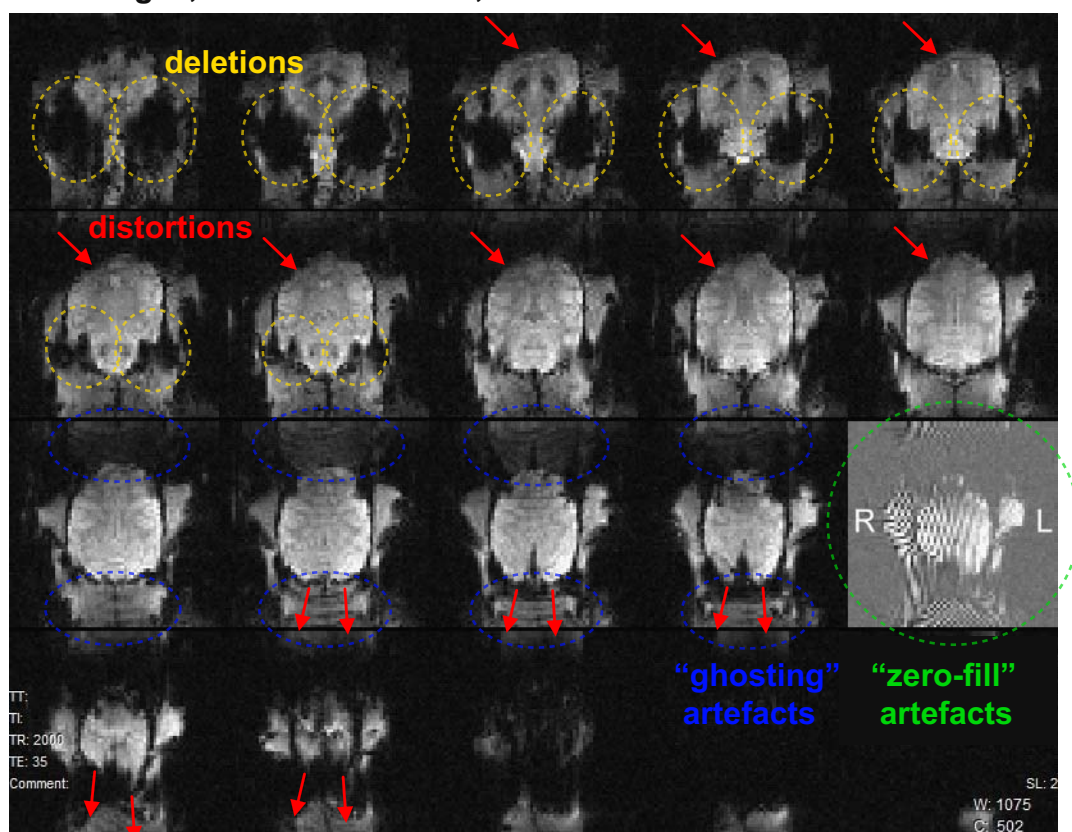


Fig. 22: Inhomogeneous illumination of surface coil configuration and distortions of functional images.

(A) Mid-sagittal (a) and transversal (b) sections of structural images measured using the surface coils that were used for functional imaging. Image brightness decreases with increasing distance from surface coil. In this configuration, occipital cortex is well illuminated, but frontal cortex is insufficiently illuminated.

(B) In order to illustrate the quality and validity of the alignment between structural (a) and spatially co-registered functional mid-sagittal sections (b), the corpus callosum and cerebellum are outlined red in (a) and the same outline is then superimposed onto the functional image. While alignment of corpus callosum in the functional section is fair with respect to its corresponding counterpart in the structural section, the cerebellum appears relatively distorted. Note that, beside the contrast (T1 vs. T2*) also spatial resolution differs between (a) and (b) (see text). Cross of green and blue line marks the location of the anterior commissure.

Structural image in (Ba) is measured using a standard knee coil, rather than the surface coils that were used in (A) and (Bb), providing a homogeneous illumination.

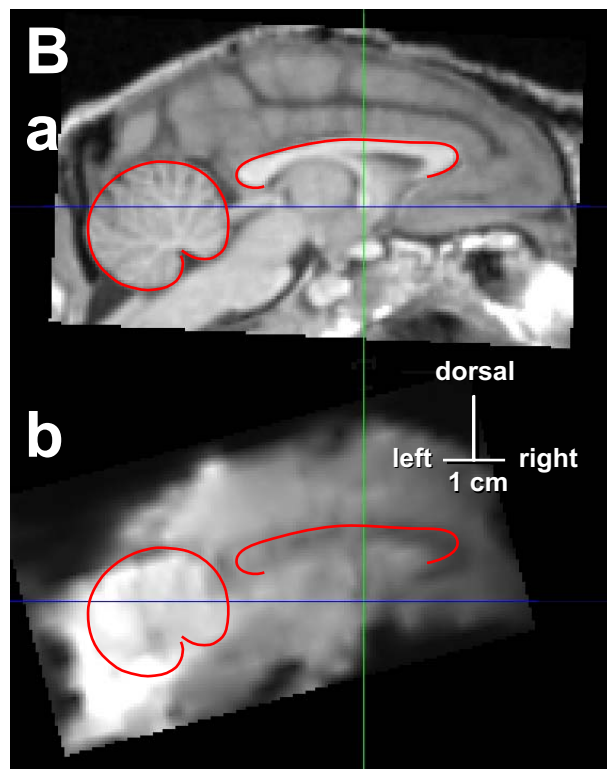
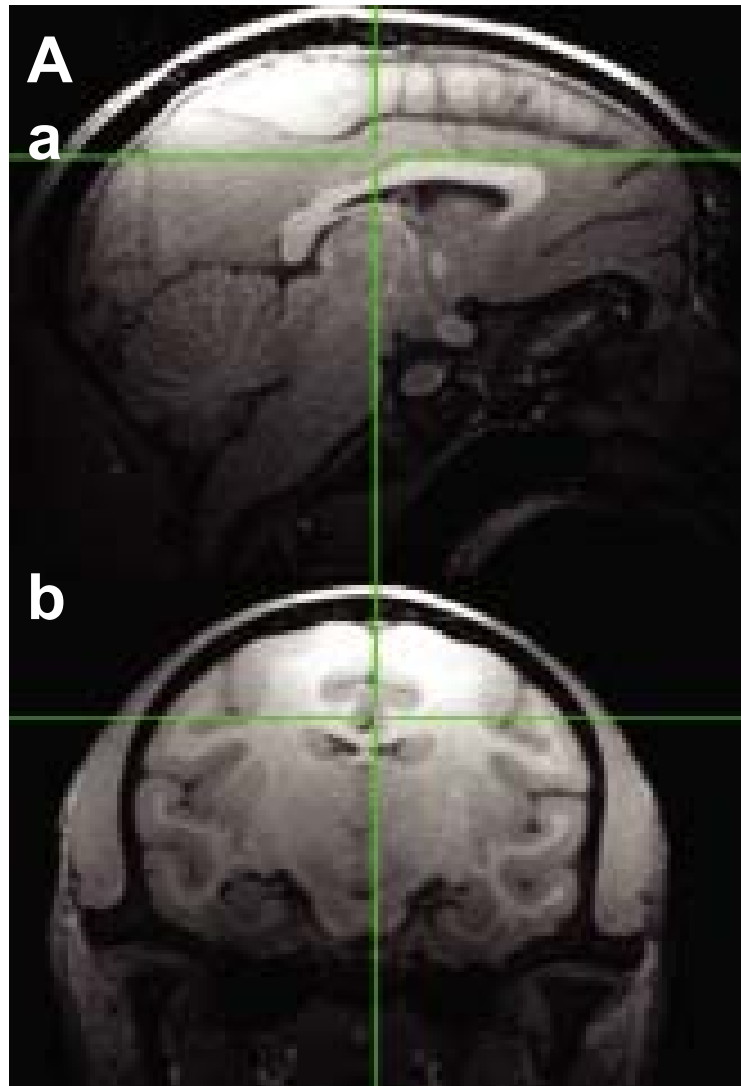


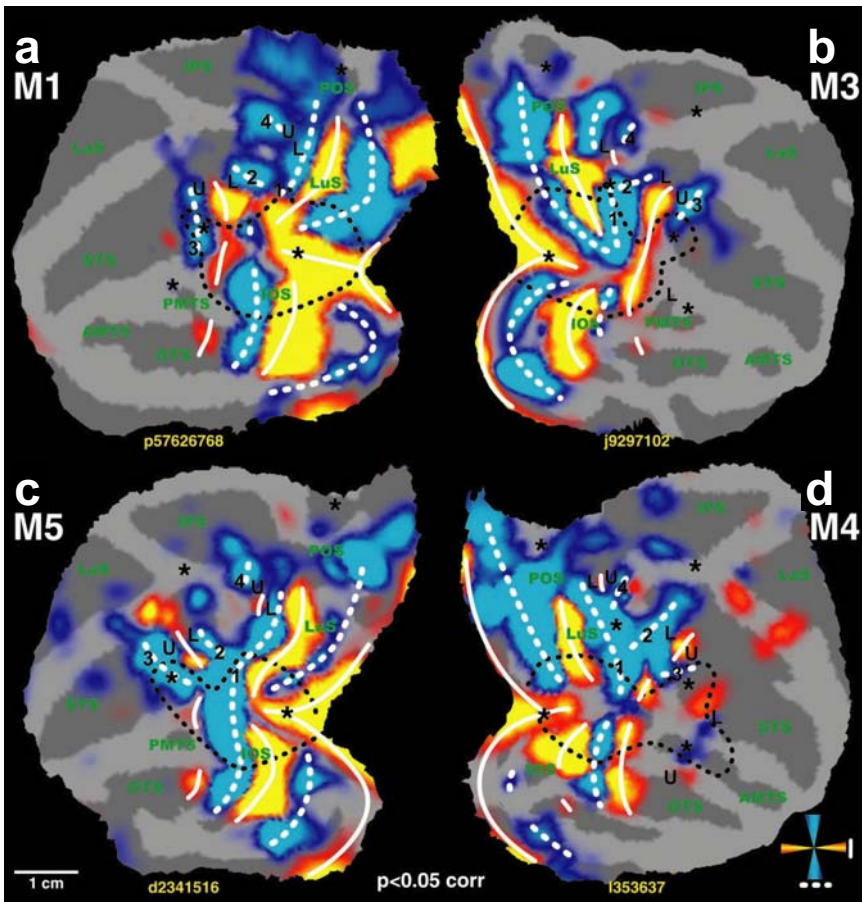
Fig. 23: Representation of meridians and different degrees of eccentricity of the visual field (figures taken, with kind permission, from Fize *et al.*, 2003).

(A) T-score maps ($p < 0.05$, corrected for multiple comparisons using *FWE*) of representations of the horizontal (red-yellow) and vertical (blue-turquoise) meridian of the visual field on flattened cortical reconstructions of left hemispheres of monkey M1 and M5 and right hemispheres of monkey M3 and M4.

(B) T-score maps ($p < 0.05$, corrected for multiple comparisons using *FWE*) of representations of central 1.5° (a), $1.5-3.5^\circ$ (b), $3.5-7^\circ$ (c), and $7-14^\circ$ (d) eccentricity of the visual field on flattened cortical reconstructions of left and right hemispheres of monkey M1.

MION (*Monocrystalline Iron Oxide Nanoparticle*) was used as as contrast agent. White solid and dashed lines represent the horizontal and vertical meridians, respectively. Labels “1”, “2” and “3” in (A) correspond to different vertical meridian representations in the region surrounding the prelunate gyrus. Label “4” (A) corresponds to the putative anterior border of *area V3A*. Black dashed line (A) indicates the contour of the central 1.5° eccentricity line. Stars indicate additional foveal activations. “L” and “U” labels indicate the locations of the lower and upper field representations. *IOS*, *inferior occipital sulcus*; *OTS*, *occipitotemporal sulcus*; *STS*, *superior temporal sulcus*; *LaS*, *lateral sulcus*; *IPS*, *intraparietal sulcus*; *POS*, *parieto-occipital sulcus*; *LuS*, *lunate sulcus*.

A



B

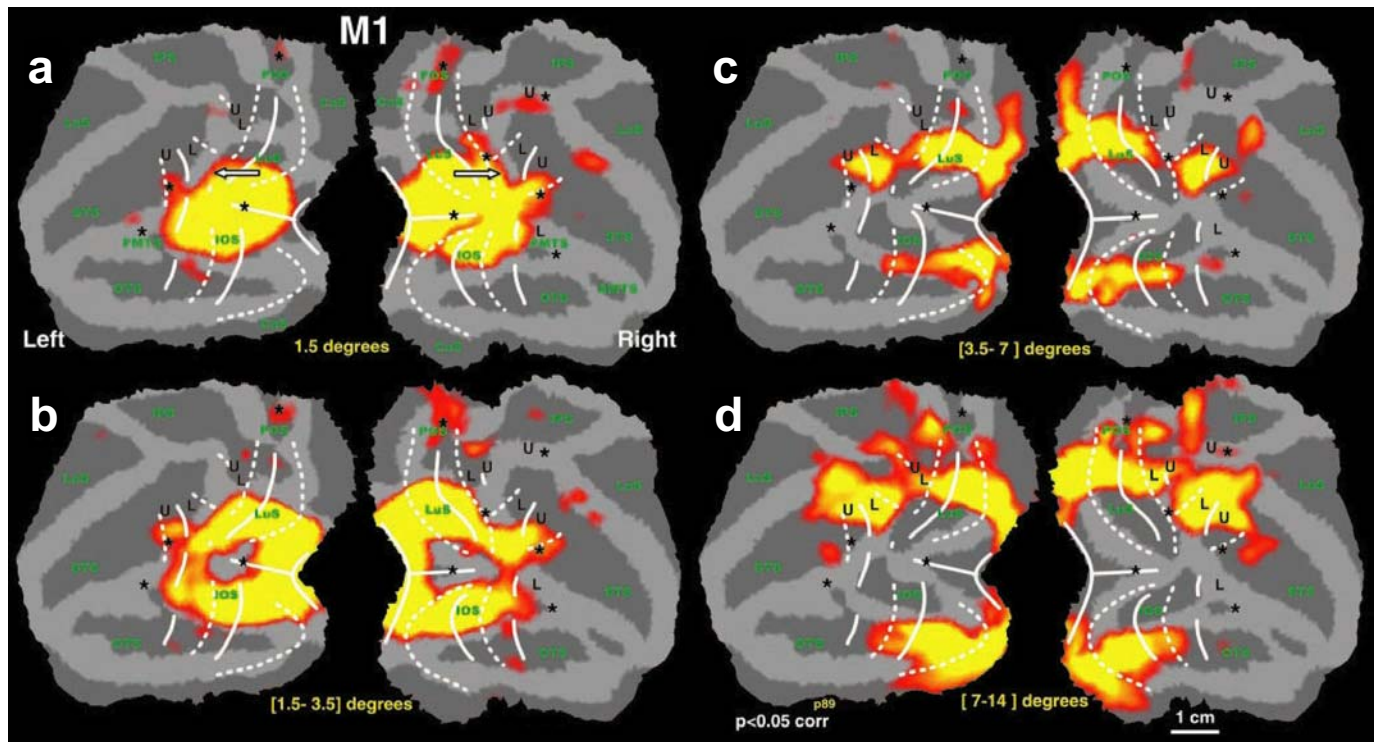


Table 5: Comparison of cortical brain areas in frontal, parietal, temporal and occipital cortex involved in saccadic eye movements and SPEMs across different studies.

		S A C C A D E S			S P E M s	
		<i>Koyama et al., 2004</i> (3 monkeys)	<i>Baker et al., 2005a</i> (2 monkeys)	<i>Present study</i> (1 monkey)	<i>Baker et al., 2005b</i> (3 monkeys)	<i>Present study</i> (1 monkey)
Cortical areas in frontal cortex						
4	Primary motor			(x)	x	
6	Premotor	x	(x)	x	x	(x)
46	Visual	x	(x)			x, unilat.
FEF	Visual	x	x	(x)	x	x
SEF	Visual	x, unilat.	x, unilat.			x, unilat.
Cortical areas in parietal cortex						
2	Somatosensory					(x)
5	Somatosensory	x		x		x
7a	Visual	x		x		x
7b	Somatosensory	x				
AIP	Visual	x				
DP	Visual	x		x		x
LIP	Visual	x	x	x		x
MDP	Visual			(x)		x
MIP	Visual			x		x
MST	Visual		x	x	x	x
PIP	Visual		x	x	x	(x)
PO	Visual			x		x
VIP	Visual	x		(x)		x
Cortical areas in temporal cortex						
Aud	Auditory			x		x
AIT	Visual					
CIT	Visual			x		
FST	Visual		x, unilat.	x	x	x
PIT	Visual			x		x
STP	Visual		x, unilat.	(x)		x
TF	Visual			(x)		
Cortical areas in occipital cortex						
MT	Visual		x	x	x	x
V1	Visual	?	x	x	x	x
V2	Visual	?	x	x	x	x
V3/V3a	Visual	x	x, unilat.	x	x	x
V4/V4t	Visual	x	x, unilat.	x	x	x
VOT	Visual			x		(x), unilat.
VP	Visual					(x)

Legend:

- BOLD response in 3 of 3 studies on saccade eye movements
- BOLD response in 2 of 3 studies on saccade eye movements
- BOLD response in 1 of 3 studies on saccade eye movements
- BOLD response exclusively to SPEMs in study of same group
- BOLD responses to saccades and SPEMs in study of same group
- x Area with peak BOLD response
- (x) Area adjacent to area with peak BOLD response
- unilat. unilateral BOLD response

3. Results

3. Results

3.1: Presentation of BOLD responses.

SPMs are represented, superimposed onto structural images or projected onto cortical surface reconstructions as T -score maps ($p < 0.05$, corrected for multiple comparisons, using false discovery rate, FDR). Additionally, loci of BOLD responses to optic flow and to oculomotor activity are summarized in tables showing coordinates of peak T -score values (local maxima, manually defined, based on projected *statistical parametric maps*, SPMs) and corresponding area names. Area borders and names are superimposed onto flat cortical surface reconstructions based on an atlas (Felleman and Van Essen, 1991) that was morphed onto the cortical surface reconstructions of monkey S (see *section 2.6*). For abbreviations of cortical area names, see Fig. 11. In the following, I refer to BOLD responses as evoked by the *processing* of optic flow/saccade/SPEM stimuli just as BOLD responses to optic flow/saccades/SPEMs.

3.2: Visual field mapping

Representation of meridians of the visual field. Fig. 12A-B shows the representation of the horizontal and vertical meridian of the visual field. SPMs in proposed areas include, among a few others, bilaterally, visual cortical *area V1* through *area V4*, *central inferotemporal area, CIT* (or *area TE*) and *posterior inferotemporal area, PIT* (or *area TEO*), as well as, bilaterally, *middle temporal visual area, MT*, *medial superior temporal visual area, MST*, *ventral intraparietal area, VIP*, *lateral intraparietal area, LIP* and *area 7a*. The SPMs of horizontal (shown in red in Fig. 12A-B) and vertical meridians (shown in green in Fig. 12A-B) show overlap of various areas (shown in yellow in Fig. 12A-B).

Representation of different degrees of eccentricity of the visual field. Fig. 12C-D shows the representation of different degrees of eccentricity of the visual field. The overall extent of the SPM representing annuli covering 2-3.5° and 18-22° is comparable to the overall extent of the SPM representing the meridians. While BOLD responses to the more central annulus (shown in red in Fig. 12C-D) are centred on more rostral parts of the primary visual cortex, the more peripheral annulus (shown in green in Fig. 12C-D) is represented along the *calcarine sulcus*.

3.3: Optic flow

Fig. 13 shows BOLD responses to optic flow stimuli, either covering the right visual hemifield (A, only left cortex shown) or covering the left visual hemifield (B, only right hemisphere shown). Maximum T -values of the SPM (Fig. 13 and Table 2), include visual areas $V1$, $V2$ and $V3$, $V3a$ and MT in the occipital lobe and areas $7a$, DP , LIP , MDP , $MSTd$, PIP and VIP in the parietal lobe; non-visual areas showing strong BOLD responses were area 5 as well as a locus within the auditory cortex. All mentioned areas responded bilaterally, albeit with different levels of significance (see T -value legend in Fig. 13). BOLD responses and especially peaks of BOLD responses often covered brain areas only partly and often spread to adjacent brain areas. Fig. 14 shows bilateral BOLD responses within the motion complex MT/MST ($MSTd$) on a transversal brain section.

3.4: Voluntary eye movements

Saccadic eye movements. Fig. 15 shows BOLD responses to 15° horizontal saccadic eye movements. Maximum T -values of the SPM (Fig. 15 and Table 3), include visual areas $V1$, $V2$ and $V3$, $V4$, $V4t$, VOT and MT in the occipital lobe and areas $7a$, DP , LIP , MIP , $MSTd$, $MSTl$, PIP and PO in the parietal lobe; non-visual areas showing strong BOLD responses were area 5, 6, 24, 29, $CA3$, as well as a locus within the auditory cortex. All mentioned areas responded bilaterally, albeit with different levels of significance (see T -value legend in Fig. 13), except a locus centred at $CA3$ that responded unilateral only in the left hemisphere. BOLD responses and especially peaks of BOLD responses, often covered brain areas only partly and often spread to adjacent brain areas. Beside area names, Table 3 lists names of adjacent areas whenever the peaks of BOLD responses were projected close to area borders on the cortical surface reconstruction. Fig. 16 shows parietal BOLD responses including areas DP , LIP , MIP , VIP and others on a transverse brain section (Fig. 16A), the FEF in frontal cortex on a cut-out transverse section (Fig. 16B) and BOLD responses along the STS , including areas MT and MST on a parasagittal section (Fig. 16C).

Smooth pursuit eye movements. Fig. 17 shows BOLD responses to 15° horizontal SPEMs. Maximum T -values of the SPM (Fig. 17 and Table 4), include visual areas $V1$, $V2$ and $V3$, $V4$ and MT in the occipital lobe; areas $7a$, DP , LIP , MDP , MIP , $MSTl$, PO and VIP in the parietal lobe; areas FST , $PITd$, $PITv$ and $STPp$ in the temporal lobe; non-visual areas showing strong BOLD responses were area 5, as well as a locus within the auditory cortex. All mentioned areas responded bilaterally, albeit with different levels of significance (see T -value legend in Fig. 13). BOLD responses and especially peaks of BOLD responses often covered brain areas only partly and often spread to adjacent brain areas. Beside area names, Table 4 lists names of adjacent areas, whenever the peak of a BOLD response was projected close to area borders on the cortical surface reconstruction. Fig. 18 shows BOLD

responses superimposed onto structural brain sections in frontal cortex, including the *FEF* (Fig. 18A and 18B), and along the *STS*, including *areas MT* and *MST* (Fig. 18B).

Saccadic vs. smooth pursuit eye movements. Fig. 19 combines the SPMs of Fig. 15 and Fig. 17 on a single cortical surface reconstruction. In the resulting SPM, fractions specific to saccades are shown in green, fractions specific to SPEMs are shown in red and fractions showing overlap are shown in yellow. BOLD responses overlap at various locations, most strongly and bilaterally in areas 4, 6, 7a, 29, 30, *FEF*, *FST*, *PITd*, *PO*, *MDP*, *MIP*, *MSTd*, *MSTl*, *PIP*, *STPp*, *TF*, *V1*, *V2*, *V3*, *V3a*, *V4* and *VIP*.

3. Results

4. Discussion & Conclusions

4.1: Technical constraints

Due to the presence of strong artefacts and distortions in functional images, the correct assignment of sites of BOLD responses to identified anatomical substrates is likely to be erroneous at affected sites in the present study. In addition to prevent reliable *localization* of the observed BOLD responses, technical constraints may also have prevented the *detection* of BOLD responses. For example, BOLD responses could not be reliably and reproducibly observed in the cerebellum and at subcortical brain sites in the present study. Therefore, we were not able to answer one of the main questions of the present study, regarding a possible involvement of the cerebellum in motion processing.

Before discussing the results of the present study in more detail, I will summarize the present technical constraints.

Image artefacts. In the following, I will discuss prominent functional image artefacts which could be observed in the present study, including examples shown in Fig. 21. MR images can contain various types of artefacts that represent limitations in the hard-/software of the MR scanner, reflect environmental influences or are induced by objects that are present in the MR scanner (<http://www.mr-tip.com>). Artefacts representing the limitations in the hard-/software of the MR scanner may occur spontaneously, but only at rare instances, such as *zero-fill artefacts* that produce zebra stripe patterns in MR images and are caused by zero filled data in k-space (see *section 1.1*) prior to Fourier transformation.

The most prominent artefacts in the present study were caused by body movements of the monkey. Body movements can cause various types of MR image artefacts. As mentioned earlier, *field shimming* procedures can be applied in order to compensate for field homogeneity changes before the start of image acquisition. Object movements during scanning lead to new changes in the magnetic field that

are not compensated and thus induce MR image artefacts.

Distortions of images reflect field homogeneity changes. Those changes are induced by magnetic susceptibility properties inherent in all objects (e.g. the subject, implants, primate chair, camera, reward system etc.) that are brought into the B_0 field of the MR scanner. MR sequences for EPI, *designed to detect* slight magnetic susceptibility differences between Hb and dHb , are also especially prone to those *unwanted* susceptibility effects of objects present in the MR scanner. EPI images obtained in the present study were mostly affected by distortions in occipital lobe and cerebellum which appeared app. 8 mm stretched in phase encoding (caudal) direction (Fig. 22B). Magnetic field inhomogeneities in regions of the brain close to bone, air-filled sinuses (especially in the temporal lobe, close to the *ossis temporalis* and *tympanum*) or liquor-filled ventricles result in reduced signal-to-noise ratio and signal loss which constitutes *deletions*.

Field homogeneity changes due to object movements commonly cause *ghosting artefacts* in EPI. Inhomogeneities in the B_0 field cause a modulation in k-space, leading to one or more ghost images at relatively shifted positions in phase encode direction (Clare, 1997). In the present study, ghosting artefacts occurred occasionally.

EPI sequence parameters. We did not systematically analyse the effects of variations in sequence parameters on the quality of functional MR images, which would be critical to find the optimal settings. In an attempt to reduce image artefacts and yield a high SNR, we nevertheless varied parameters such as phase encoding direction, orientation of slices or TE. For BOLD contrasts, it has been demonstrated that decreasing the TE increases the SNR and reduces the amount of susceptibility artefacts (Gorno-Tempini *et al.*, 2002). Due to the fact that BOLD contrasts are dependent on the TE, it can only be varied within a limited range.

Coil configuration. The SNR of MR signals was better for parts of the brain lying close to the coils than for those lying at a distance (Fig. 22). BOLD responses

observed in areas lying in frontal brain parts and that were expected to respond strongly to stimuli – as e.g. the frontal eye fields during oculomotor activity – showed only low statistical significance in *T*-score maps, a fact, which may reflect the lowered SNR, relatively to occipital brain parts. Despite the fact that positioning of the surface coils above the skull was suitable to cover the cerebellum, we could not reliably and reproducibly show BOLD responses within the *cerebellum* and most subcortical structures. This might have to be attributed to the profound image distortions present in those brain structures.

In order to obtain homogeneous *structural* images, we used a standard knee coil that covered all parts of the brain. In those experiments, the monkey had to be anaesthetized in order to position the head of the monkey inside the coil and scan for long periods of time without movements.

Eye-gaze-control. Although *eye-gaze-control* was used for behavioural control (see *section 2.2*), occasionally, the control mechanism had to be deactivated due to the presence of strong artefacts in the video signal that originated from MR scanning procedures. Fig. 7 shows representative eye position traces for saccades, SPEMs and fixation recorded during MR scanning with artefacts marked in red colour. *Eye-gaze-control* was deactivated (a) permanently during image acquisition in the visual field mapping paradigm in the early phase of the present study when procedures were still to be improved, (b) never in the optic flow paradigm and (c) temporarily (15-25%) in saccadic eye movement and SPEM paradigms. Eye position and oculomotor behaviour was still observed by the experimenters during periods of deactivation of *eye-gaze-control* and trials were interrupted immediately whenever the monkey did not fulfil the (oculomotor) requirements of the task. It is possible, albeit unlikely, that accuracy and proper performance of eye movements were different in periods in which *eye-gaze-control* was deactivated with respect to those periods when *eye-gaze-control* was activated. Consequently, the monkey may have performed unwanted eye movements in periods

requiring fixation. In the saccadic eye movements and SPEMs paradigms, amplitudes of eye movements may have been too long or too short. Furthermore, by moving eyes away from the target, the visual field may have been stimulated differently than intended. However, monkey S was trained extensively to perform tasks and fulfil the oculomotor requirements with high accuracy in the dummy scanner, where eye-gaze-control was always active.

Presentation screen. Back-projection of stimuli using a conventional LCD projector has the disadvantage that it produces background luminance within the projection area that cannot be eliminated by varying contrast and brightness parameters of the projector control software. Therefore, eye movements relative to the screen (as requested during saccadic eye movements and SPEM paradigm, or resulting from eye movements inside the tolerance window during fixation) represented relative movements of the weakly illuminated area of the screen and the dark surrounding within the visual field. As a consequence, screen borders exhibited undesirable contrast changes. Additionally, reflections of light at the walls of the MR scanner bore were likely to constitute undesirable peripheral stimuli.

Auditory noise. The monkey wore ear protection and was adapted to the presence of noise. Therefore, it is unlikely that the monkey was distracted by scanner noise. Unexpectedly, parts of the auditory cortex were included in SPMs of all stimulus contrasts discussed here (Fig. 12, 13, 15 and 17). Since auditory noise originating from the MR scanner was equal in all experimental conditions and because there is no obvious reason why the acoustics should have differed between stimulation conditions, we have to consider it as artefact that probably originated from misalignment or misprojection of functional data (see below).

Misalignment of functional and structural images. While alignment between functional images and structural images was accurate in some parts of the brain, such as the *corpus callosum* in Fig. 22B, other brain parts of functional images were shifted and distorted relative to structural images, such as e.g. occipital cortex or

the *cerebellum* in Fig. 22B. Because most brain areas were identified on the basis of the high-resolution structural images that revealed anatomical details better than functional images, misinterpretation may have been made whenever misalignment between functional and structural data was present. The occipital cortex and the *cerebellum* seemed to be stretched out in caudal direction in functional images relatively to structural images. Such distortions cannot be expected to be linear and it is very hard to define portions of the brain volume which are affected. Available methods for compensating field distortions in functional images are optimized for human brains (dependent on spatial normalizations) and cannot be applied to monkey brains, without adaptations. We cannot quantitatively report the dimensions and impact of artefacts in the present study. However, a visual inspection, as e.g. in the example shown in Fig. 22B, can provide a rough estimate. The occipital lobe and the *cerebellum* appeared to be mostly affected by image distortions. While frontal brain parts suffered from a low SNR, occipital brain parts were heavily subjected to image distortions and deletions were present in the temporal lobes. The parietal lobes may have exhibited the best alignment accuracy between structural and functional brain volumes.

Misprojection of functional data onto cortical surface reconstructions. Similar problems to the above mentioned, apply to projections of SPMs onto the cortical surface reconstructions: whenever functional and structural brain volumes were misaligned, projections onto the surface reconstructions were incorrect. Therefore, the superimposed atlas onto the cortical surface reconstruction may have led to wrong assumptions when attributing (miss-projected) BOLD responses to brain areas. Voxel projected onto the cortical surface reconstruction were those contained within both the SPM and a cube of a dimension of $5 \times 5 \times 5$ mm, centred at each node of the triangulated cortical surface reconstruction. If, however, due to image distortions, voxel of the SPM were shifted with respect to structural images, the assignment of voxel to nodes of the cortical surface reconstruction were

erroneous. This may have resulted in either misprojection, or a complete loss of functional data projections onto the cortical surface reconstruction.

Deviations of brain areas from atlas. Besides the fact that the projection of functional data onto the surface reconstructions may be partly incorrect, the atlas (Felleman and Van Essen, 1991) may also deviate from the functional architecture of the individual. The atlas was morphed onto the surface reconstruction using landmarks, including various sulci and gyri (Fig. 10). Even an accurate alignment of surface structures (as e.g. gyri and sulci) does not exclude the possibility that atlas area-borders may locally vary, with respect to landmarks between atlas template and individual. Therefore, all area borders, as shown superimposed onto cortical reconstruction, can only approximate the actual area borders of the individual. However, whenever “functional localizers” are used, i.e. stimuli that allow a prediction of sites of BOLD responses, area localization can be validated. Such a functional localizer could be represented by visual motion stimuli that are expected to elicit BOLD responses within ‘*motion complex*’ MT/MST (Fig. 13).

Definition of BOLD response peaks. As mentioned earlier, BOLD response peaks were manually defined, based on projections of BOLD responses onto the cortical surface (see spherical symbols in Fig. 13, 15 and 17). However, the definition of peak responses underlie subjective criteria, since smoothing and minimal peak separation parameters are arbitrary, chosen at best estimate by the experimenter. Consequently, loci adjacent to BOLD response peaks should be taken into consideration. Tables 2, 3 and 4 list names of adjacent areas that appeared to be associated with the defined peak locations.

4.2: Visual field mapping

In initial monkey fMRI experiments of the present study, stimuli were chosen that allowed validation of the methods. Visual field mapping stimuli were selected, because of the availability of retinotopic maps provided by fMRI studies on anaesthetized (Logothetis *et al.*, 1999; Brewer *et al.*, 2002) or awake (Fize *et al.*, 2003) monkeys. Although properties of stimuli used in the present study – including spatial frequency, flicker frequency, stimulus contrast, incorporation of the retinal magnification factor – were not chosen optimally, SPMs bilaterally included areas known to have a retinotopic organization *area V1* through *area V4*, *area CIT* (or *area TE*), *area PIT* (or *area TEO*), as well as, *area MT*, *area MST*, *area VIP*, *area LIP* and *area 7a* (Felleman and Van Essen, 1991; Logothetis *et al.*, 1999; Brewer *et al.*, 2002; Fize *et al.*, 2003; Tootell *et al.*, 2003; Van Essen, 2003).

In the following, I will discuss similarities and differences of retinotopic maps obtained in the present study and the study of Fize *et al.* (2003). In their study, Fize and coworkers (2003) presented a set of stimuli to four rhesus monkeys in order to map the retinotopic organization throughout the visual cortex. Fize and coworkers (2003) used a contrast agent (*MION*, *Monocrystalline Iron Oxide Nanoparticle*, a dextran-coated iron oxide agent) at a conventional 1.5 T scanner to improve SNR by a factor of app. 3-5 (Vanduffel *et al.*, 2001; Leite *et al.*, 2002; Vanduffel *et al.*, 2002; Fize *et al.*, 2003). Other than BOLD fMRI responses, MION fMRI responses are dependent on blood volume rather than on blood oxygenation.

Representation of meridians of the visual field. Borders between early visual areas *V1*, *V2*, *V3* and *V4* are characterized by representations of meridians illustrated in Fig. 23A of Fize and coworkers (2003). The first vertical meridian representation is known to be confined to the anterior border of *area V1*, the second horizontal meridian, to the anterior border of *area V2* and the second vertical meridian representation to the anterior border of *area V3* in dorsal and ventral occipital cortex (Daniel and Whitteridge, 1961; Van Essen *et al.*, 1984). We failed to

obtain a similarly ordered pattern in monkey S (Fig. 12A-B). Representations of horizontal and vertical meridians largely overlapped, spanned multiple areas and did not appear to delineate area borders. A possible explanation could be undesired eye movements of the monkey during periods in which eye-gaze-control was deactivated (see above). Eye movements of the monkey would have prevented the consistent stimulation of defined parts of the visual field.

Representation of different degrees of eccentricity of the visual field. SPMs obtained for monkey S, using annuli of different eccentricities, appear to match the meridian representations of corresponding stimuli that were obtained by Fize and coworkers (2003) more closely (Fig. 23B). However, stimuli that were used in the present study differed from those used by Fize and coworkers (2003) in their degree of eccentricity. In the present study the more central annulus spanned app. 2-3.5° (Fig. 12C-D, red colour) – in the study of Fize and coworkers (2003) the central stimulus covered the central 1.5° (Fig. 23Ba). The more peripheral annulus in the present study spanned 18-22° (Fig. 12C-D, green colour) – whereas the most eccentric stimulus of Fize and coworkers (2003) covered 7-14° (Fig. 23Bd). Additionally they included annuli spanning 1.5-3.5° (Fig. 23Bb) and 3.5-7° (Fig. 23Bc). Fig. 23Ba-d shows how SPMs resulting from consecutive stimulation of *central* parts towards *peripheral* parts of the visual field extend from *rostral* parts of the visual cortex along the *calcarine sulcus*. Similarly, the representation of the annulus spanning 2-3.5° in the present study lies more rostral than the representation of the annulus spanning 18-22°, which appears centred along the *calcarine sulcus*. Hence, despite the fact that representations of the meridians shared only a low degree of similarity with those of Fize and coworkers (2003), representations of different degrees of eccentricity fulfilled expectations.

4.3: Optic flow

Motion processing has been investigated using fMRI in anaesthetized (Tolias *et al.*, 2001) and alert (Vanduffel *et al.*, 2001; Vanduffel *et al.*, 2002) monkeys (for review of monkey fMRI studies and comparison to human fMRI studies, see Orban *et al.*, 2003). With moving dots (comprising *coherent motion* in one of eight randomly selected directions) Vanduffel and coworkers (2001) – in their fMRI study, using conventional 1.5 T scanners and *MION* as contrast agent (see *section 4.2*) – could demonstrate motion sensitivity in *areas V2, V3, MT, MSTv* (or *MSTl*, ventral-lateral), *FST, VIP* and *FEF* in alert, fixating monkeys. Furthermore, when random lines were presented instead of random dots, the following areas added to the list: *areas V4, CIT (TE), LIP* and *PIP*. The present study confirmed motion sensitivity in all above-listed areas, by using moving dots (comprising *optic flow*, see *section 2.3*) (Fig. 13), with exception of the *FEF* and *area CIT*.

Areas MT/MST. As expected, contralateral BOLD responses were found prominently within the motion sensitive *areas MT/MST* (Desimone and Ungerleider, 1986; Ungerleider and Desimone, 1986a; Ungerleider and Desimone, 1986b) (Fig. 14). The observed BOLD responses to optic flow stimuli in *area MST* in the present study are also in line with human fMRI studies. A recent fMRI study (Smith *et al.*, 2006) has investigated BOLD responses to optic flow in human areas homologous to macaque *areas MT* and *MST* and, similar to previous human fMRI studies (Zeki *et al.*, 1991; Tootell *et al.*, 1995), contributed with evidence for the existence of those homologues. While human *area MT* was demonstrated to respond to a variety of moving dot patterns – including random motion – human *area MST* was shown to be strongly driven by optic flow stimuli, which contained multiple flow components (as e.g. expansion, contraction and rotation).

Motion sensitivity. Results of the present study are in agreement with single unit data on motion sensitive brain areas (for review, see Orban *et al.*, 1986). *Areas MT, MST, VIP, PO* and layers *4B* and *6* of *area V1* contain more than 60%, *area V3*

and the *thick stripes* of *area V2* contain nearly 40% direction-selective neurons (Felleman and Van Essen, 1987; Peterhans and von der Heydt, 1993; Levitt *et al.*, 1994; Gegenfurtner *et al.*, 1997; as cited by Vanduffel *et al.*, 2001). With exception of *PO*, SPMs covered all the above mentioned areas in the present study, similar to SPMs shown by Vanduffel and coworkers (2001), with the exception that *area V1* was not included in SPMs of their study (see below). Similar to the SPMs shown by Vanduffel and coworkers (2001), SPMs in the present study also included areas that were not specifically implicated in motion processing previously, such as *areas PIP, LIP* and *V4*. We cannot exclude the possibility that the observed BOLD response in *area LIP* in the present study reflect overt or suppressed eye movements, although the latter is unlikely (Gottlieb and Goldberg, 1999; as cited by Vanduffel *et al.*, 2001). By including eye movement information as covariates of no interest into the general linear model of their statistical analysis, Vanduffel and coworkers (2001) explicitly removed effects of overt eye movements in the statistical analysis for one of their monkeys and still observed fMRI responses in *area LIP*.

In addition to areas reported by Vanduffel and coworkers (2001), in the present study SPMs included large parts of *area V1* and were also present in *areas V3a, 7a, DP, MDP, 5* and parts of auditory cortex.

Area V3a was reported to be motion-sensitive in humans, but possibly not in non-human primates (Vanduffel *et al.*, 2001; Vanduffel *et al.*, 2002; for review, see Orban *et al.*, 2003). As an alternative explanation for the previously observed absence of *area V3a*, a difference in functional sensitivity of *area V3a* between species is discussed (Tootell *et al.*, 1997). We cannot give evidence for true motion-sensitivity of *area V3a* in the present study, since the observed responses could as well be assigned to stimulus attributes other than motion, as also discussed in the following paragraph for *area V1*.

Differences between SPMs obtained in the present study and those obtained in

the study of Vanduffel and coworkers (2001) can be explained by the different types of stimuli used (coherent movement vs. optic flow) as well as by the chosen stimulus contrast. While stimulus contrast in their study consisted of random dot or line displays, comprising '*coherent motion vs. no motion*', in the present study, stimulus contrast consisted of random dot displays, comprising centrifugal motion (optic flow), covering '*left vs. right visual hemifield*'. By separately testing stimulated hemispheres against each other, we could avoid creating an extra baseline condition against which the main stimulus was tested. In order to separately test the effect of motion, such a baseline condition would have been identical to the moving random dot stimulus in all aspects (as e.g. the lifetime of dots etc.), except the motion of the dots. In the design of the present study, however, the moving random dot stimulus was present in one visual hemifield at a time and tested against the same hemifield of blocks in which the contralateral hemifield contained the moving random dot stimulus. This may have caused BOLD responses in *V1* – and possibly also in other visual areas, including *area V3a*.

In the study of Vanduffel and coworkers (2001), stimulus aspects, apart from motion, were present in all stimulation conditions and thereby were removed from analysis, which would explain the fact that Vanduffel and coworkers (2001) could not demonstrate BOLD responses in *V1* consistently across subjects and hemispheres. However, since *area V1* is known to contain direction-selective neurons, the observed BOLD responses in the present study may reflect true motion sensitivity.

The fact that, in the present study, fMRI responses included brain areas in addition to those reported by Vanduffel and coworkers could be explained by the relatively enhanced complexity of stimuli used and by the fact that larger portions of the visual field were stimulated (aperture diameter 60° vs. 14°). *Areas 7a*, *MSTd* and *STP*, which showed BOLD responses in the present study, but not in the study of Vanduffel and coworkers (2001), have all previously been implicated in

motion processing especially for large and complex stimuli, such as optic flow and biological motion (Tanaka *et al.*, 1986b; Lagae *et al.*, 1994; Oram and Perrett, 1994; Siegel and Read, 1997).

Cerebellum. As mentioned earlier, we hardly observed any BOLD responses within the *cerebellum*. Therefore, we cannot give evidence for or against cerebellar involvement in motion processing. The reason of the observed lack of BOLD responses in the *cerebellum* is unclear but could lie in the observed image distortions present in that particular part of the brain.

4.4: Voluntary eye movements

Comparison across studies. When comparing SPMs on frontal, parietal, temporal and occipital cortex for saccades and SPEMs across studies of (a) Koyama and coworkers (2004), (b) Baker and coworkers (2005a and 2005b) and (c) the present study (Table 5), areas most consistently reported for both saccades and SPEMs are: *areas 6, FEF, LIP, V3/V3a and V4/V4t*. These areas are present in all above mentioned studies, with exception of *area LIP* in the study of Baker and coworkers (2005b). Since Koyama and coworkers (2004) did not identify all peaks in observed SPMs, specific brain areas might be missed in Table 5 for their study.

Identified cortical areas in the study of Koyama and coworkers (2004) were *areas LIPd & LIPv, LIPv/VIP* (listed in Table 5 as “LIP” and “VIP”), *7a, 7a/7b* (listed as “7a” and “7b” in Table 5), *DP, AIP, FEF (BA 8), PMv & PMd (BA 6)* (listed as “6” in Table 5) and *BA 46/8* (listed as “46” in Table 5).

Identified cortical areas in the study of Baker and coworkers (2005a) were *areas FEF, SEF, LIP, PIP, MST, MT, FST, STP, V1, V3a* (listed in Table 5 as “V3/V3a”) and *V4* (listed in Table 5 as “V4/V4t”). Both saccades and SPEMs were examined by Baker and coworkers (2005b) in three monkeys; however, results from that particular study, presented in Table 5, are still preliminary (conference proceeding).

Identified cortical areas in the present study were *areas CITd & CITv, areas MSTd & MSTl, areas PITd & PITv, area STPp, areas V3 & V3a and areas V4 & V4t* (listed in Table 5 as “CIT”, “MST”, “PIT”, “STP”, “V3/V3a”, “V4/V4t”, respectively).

In studies of Baker and coworkers (2005a and 2005b) a conventional 3 T MR scanner was used; Koyama and coworkers (2004) scanned at a 4.7 T MR scanner.

Areas LIP, FEF and SEF. As reviewed in the introduction (see *section 1.3*), previous studies have implicated *areas LIP, FEF and SEF* as the most essential cortical areas involved in saccades and also as crucial for SPEMs. The consistent observations of BOLD responses within the *FEF* (Bruce *et al.*, 1985; Tehovnik *et al.*, 2000) and *area LIP* (Barash *et al.*, 1991a; Barash *et al.*, 1991b; Thier and Andersen, 1998;

Goldberg *et al.*, 2002) (Table 5) in the present study are therefore in good agreement with the literature. In the studies of Koyama and coworkers (2004) and Baker and coworkers (2005a and 2005b) the *SEF* (Schlag and Schlag-Rey, 1987; Tehovnik, 1995; Tehovnik *et al.*, 2000) responded only weakly and could only be observed unilaterally. In the present study the *SEF* could not be observed at all in the saccadic eye movements paradigm, but only in the SPEM paradigm. As a possible explanation for the weak response in the *SEF*, Koyama and coworkers (2004) argue that simplicity of the task and overtraining of the subjects might have led to a decrease in neural responses due to habituation effects (Chen and Wise, 1995b), this might also apply to the present study. Unlike *FEF* neurons, *SEF* neurons appear to respond maximal to complex or cognitively challenging saccade tasks (Olson and Gettner, 1995; Chen and Wise, 1995a; Amador *et al.*, 2004).

Area 6. *Area 6* has been associated with visually-guided skeletomotor behaviour, but rostral *area 6* may as well be involved in oculomotor activity (Moschovakis *et al.*, 2004; as cited in Baker *et al.*, 2005a). The idea that *area 6* plays a role in eye movements is supported by the results of all the studies listed in Table 5.

Area 46. In the posterior principle sulcus (possibly including *area 46*), where saccade-related activity has been previously demonstrated (Funahashi *et al.*, 1990; Funahashi *et al.*, 1991; Takeda and Funahashi, 2002; as cited in Baker *et al.*, 2005a), BOLD responses to saccades could be observed by Koyama and coworkers (2004) and Baker and coworkers (2005a). In contrast, BOLD responses to saccades within *area 46* were not observed in the present study. SPMs for SPEMs included *area 46* only partly and unilaterally. Probably, these BOLD responses have to be attributed to the *FEF* at close distance, rather than to *area 46*.

Area DP and area 5. *Area DP*, where saccade-related neuronal activity was reported (Andersen *et al.*, 1997; as cited in Koyama *et al.*, 2004) and *area 5*, where neural activity is likely modulated by saccades (Snyder *et al.*, 2000; as cited in Koyama *et al.*, 2004) and eye positions (Nakamura *et al.*, 1999; as cited in Koyama *et*

al., 2004), were reported in the study of Koyama and coworkers (2004), as well as in the present study, for saccades and for SPEMs.

Areas MT/MST. BOLD responses were expected in *areas MT/MST* for SPEMs (*area MSTd* in particular, see *section 1.3*). The fact that BOLD responses were unexpectedly also present in *areas MT/MST* for saccades suggests the contributions of other factors than saccade activity. As mentioned before, due to background luminance on the projection screen, borders of the screen contrasted against the dark surrounding. It is likely that peripheral visual transients and/or visual motion was induced on the retina by eye movements due to these objects in the background. *Areas MT/MST* were also reported for saccades by Baker and coworkers (2005, 2005b), probably due to similar reasons. Baker and coworkers argue that BOLD responses in *areas MT/MST* may reflect eye-velocity-tuned motion-sensitive neurons (Thiele *et al.*, 2002).

Superior colliculus. The only subcortical structure that showed BOLD responses to both saccades and SPEMs reliably and relatively strongly was the SC (Fig. 20). The SC is well-known for its role in oculomotor function. The brain stem premotor nuclei receive commands from the SC, which, in turn, receives direct excitatory projections from the *FEF* and *area LIP* and an inhibitory projection from the *substantia nigra*. The *substantia nigra* is suppressed by the *caudate nucleus*, which receives excitatory input from the *FEF*. Thus, *FEF* acts upon the superior colliculus in a direct, excitatory way and in an indirect way by releasing it from suppression by the *substantia nigra* by exciting the *caudate nucleus*, which inhibits the *substantia nigra* (Fig. 4) (paragraph adapted from Goldberg, 2000). Furthermore, oculomotor-related information flow has been reported from the SC to the *FEF*, via the mediodorsal thalamus (Sommer and Wurtz, 2004).

Paradoxically, peak BOLD responses centred at locations similar to the proposed location of the SC in Fig. 4 were repetitively observed throughout several experiments, regardless of the type of stimuli used, and thus may reflect artefacts. How-

ever, the nature of those artefacts could not be determined in the present study.

Saccadic eye movements vs. SPEMs. Results of the present study support the idea that many similar cortical areas may be crucial for both saccades and SPEMs. Sporadic occurrences of correction saccades made during SPEMs cannot be excluded. Such correction saccades may explain BOLD responses to SPEMs in areas that are known to be saccade-specific, such as *area DP*. However, it is unlikely that correction saccades can account for the high similarity of SPMs for both saccades and SPEMs in the present study. In the present study, *areas 2, 46, SEF* and *VP* (Fig. 19, Table 5) were the only areas showing no overlap of BOLD responses to saccades and SPEMs. Nevertheless, because the present study did not allow for a fine quantitative analysis, it would be too speculative to draw conclusions about observations of brain areas that have not been earlier reported to be implicated in voluntary eye movements. A quantitative analysis would require data from several subjects.

4.5: Future improvements

Finally, the most important points that need to be improved in future experiments will be listed.

- *MR pulse sequences* have to be selected and *MR sequence parameters* such as slice orientation, phase encoding direction and echo time have to be optimized in a systematic approach to reduce image artefacts as much as possible.
- Methods for the *correction of image distortions* used in the analysis of human fMRI data should be adapted for their use in the analysis of monkey fMRI data. Ideally, it should be possible to apply standard algorithms for efficient and precise realignment of corrected functional brain volumes with structural brain volumes.
- Scanning at 3 T improves the SNR with respect to scanning at 1.5 T, but images are also more prone to distortions. It could be useful to test whether scanning at 1.5 T significantly reduces image artefacts. In order to compensate for the loss of SNR relatively to scanning at 3 T, contrast agents such as *MION* could be used.
- *Surface coil placement* should be systematically varied in order to account for the inhomogeneous illumination of the used surface coils. Alternative coils could be tested.
- For purposes of statistical analysis, the appropriate *number of measurements per sessions* has to be determined.
- *Background luminance* on the presentation screen has to be eliminated, e.g. by using grey filters in front of the lens of the LCD projector. However, stimuli have to be projected at high enough contrast and brightness levels.
- *Reflections* – e.g. on bore walls inside the MR scanner – have to be removed or reduced. This could be achieved by covering the scanner bore walls and bore opening (excluding the presentation screen).
- For *eye-position-tracking* a higher temporal resolution is recommendable to al-

low for qualitative analysis of eye position data. Artefacts present in the video image caused by magnetic field gradients during scanning and distortions of the magnetic field by the camera present inside the bore could possibly be prevented by placing the camera outside the scanner. A camera positioned at close distance to the monkey's eye occludes parts of the visual field.

- In order to reduce *movement-related image artefacts*, movements of the monkey have to be further restricted, e.g. by confining available space in which the monkey can move to a minimum. A head-post system and possibly a chin rest have to be used to securely restrain the head. In addition, it will be necessary to further train the monkey to keep motionless during fMRI experiments. Therefore, body movements of the monkey have to be detected and movement information has to be used for behavioural control by providing the monkey with feedback information about these movements.
- *Reward application* during image acquisition is problematic because the monkey licks and moves the snout. An event-related design would be better suited than a blocked design, for disentangling events of interest and effects of reward application.
- In the present study, saccade and SPEM targets moved between two extreme positions repetitively throughout blocks at a constant rate, allowing the monkey to *anticipate future target positions*. In future experiments timing parameters and target positions should be varied in order to exclude anticipation.
- Several subjects have to be tested in order to account for *inter-individual differences*.

5. Summary / Zusammenfassung

Summary.

Blood-oxygen-level-dependent (BOLD) functional magnetic resonance imaging (fMRI) performed on a conventional 3 T MR scanner was used in order to investigate brain activity in response to visual stimuli and eye movements of an alert, behaving rhesus monkey.

The current study presents functional data on representations of meridians and different degrees of eccentricity of the visual field, on optic flow and on saccade and smooth pursuit eye movements (SPEMs).

A number of technical constraints – such as distortions of functional MR images – hampered the exact localization and identification of sites showing BOLD responses. Despite these limitations, the present results are largely in agreement with both the classical literature on monkey brain functions and comparable monkey fMRI studies.

Results of the present study are in accordance with the view that processing of optic flow requires cortical *areas MT/MST (middle temporal/medial superior temporal)*. Furthermore, the present study implicates cortical areas that are well-known for their role in oculomotor function in the processing of saccadic eye movements and SPEMs, including *area LIP (lateral intraparietal)*, as well as the *FEF (frontal eye fields)* and, albeit only weakly, the *SEF (supplementary eye fields)*.

Future experiments will have to improve used material as well as experimental procedures in order to reduce artefacts in functional images. It will be of particular importance to reduce contributions of those artefacts that emerge from body movements of the monkey. Additional subjects will have to be tested in order to account for inter-individual effects.

Zusammenfassung.

Mithilfe von *Blutsauerstoff-abhängiger (BOLD) funktioneller Magnetresonanztomographie (fMRT)* wurde die Hirnaktivität als Antwort auf visuelle Stimuli und Augenbewegungen eines wachen, sich definiert verhaltenden Rhesus-Affens an einem konventionellen 3 T MR-Scanner untersucht.

Es werden funktionelle Daten zur Repräsentation von Meridianen und verschiedenen Exzentrizitäten des visuellen Feldes, zu optischen Flußfeldern, zu Sakkaden und zu glatten Augefolgebewegungen präsentiert.

Eine Reihe von technischen Schwierigkeiten – wie z.B. Verzerrungen von funktionalen MR-Bildern – erschwerten die exakte Ortsbestimmung und Identifikation derjenigen Hirngebiete, welche BOLD-Antworten zeigten. Ungeachtet dieser Limitationen sind die Ergebnisse dieser Studie jedoch weitgehend in Übereinstimmung, sowohl mit Ergebnissen der klassischen Literatur über Hirnfunktionen von Affen, als auch mit vergleichbaren fMRT-Studien an Affen.

Die Ergebnisse der vorliegenden Studie stimmen mit der Annahme überein, dass die Verarbeitung optischer Flußfelder die kortikalen Areale *MT/MST (middle temporal/medial superior temporal)* benötigt. Weiterhin implizieren die Ergebnisse dieser Studie kortikale Areale in der Verarbeitung von Sakkaden und glatten Augefolgebewegungen, deren Rolle in okulomotorischen Funktionen bekannt ist, einschließlich des Areals *LIP (lateral intraparietal)*, der *FEF (frontale Augenfelder)* sowie, wenn auch nur schwach, der *SEF (supplementäre Augenfelder)*.

Für zukünftige Experimente wird es erforderlich sein, das verwendete Material und die experimentellen Prozeduren zu verbessern, um Artefakte in den funktionalen Bildern zu reduzieren. Eine besondere Bedeutung wird dabei die Vermeidung von Artefakten spielen, die durch Körperbewegungen des Affen hervorgerufen werden. Weitere Affen werden untersucht werden müssen, um interindividuellen Unterschieden gerecht zu werden.

6. Acknowledgements

The current work was supported by *HFSP RGP 0023/2001-B*, *DFG SFB 550-A2* and *A7*, by the *clinical neurosciences programme* of the *Hermann and Lilly Schilling Foundation* and by the *Hertie-Foundation*, which supported the creation of the *Hertie-Institute for Clinical Brain Research (HIH)* at the *University of Tübingen*.

I thank my supervisor, *Prof. Dr. Hans-Peter Thier*, *HIH*, *Department of Cognitive Neurology*, *University of Tübingen*, for advice, discussions, helpful critics and support. Thanks to my colleagues, *Friedemann Bunjes*, *Nicolas Catz*, *Suryadeep Dash*, *Dr. Peter Dicke*, *Alla Ignashchenkova*, *Simone Kamphuis* and *Konstantin Tziridis* and the remaining colleagues of the department for discussions, help and support during the long time that we have been working together.

Special thanks to *Rocky*, *Boris*, *Zeppelin*, *Spock*, *Zeus* & *Herkules*.

MRI experiments were mainly conducted by *Dr. Peter Dicke* and my person, with help of *Friedemann Bunjes* and *Simon Bock* and in cooperation with the *Section MR of CNS*, *Department of Neuroradiology*, *University of Tübingen*: I thank *Prof. Dr. Wolfgang Grodd* and especially *Dr. Michael Erb* for help in numerous issues regarding MR experiments, image acquisition & analysis. Thanks for valuable MRI tips to *Michael Wibrall*, *Max Planck Institute for Brain Research*, *Frankfurt/Main*.

Thanks to *Hubert Willmann* (primate chair and materials), *Rüdiger Bernd* (electronics) and their teams, to *Mark Repnow*, *Friedemann Bunjes* and *Dr. Peter Dicke* (software) and to *Helmut Stark* (MR coils) for excellent technical support and to *Dagmar Heller-Schmerold* and *Ute Großhennig* for practical help.

My advisors and mentors during all projects of my PhD studentship – *Prof. Dr. Dr. h.c. Valentino Braitenberg & Prof. Dr. Almut Schüz, Max Planck Institute for Biological Cybernetics, Tübingen* and *Prof. Dr. Werner J. Schmidt, Department of Neuropharmacology, University of Tübingen* – thank you for motivating, supporting and helping!

I am especially indebted to the *Graduate School of Neural & Behavioural Sciences – International Max Planck Research School, University of Tübingen* for providing me, as one of the first students, an excellent education within its *master's and doctoral degree program* with theoretical and practical training in a wide spectrum of neuroscience topics – thanks to organisers, lecturers and fellow students!

Special thank to programme coordinator of the *Graduate School, Prof. Dr. Horst Herbert*, for help in all aspects regarding studies and much more.

And last but not least, I thank my *family* and *friends* for always supporting me and for sharing my fascinations.

7. References

Amador N, Schlag-Rey M, Schlag J (2004) Primate antisaccade. II. Supplementary eye field neuronal activity predicts correct performance. *J Neurophysiol* 91:1672-1689.

Andersen AH, Zhang Z, Barber T, Rayens WS, Zhang J, Grondin R, Hardy P, Gerhardt GA, Gash DM (2002) Functional MRI studies in awake rhesus monkeys: methodological and analytical strategies. *J Neurosci Methods* 118:141-152.

Andersen RA, Snyder LH, Bradley DC, Xing J (1997) Multimodal representation of space in the posterior parietal cortex and its use in planning movements. *Annu Rev Neurosci* 20:303-330.

Attwell D, Iadecola C (2002) The neural basis of functional brain imaging signals. *Trends in Neurosciences* 25:621-625.

Attwell D, Laughlin SB (2001) An energy budget for signaling in the grey matter of the brain. *J Cereb Blood Flow Metab* 21:1133-1145.

Baker JT, Patel GH, Corbetta M, Snyder LH (2005a) Distribution of activity across the monkey cerebral cortical surface, thalamus and midbrain during rapid, visually guided saccades. *Cereb Cortex*.

Baker JT, Patel GH, Corbetta M, Snyder LH (2005b) FMRI comparison of the macaque cortical substrates for smooth pursuit and saccadic eye movements. Conference poster abstract #166.9, annual meeting of the Society for Neuroscience, 2005, Washington DC.

Bandettini PA, Wong EC, Hinks RS, Tikofsky RS, Hyde JS (1992) Time course EPI of human brain function during task activation. *Magn Reson Med* 25:390-397.

Barash S, Bracewell RM, Fogassi L, Gnadt JW, Andersen RA (1991a) Saccade-related activity in the lateral intraparietal area. I. Temporal properties; comparison with area 7a. *J Neurophysiol* 66:1095-1108.

Barash S, Bracewell RM, Fogassi L, Gnadt JW, Andersen RA (1991b) Saccade-related activity in the lateral intraparietal area. II. Spatial properties. *J Neurophysiol* 66:1109-1124.

Barash S, Melikyan A, Sivakov A, Zhang M, Glickstein M, Thier P (1999) Saccadic dysmetria and adaptation after lesions of the cerebellar cortex. *J Neurosci* 19:10931-10939.

7. References

- Beusmans JM (1993) Computing the direction of heading from affine image flow. *Biol Cybern* 70:123-136.
- Blinkov, S.M., Glezer II (1968) *The Human Brain in Figures and Tables. A Quantitative Handbook*. New York: Plenum Press.
- Boxerman JL, Bandettini PA, Kwong KK, Baker JR, Davis TL, Rosen BR, Weisskoff RM (1995) The intravascular contribution to fMRI signal change: Monte Carlo modeling and diffusion-weighted studies in vivo. *Magn Reson Med* 34:4-10.
- Bremmer F, Kubischik M, Pekel M, Lappe M, Hoffmann KP (1999) Linear vestibular self-motion signals in monkey medial superior temporal area. *Ann N Y Acad Sci* 871:272-281.
- Brewer AA, Press WA, Logothetis NK, Wandell BA (2002) Visual areas in macaque cortex measured using functional magnetic resonance imaging. *J Neurosci* 22:10416-10426.
- Bruce CJ, Goldberg ME, Bushnell MC, Stanton GB (1985) Primate frontal eye fields. II. Physiological and anatomical correlates of electrically evoked eye movements. *J Neurophysiol* 54:714-734.
- Buxton RB, Frank LR (1997) A model for the coupling between cerebral blood flow and oxygen metabolism during neural stimulation. *J Cereb Blood Flow Metab* 17:64-72.
- Caesar K, Thomsen K, Lauritzen M (2003) Dissociation of spikes, synaptic activity, and activity-dependent increments in rat cerebellar blood flow by tonic synaptic inhibition. *Proc Natl Acad Sci U S A* 100:16000-16005.
- Catz N, Dicke PW, Thier P (2005) Cerebellar complex spike firing is suitable to induce as well as to stabilize motor learning. *Curr Biol* 15:2179-2189.
- Cauli B, Tong XK, Rancillac A, Serluca N, Lambolez B, Rossier J, Hamel E (2004) Cortical GABA interneurons in neurovascular coupling: relays for subcortical vasoactive pathways. *J Neurosci* 24:8940-8949.
- Chen LL, Wise SP (1995a) Supplementary eye field contrasted with the frontal eye field during acquisition of conditional oculomotor associations. *J Neurophysiol* 73:1122-1134.
- Chen LL, Wise SP (1995b) Neuronal activity in the supplementary eye field during acquisition of conditional oculomotor associations. *J Neurophysiol* 73:1101-1121.

Chen Q, Andersen AH, Zhang Z, Ovadia A, Cass WA, Gash DM, Avison MJ (1999) Functional MRI of basal ganglia responsiveness to levodopa in parkinsonian rhesus monkeys. *Exp Neurol* 158:63-75.

Chen Q, Andersen AH, Zhang Z, Ovadia A, Gash DM, Avison MJ (1996) Mapping drug-induced changes in cerebral R2* by Multiple Gradient Recalled Echo functional MRI. *Magn Reson Imaging* 14:469-476.

Clare S (1997) Functional MRI: methods and applications. University of Nottingham, Great Britain.

Cui DM, Yan YJ, Lynch JC (2003) Pursuit subregion of the frontal eye field projects to the caudate nucleus in monkeys. *J Neurophysiol* 89:2678-2684.

Daniel PM, Whitteridge D (1961) The representation of the visual field on the cerebral cortex in monkeys. *J Physiol (Paris)* 159:203-221.

Denys K, Vanduffel W, Fize D, Nelissen K, Sawamura H, Georgieva S, Vogels R, Van Essen D, Orban GA (2004) Visual activation in prefrontal cortex is stronger in monkeys than in humans. *J Cogn Neurosci* 16:1505-1516.

Desimone R, Ungerleider LG (1986) Multiple visual areas in the caudal superior temporal sulcus of the macaque. *J Comp Neurol* 248:164-189.

DeYoe EA, Carman GJ, Bandettini P, Glickman S, Wieser J, Cox R, Miller D, Neitz J (1996) Mapping striate and extrastriate visual areas in human cerebral cortex. *Proc Natl Acad Sci U S A* 93:2382-2386.

Dietrich H, Dicke PW, Catz N, Glickstein M, Haarmeier T, Thier P (2003) Lesions of rhesus monkey posterior vermis cause deficits in visual motion perception. Conference talk abstract #882.7, annual meeting of the Society for Neuroscience, 2003, New Orleans.

Disbrow EA, Slutsky DA, Roberts TP, Krubitzer LA (2000) Functional MRI at 1.5 tesla: a comparison of the blood oxygenation level-dependent signal and electrophysiology. *Proc Natl Acad Sci U S A* 97:9718-9723.

Dow BM, Snyder AZ, Vautin RG, Bauer R (1981) Magnification factor and receptive field size in foveal striate cortex of the monkey. *Exp Brain Res* 44:213-228.

Dubowitz DJ, Bernheim KA, Chen DY, Bradley Jr WG, Andersen RA (2001a) Enhancing fMRI contrast in awake-behaving primates using intravascular magnetite dextran nanoparticles. *Neuroreport* 12:2335-2340.

Dubowitz DJ, Chen DY, Atkinson DJ, Grieve KL, Gillikin B, Bradley WG, Jr., An-

7. References

- Andersen RA (1998) Functional magnetic resonance imaging in macaque cortex. *Neuroreport* 9:2213-2218.
- Dubowitz DJ, Chen DY, Atkinson DJ, Scadeng M, Martinez A, Andersen MB, Andersen RA, Bradley WG, Jr. (2001b) Direct comparison of visual cortex activation in human and non-human primates using functional magnetic resonance imaging. *J Neurosci Methods* 107:71-80.
- Duffy CJ (1998) MST neurons respond to optic flow and translational movement. *J Neurophysiol* 80:1816-1827.
- Duffy CJ, Wurtz RH (1991a) Sensitivity of MST neurons to optic flow stimuli. I. A continuum of response selectivity to large-field stimuli. *J Neurophysiol* 65:1329-1345.
- Duffy CJ, Wurtz RH (1997) Multiple temporal components of optic flow responses in MST neurons. *Exp Brain Res* 114:472-482.
- Duffy CJ, Wurtz RH (1991b) Sensitivity of MST neurons to optic flow stimuli. II. Mechanisms of response selectivity revealed by small-field stimuli. *J Neurophysiol* 65:1346-1359.
- Engel SA, Rumelhart DE, Wandell BA, Lee AT, Glover GH, Chichilnisky EJ, Shadlen MN (1994) fMRI of human visual cortex. *Nature* 369:525.
- Felleman DJ, Van Essen DC (1987) Receptive field properties of neurons in area V3 of macaque monkey extrastriate cortex. *J Neurophysiol* 57:889-920.
- Felleman DJ, Van Essen DC (1991) Distributed hierarchical processing in the primate cerebral cortex. *Cereb Cortex* 1:1-47.
- Fize D, Vanduffel W, Nelissen K, Denys K, Chef dC, Faugeras O, Orban GA (2003) The retinotopic organization of primate dorsal V4 and surrounding areas: A functional magnetic resonance imaging study in awake monkeys. *J Neurosci* 23:7395-7406.
- Fox PT, Miezin FM, Allman JM, Van E, Raichle ME (1987) Retinotopic organization of human visual cortex mapped with positron-emission tomography. *J Neurosci* 7:913-922.
- Fox PT, Raichle ME (1986) Focal physiological uncoupling of cerebral blood flow and oxidative metabolism during somatosensory stimulation in human subjects. *Proc Natl Acad Sci U S A* 83:1140-1144.
- Fox PT, Raichle ME, Mintun MA, Dence C (1988) Nonoxidative glucose consump-

tion during focal physiologic neural activity. *Science* 241:462-464.

Friedman DP (1983) Laminar patterns of termination of cortico-cortical afferents in the somatosensory system. *Brain Res* 273:147-151.

Friston KJ (2003) Experimental design and statistical parametric mapping. In: *Human Brain Function* (Frackowiak RSJ, Friston KJ, Frith C, Dolan R, Price CJZS, Ashburner J, Penny WD, eds), Academic Press.

Funahashi S, Bruce CJ, Goldman-Rakic PS (1990) Visuospatial coding in primate prefrontal neurons revealed by oculomotor paradigms. *J Neurophysiol* 63:814-831.

Funahashi S, Bruce CJ, Goldman-Rakic PS (1991) Neuronal activity related to saccadic eye movements in the monkey's dorsolateral prefrontal cortex. *J Neurophysiol* 65:1464-1483.

Gegenfurtner KR, Kiper DC, Levitt JB (1997) Functional properties of neurons in macaque area V3. *J Neurophysiol* 77:1906-1923.

Genovese CR, Lazar NA, Nichols T (2002) Thresholding of statistical maps in functional neuroimaging using the false discovery rate. *Neuroimage* 15:870-878.

Gibson JJ (1966) *The senses considered as perceptual systems*. Boston: Houghton Mifflin.

Goebel R, Khorram-Sefat D, Muckli L, Hacker H, Singer W (1998) The constructive nature of vision: direct evidence from functional magnetic resonance imaging studies of apparent motion and motion imagery. *Eur J Neurosci* 10:1563-1573.

Gold L, Lauritzen M (2002) Neuronal deactivation explains decreased cerebellar blood flow in response to focal cerebral ischemia or suppressed neocortical function. *Proc Natl Acad Sci U S A* 99:7699-7704.

Goldberg JH, Tamas G, Aronov D, Yuste R (2003) Calcium microdomains in aspiny dendrites. *Neuron* 40:807-821.

Goldberg ME (2000) The control of gaze. In: *Principles Of Neural Science* (Kandel ER, Schwartz JH, Jessel TM, eds), pp 782-800. New York, St. Louis, San Francisco, Auckland, Bogotá, Caracas, Lisbon, London, Madrid, Mexico City, Milan, Montreal, New Delhi, San Juan, Singapore, Sydney, Tokyo, Toronto: McGraw-Hill.

Goldberg ME, Bisley J, Powell KD, Gottlieb J, Kusunoki M (2002) The role of the lateral intraparietal area of the monkey in the generation of saccades and visuospatial attention. *Ann N Y Acad Sci* 956:205-215.

7. References

- Gorno-Tempini ML, Hutton C, Josephs O, Deichmann R, Price C, Turner R (2002) Echo time dependence of BOLD contrast and susceptibility artifacts. *Neuroimage* 15:136-142.
- Gottlieb J, Goldberg ME (1999) Activity of neurons in the lateral intraparietal area of the monkey during an antisaccade task. *Nat Neurosci* 2:906-912.
- Graziano MS, Andersen RA, Snowden RJ (1994) Tuning of MST neurons to spiral motions. *J Neurosci* 14:54-67.
- Grill-Spector K, Kushnir T, Hendler T, Malach R (2000) The dynamics of object-selective activation correlate with recognition performance in humans. *Nat Neurosci* 3:837-843.
- Grodd W (1998) Introduction to magnetic resonance imaging and spectroscopy in medicine and zoology. *Zoology* 101:174-199.
- Gunter TE, Yule DI, Gunter KK, Eliseev RA, Salter JD (2004) Calcium and mitochondria. *FEBS Lett* 567:96-102.
- Hadjikhani N, Roland PE (1998) Cross-modal transfer of information between the tactile and the visual representations in the human brain: A positron emission tomographic study. *J Neurosci* 18:1072-1084.
- Hamel E (2004) Cholinergic modulation of the cortical microvascular bed. *Prog Brain Res* 145:171-178.
- Hayashi T, Konishi S, Hasegawa I, Miyashita Y (1999) Short communication: mapping of somatosensory cortices with functional magnetic resonance imaging in anaesthetized macaque monkeys. *Eur J Neurosci* 11:4451-4456.
- Heeger DJ, Huk AC, Geisler WS, Albrecht DG (2000) Spikes versus BOLD: what does neuroimaging tell us about neuronal activity? *Nat Neurosci* 3:631-633.
- Huk AC, Dougherty RF, Heeger DJ (2002) Retinotopy and functional subdivision of human areas MT and MST. *J Neurosci* 22:7195-7205.
- Iadecola C (2004) Neurovascular regulation in the normal brain and in Alzheimer's disease. *Nat Rev Neurosci* 5:347-360.
- Kastner S, De WP, Desimone R, Ungerleider LG (1998) Mechanisms of directed attention in the human extrastriate cortex as revealed by functional MRI. *Science* 282:108-111.
- Kayser C, Kim M, Ugurbil K, Kim DS, Konig P (2004) A comparison of hemody-

dynamic and neural responses in cat visual cortex using complex stimuli. *Cerebral Cortex* 14:881-891.

Koyama M, Hasegawa I, Osada T, Adachi Y, Nakahara K, Miyashita Y (2004) Functional magnetic resonance imaging of macaque monkeys performing visually guided saccade tasks: comparison of cortical eye fields with humans. *Neuron* 41:795-807.

Krauzlis RJ (2005) The control of voluntary eye movements: new perspectives. *Neuroscientist* 11:124-137.

Kwong KK, Belliveau JW, Chesler DA, Goldberg IE, Weisskoff RM, Poncelet BP, Kennedy DN, Hoppel BE, Cohen MS, Turner R, . (1992) Dynamic magnetic resonance imaging of human brain activity during primary sensory stimulation. *Proc Natl Acad Sci U S A* 89:5675-5679.

Lagae L, Maes H, Raiguel S, Xiao DK, Orban GA (1994) Responses of macaque STS neurons to optic flow components: a comparison of areas MT and MST. *J Neurophysiol* 71:1597-1626.

Lappe M, Rauschecker JP (1993) A neural network for the processing of optic flow from ego-motion in higher mammals. *Neural Computation* 5:374-391.

Lauritzen M (2001) Relationship of spikes, synaptic activity, and local changes of cerebral blood flow. *J Cereb Blood Flow Metab* 21:1367-1383.

Lauritzen M (2005) Reading vascular changes in brain imaging: is dendritic calcium the key? *Nature Reviews Neuroscience* 6:77-85.

Leite FP, Tsao D, Vanduffel W, Fize D, Sasaki Y, Wald LL, Dale AM, Kwong KK, Orban GA, Rosen BR, Tootell RB, Mandeville JB (2002) Repeated fMRI using iron oxide contrast agent in awake, behaving macaques at 3 Tesla. *Neuroimage* 16:283-294.

Letelier JC, Varela F (1984) Why the cortical magnification factor in rhesus is isotropic. *Vision Res* 24:1091-1095.

LeVay S, Hubel DH, Wiesel TN (1975) The pattern of ocular dominance columns in macaque visual cortex revealed by a reduced silver stain. *J Comp Neurol* 159:559-576.

Levitt JB, Kiper DC, Movshon JA (1994) Receptive fields and functional architecture of macaque V2. *J Neurophysiol* 71:2517-2542.

Logothetis NK (2003a) MR imaging in the non-human primate: studies of function

and of dynamic connectivity. *Curr Opin Neurobiol* 13:630-642.

Logothetis NK (2003b) The underpinnings of the BOLD functional magnetic resonance imaging signal. *J Neurosci* 23:3963-3971.

Logothetis NK (2002) The neural basis of the blood-oxygen-level-dependent functional magnetic resonance imaging signal. *Philos Trans R Soc Lond B Biol Sci* 357:1003-1037.

Logothetis NK, Guggenberger H, Peled S, Pauls J (1999) Functional imaging of the monkey brain. *Nat Neurosci* 2:555-562.

Logothetis NK, Pauls J, Augath M, Trinath T, Oeltermann A (2001) Neurophysiological investigation of the basis of the fMRI signal. *Nature* 412:150-157.

Logothetis NK, Wandell BA (2004) Interpreting the BOLD signal. *Annu Rev Physiol* 66:735-769.

Mathiesen C, Caesar K, Akgoren N, Lauritzen M (1998) Modification of activity-dependent increases of cerebral blood flow by excitatory synaptic activity and spikes in rat cerebellar cortex. *J Physiol* 512:555-566.

Maunsell JH, Van Essen DC (1983) The connections of the middle temporal visual area (MT) and their relationship to a cortical hierarchy in the macaque monkey. *J Neurosci* 3:2563-2586.

Moschovakis AK, Gregoriou GG, Ugolini G, Doldan M, Graf W, Guldin W, Hadjimitsakis K, Savaki HE (2004) Oculomotor areas of the primate frontal lobes: a transneuronal transfer of rabies virus and [14C]-2-deoxyglucose functional imaging study. *J Neurosci* 24:5726-5740.

Munoz DP (2002) Commentary: saccadic eye movements: overview of neural circuitry. *Prog Brain Res* 140:89-96.

Nakahara K, Hayashi T, Konishi S, Miyashita Y (2002) Functional MRI of macaque monkeys performing a cognitive set-shifting task. *Science* 295:1532-1536.

Nakamura K, Chung HH, Graziano MS, Gross CG (1999) Dynamic representation of eye position in the parieto-occipital sulcus. *J Neurophysiol* 81:2374-2385.

Nelissen K, Luppino G, Vanduffel W, Rizzolatti G, Orban GA (2005) Observing others: multiple action representation in the frontal lobe. *Science* 310:332-336.

Nessaiver M (1996) All you really need to know about MRI physics. Rittenhouse Book Distributors.

Nichols T, Hayasaka S (2003) Controlling the familywise error rate in functional neuroimaging: a comparative review. *Stat Methods Med Res* 12:419-446.

Noda H, Mikami A (1986) Discharges of neurons in the dorsal paraflocculus of monkeys during eye movements and visual stimulation. *J Neurophysiol* 56:1129-1146.

Ogawa S, Lee TM (1990) Magnetic resonance imaging of blood vessels at high fields: in vivo and in vitro measurements and image simulation. *Magn Reson Med* 16:9-18.

Ogawa S, Lee TM, Kay AR, Tank DW (1990a) Brain magnetic resonance imaging with contrast dependent on blood oxygenation. *Proc Natl Acad Sci U S A* 87:9868-9872.

Ogawa S, Lee TM, Nayak AS, Glynn P (1990b) Oxygenation-sensitive contrast in magnetic resonance image of rodent brain at high magnetic fields. *Magn Reson Med* 14:68-78.

Ogawa S, Menon RS, Kim SG, Ugurbil K (1998) On the characteristics of functional magnetic resonance imaging of the brain. *Annu Rev Biophys Biomol Struct* 27:447-74.:447-474.

Ogawa S, Tank DW, Menon R, Ellermann JM, Kim SG, Merkle H, Ugurbil K (1992) Intrinsic signal changes accompanying sensory stimulation: functional brain mapping with magnetic resonance imaging. *Proc Natl Acad Sci U S A* 89:5951-5955.

Olson CR, Gettner SN (1995) Object-centered direction selectivity in the macaque supplementary eye field. *Science* 269:985-988.

Optican LM, Quaia C (2002) Distributed model of collicular and cerebellar function during saccades. *Ann N Y Acad Sci* 956:164-177.

Optican LM, Robinson DA (1980) Cerebellar-dependent adaptive control of primate saccadic system. *J Neurophysiol* 44:1058-1076.

Oram MW, Perrett DI (1994) Responses of anterior superior temporal polysensory (STPa) neurons to "biological motion" stimuli. *J Cogn Neurosci* 6:99-116.

Orban GA, Fize D, Peuskens H, Denys K, Nelissen K, Sunaert S, Todd J, Vanduffel W (2003) Similarities and differences in motion processing between the human and macaque brain: evidence from fMRI. *Neuropsychologia* 41:1757-1768.

Orban GA, Kennedy H, Bullier J (1986) Velocity sensitivity and direction selectiv-

7. References

ity of neurons in areas V1 and V2 of the monkey: influence of eccentricity. *J Neurophysiol* 56:462-480.

Orban GA, Lagae L, Verri A, Raiguel S, Xiao D, Maes H, Torre V (1992) First-order analysis of optical flow in monkey brain. *Proc Natl Acad Sci U S A* 89:2595-2599.

Pauling L, Coryell C (1936) The magnetic properties and structure of hemoglobin, oxyhemoglobin and carbonmonoxyhemoglobin. *Proc Natl Acad Sci U S A* 22:210-216.

Peterhans E, von der Heydt R (1993) Functional organization of area V2 in the alert macaque. *Eur J Neurosci* 5:509-524.

Petit L, Haxby JV (1999) Functional anatomy of pursuit eye movements in humans as revealed by fMRI. *J Neurophysiol* 82:463-471.

Pinsk MA, Desimone K, Moore T, Gross CG, Kastner S (2005) Representations of faces and body parts in macaque temporal cortex: A functional MRI study. *Proc Natl Acad Sci U S A*.

Pinsk MA, Moore T, Richter MC, Gross CG, Kastner S (2004) Methods for functional magnetic resonance imaging in normal and lesioned behaving monkeys. *J Neurosci Methods* 143:179-195.

Porter JT, Cauli B, Staiger JF, Lambolez B, Rossier J, Audinat E (1998) Properties of bipolar VIPergic interneurons and their excitation by pyramidal neurons in the rat neocortex. *Eur J Neurosci* 10:3617-3628.

Rainer G, Augath M, Trinath T, Logothetis NK (2001) Nonmonotonic noise tuning of BOLD fMRI signal to natural images in the visual cortex of the anesthetized monkey. *Curr Biol* 11:846-854.

Rees G, Friston K, Koch C (2000) A direct quantitative relationship between the functional properties of human and macaque V5. *Nat Neurosci* 3:716-723.

Robinson DA (1963) A method of measuring eye movement using a scleral search coil in a magnetic field. *IEEE Trans Biomed Eng* 10:137-145.

Rockland KS, Pandya DN (1979) Laminar origins and terminations of cortical connections of the occipital lobe in the rhesus monkey. *Brain Res* 179:3-20.

Rosano C, Krisky CM, Welling JS, Eddy WF, Luna B, Thulborn KR, Sweeney JA (2002) Pursuit and saccadic eye movement subregions in human frontal eye field: a high-resolution fMRI investigation. *Cereb Cortex* 12:107-115.

Saito H, Yukie M, Tanaka K, Hikosaka K, Fukada Y, Iwai E (1986) Integration of direction signals of image motion in the superior temporal sulcus of the macaque monkey. *J Neurosci* 6:145-157.

Sakitt B (1982) Why the cortical magnification factor in rhesus can not be isotropic. *Vision Res* 22:417-421.

Sawamura H, Georgieva S, Vogels R, Vanduffel W, Orban GA (2005) Using functional magnetic resonance imaging to assess adaptation and size invariance of shape processing by humans and monkeys. *J Neurosci* 25:4294-4306.

Schlag J, Schlag-Rey M (1987) Evidence for a supplementary eye field. *J Neurophysiol* 57:179-200.

Scudder CA, Kaneko CS, Fuchs AF (2002) The brainstem burst generator for saccadic eye movements: a modern synthesis. *Exp Brain Res* 142:439-462.

Sereno MI, Dale AM, Reppas JB, Kwong KK, Belliveau JW, Brady TJ, Rosen BR, Tootell RB (1995) Borders of multiple visual areas in humans revealed by functional magnetic resonance imaging. *Science* 268:889-893.

Siegel RM, Read HL (1997) Analysis of optic flow in the monkey parietal area 7a. *Cereb Cortex* 7:327-346.

Smith AT, Wall MB, Williams AL, Singh KD (2006) Sensitivity to optic flow in human cortical areas MT and MST. *Eur J Neurosci* 23:561-569.

Snyder LH, Batista AP, Andersen RA (2000) Saccade-related activity in the parietal reach region. *J Neurophysiol* 83:1099-1102.

Sommer MA, Wurtz RH (2004) What the brain stem tells the frontal cortex. I. Oculomotor signals sent from superior colliculus to frontal eye field via mediodorsal thalamus. *J Neurophysiol* 91:1381-1402.

Southam E, Morris R, Garthwaite J (1992) Sources and targets of nitric oxide in rat cerebellum. *Neurosci Lett* 137:241-244.

Spees WM, Yablonskiy DA, Oswood MC, Ackerman JJ (2001) Water proton MR properties of human blood at 1.5 Tesla: magnetic susceptibility, T(1), T(2), T*(2), and non-Lorentzian signal behavior. *Magn Reson Med* 45:533-542.

Stefanacci L, Reber P, Costanza J, Wong E, Buxton R, Zola S, Squire L, Albright T (1998) fMRI of monkey visual cortex. *Neuron* 20:1051-1057.

Stein JF (1986) Role of the cerebellum in the visual guidance of movement. *Nature*

323:217-221.

Takeda K, Funahashi S (2002) Prefrontal task-related activity representing visual cue location or saccade direction in spatial working memory tasks. *J Neurophysiol* 87:567-588.

Tanaka K, Hikosaka K, Saito H, Yukie M, Fukada Y, Iwai E (1986a) Analysis of local and wide-field movements in the superior temporal visual areas of the macaque monkey. *J Neurosci* 6:134-144.

Tanaka K, Hikosaka K, Saito H, Yukie M, Fukada Y, Iwai E (1986b) Analysis of local and wide-field movements in the superior temporal visual areas of the macaque monkey. *J Neurosci* 6:134-144.

Tehovnik EJ (1995) The dorsomedial frontal cortex: eye and forelimb fields. *Behav Brain Res* 67:147-163.

Tehovnik EJ, Sommer MA, Chou IH, Slocum WM, Schiller PH (2000) Eye fields in the frontal lobes of primates. *Brain Res Brain Res Rev* 32:413-448.

Thiele A, Henning P, Kubischik M, Hoffmann KP (2002) Neural mechanisms of saccadic suppression. *Science* 295:2460-2462.

Thielert CD, Thier P (1993) Patterns of projections from the pontine nuclei and the nucleus reticularis tegmenti pontis to the posterior vermis in the rhesus monkey: a study using retrograde tracers. *J Comp Neurol* 337:113-126.

Thier P, Andersen RA (1998) Electrical microstimulation distinguishes distinct saccade-related areas in the posterior parietal cortex. *J Neurophysiol* 80:1713-1735.

Thier P, Dicke PW, Haas R, Thielert CD, Catz N (2002) The role of the oculomotor vermis in the control of saccadic eye movements. *Ann N Y Acad Sci* 978:50-62.

Thier P, Erickson RG (1992) Responses of Visual-Tracking Neurons from Cortical Area MST-I to Visual, Eye and Head Motion. *Eur J Neurosci* 4:539-553.

Thier P, Haarmer T, Treue S, Barash S (1999) Absence of a common functional denominator of visual disturbances in cerebellar disease. *Brain* 122 (Pt 11):2133-2146.

Thomsen K, Offenhauser N, Lauritzen M (2004) Principal neuron spiking: neither necessary nor sufficient for cerebral blood flow in rat cerebellum. *Journal of Physiology-London* 560:181-189.

Tian JR, Lynch JC (1996b) Functionally defined smooth and saccadic eye move-

ment subregions in the frontal eye field of Cebus monkeys. *J Neurophysiol* 76:2740-2753.

Tian JR, Lynch JC (1996a) Corticocortical input to the smooth and saccadic eye movement subregions of the frontal eye field in Cebus monkeys. *J Neurophysiol* 76:2754-2771.

Tolias AS, Smirnakis SM, Augath MA, Trinath T, Logothetis NK (2001) Motion processing in the macaque: revisited with functional magnetic resonance imaging. *J Neurosci* 21:8594-8601.

Tootell RB, Hadjikhani N (2001) Where is 'dorsal V4' in human visual cortex? Retinotopic, topographic and functional evidence. *Cereb Cortex* 11:298-311.

Tootell RB, Mendola JD, Hadjikhani NK, Ledden PJ, Liu AK, Reppas JB, Sereno MI, Dale AM (1997) Functional analysis of V3A and related areas in human visual cortex. *J Neurosci* 17:7060-7078.

Tootell RB, Reppas JB, Kwong KK, Malach R, Born RT, Brady TJ, Rosen BR, Belliveau JW (1995) Functional analysis of human MT and related visual cortical areas using magnetic resonance imaging. *J Neurosci* 15:3215-3230.

Tootell RB, Silverman MS, Switkes E, De Valois RL (1982) Deoxyglucose analysis of retinotopic organization in primate striate cortex. *Science* 218:902-904.

Tootell RB, Tsao D, Vanduffel W (2003) Neuroimaging weighs in: humans meet macaques in "primate" visual cortex. *J Neurosci* 23:3981-3989.

Tsao DY, Vanduffel W, Sasaki Y, Fize D, Knutsen TA, Mandeville JB, Wald LL, Dale AM, Rosen BR, Van Essen DC, Livingstone MS, Orban GA, Tootell RB (2003) Stereopsis activates V3A and caudal intraparietal areas in macaques and humans. *Neuron* 39:555-568.

Tsay D, Yuste R (2004) On the electrical function of dendritic spines. *Trends Neurosci* 27:77-83.

Ungerleider LG, Desimone R (1986a) Cortical connections of visual area MT in the macaque. *J Comp Neurol* 248:190-222.

Ungerleider LG, Desimone R (1986b) Projections to the superior temporal sulcus from the central and peripheral field representations of V1 and V2. *J Comp Neurol* 248:147-163.

Van Essen DC (1985) Functional organization of primate visual cortex. In: *Cerebral cortex, Vol 3* (Peters A, Jones EG, eds), pp 259-329. New York: Plenum.

7. References

- Van Essen DC (2003) Organization of Visual Areas in Macaque and Human Cerebral Cortex. In: *Visual Neurosciences* (Chalupa L, Werner J, eds).
- Van Essen DC, Drury HA, Dickson J, Harwell J, Hanlon D, Anderson CH (2001) An integrated software suite for surface-based analyses of cerebral cortex. *J Am Med Inform Assoc* 8:443-459.
- Van Essen DC, Newsome WT, Maunsell JH (1984) The visual field representation in striate cortex of the macaque monkey: asymmetries, anisotropies, and individual variability. *Vision Res* 24:429-448.
- Vanduffel W, Fize D, Mandeville JB, Nelissen K, Van Hecke P, Rosen BR, Tootell RB, Orban GA (2001) Visual motion processing investigated using contrast agent-enhanced fMRI in awake behaving monkeys. *Neuron* 32:565-577.
- Vanduffel W, Fize D, Peuskens H, Denys K, Sunaert S, Todd JT, Orban GA (2002) Extracting 3D from motion: differences in human and monkey intraparietal cortex. *Science* 298:413-415.
- Vaucher E, Tong XK, Cholet N, Lantin S, Hamel E (2000) GABA neurons provide a rich input to microvessels but not nitric oxide neurons in the rat cerebral cortex: a means for direct regulation of local cerebral blood flow. *J Comp Neurol* 421:161-171.
- Verri A, Girosi F, Torre V (1989) Mathematical properties of the twodimensional motion field: From singular points to motion parameters. *J Opt Soc Am A* 6:698-712.
- Waespe W, Buttner U, Henn V (1981) Visual-vestibular interaction in the flocculus of the alert monkey. I. Input activity. *Exp Brain Res* 43:337-348.
- Wandell BA (1999) Computational neuroimaging of human visual cortex. *Annu Rev Neurosci* 22:145-173.
- Werkhoven P, Koenderink JJ (1990a) Extraction of motion parallax structure in the visual system. I. *Biol Cybern* 63:185-191.
- Werkhoven P, Koenderink JJ (1990b) Extraction of motion parallax structure in the visual system. II. *Biol Cybern* 63:193-199.
- Wurtz RH, Kandel ER (2000) Perception of motion, depth and form. In: *Principles Of Neural Science* (Kandel ER, Schwartz JH, Jessel TM, eds), pp 548-571. New York, St. Louis, San Francisco, Auckland, Bogotá, Caracas, Lisbon, London, Madrid, Mexico City, Milan, Montreal, New Delhi, San Juan, Singapore, Sydney, Tokyo, Toronto: McGraw-Hill.

Zee DS (1984) New concepts of cerebellar control of eye movements. *Otolaryngol Head Neck Surg* 92:59-62.

Zeki S, Watson JD, Lueck CJ, Friston KJ, Kennard C, Frackowiak RS (1991) A direct demonstration of functional specialization in human visual cortex. *J Neurosci* 11:641-649.

Zeki SM (1977) Colour coding in the superior temporal sulcus of rhesus monkey visual cortex. *Proc R Soc Lond B Biol Sci* 197:195-223.

Zhang ET, Mikkelsen JD, Fahrenkrug J, Moller M, Kronborg D, Lauritzen M (1991) Prepro-vasoactive intestinal polypeptide-derived peptide sequences in cerebral blood vessels of rats: on the functional anatomy of metabolic autoregulation. *J Cereb Blood Flow Metab* 11:932-938.

Zhang Z, Andersen A, Grondin R, Barber T, Avison R, Gerhardt G, Gash D (2001) Pharmacological MRI mapping of age-associated changes in basal ganglia circuitry of awake rhesus monkeys. *Neuroimage* 14:1159-1167.

Zhang Z, Andersen AH, Avison MJ, Gerhardt GA, Gash DM (2000) Functional MRI of apomorphine activation of the basal ganglia in awake rhesus monkeys. *Brain Res* 852:290-296.